Exploring the Anatomy of QCD and Related Strongly Coupled Theories

A Dissertation presented

by

Moshe Kellerstein

to

The Graduate School

in Partial Fulfillment of the

Requirements

for the Degree of

Doctor of Philosophy

in

Physics

Stony Brook University

July 2019

Stony Brook University

The Graduate School

Moshe Kellerstein

We, the dissertation committee for the above candidate for the

Doctor of Philosophy degree, hereby recommend

acceptance of this dissertation

Prof. Jacobus Verbaarschot - Dissertation Advisor
Professor, Department of Physics and Astronomy

Prof. Derek Teaney - Chairperson of Defense
Associate Professor, Department of Physics and Astronomy

Prof. Robert L. McCarthy - Committee Member
Professor, Department of Physics and Astronomy

Prof. Swagato Mukherjee - External Member
Professor, Brookhaven National Laboratory

This dissertation is accepted by the Graduate School

Eric Wertheimer
Dean of the Graduate School

Abstract of the Dissertation

Exploring the Anatomy of QCD and Related Strongly Coupled Theories

by

Moshe Kellerstein

Doctor of Philosophy

in

Physics

Stony Brook University

2019

Following a brief review introducing Chiral Random Matrix Theory as the low energy limit of QCD, and of two methods for non-perturbative computation of partition functions, we consider bosonic random matrix partition functions at nonzero chemical potential and compare the chiral condensate, the baryon number density and the baryon number susceptibility to the result of the corresponding fermionic partition function. We find that as long as results are finite, the phase transition of the fermionic theory persists in the bosonic theory. However, in case that bosonic partition function diverges and has to be regularized, the phase transition of the fermionic theory does not occur in the bosonic theory, and the bosonic theory is always in the broken phase.

We present preliminary results from a perturbative study of gauge invariant correlators in coordinate space. These correlators are comprised of the flavor-off-diagonal, dimension-5 chromelectric dipole moment (CEDM), and the chromomagnetic dipole moment (CMDM) operators, and have been calculated up to $\mathcal{O}(g^4)$ in the QCD coupling constant. Using results for the correlators, we discuss the renormalization and mixing of the CEDM and CMDM with lower dimensional operators, and present the renormalization matrices for the CEDM to CEDM and CMDM to CMDM correlators in the

$\overline{MS}$ scheme. We compute the matching factors necessary to convert the non-perturbative renormalization factors found for these correlators in the X-space scheme into $\overline{MS}$ so that CEDM and CMDM lattice calculations can be utilized in current studies. We have also computed the renormalization group coefficients, and the renormalization group flow of the correlatros necessary to express these operators at an arbitrary renormalizatoin point.

To my parents, Shirley and Joseph Kellerstein

Contents

List of Figures

Acknowledgements

I would like to thank Professors Jacobus Verbaarschot and Sergey Syritsyn for giving me the opportunity to learn, study, and contribute to the exciting fields of random matrix theory, and lattice field theory. Throughout the duration of my Ph.D, they always took the time to answer my questions, and discuss ideas.

I would like to thank my committee for their time, and assistance in my academic pursuits.

I would like to thank my Stony Brook family, Hualong Gervais, Bing Wang, Mehdi Namazi, Taeho Ryu, Harikrishnan Ramani, Oumarou Njoya, Yachao Qian and Scott Mills for being great friends, and making my time in Stony Brook amazing.

Thanks to my friend and colleague, Dr. Asaf Jeff Dror, for the support, fun physics discussions and advice throughout the duration of our physics careers.

Thank you to my family, Aaron, Joseph and Shirley Kellerstein for your constant support, and for encouraging me to pursue my passion.

Chapter 1

Introduction To Chiral Random Matrix Theory

Chiral Symmetry

Quantum chromodynamics (QCD), is the theory of the strong nuclear force. It is a non-abelian, $SU(3)$ color gauge theory, defining quark and gluon fields, and their interactions via the QCD lagrangian

$$\mathcal{L}_{QCD} = -\frac{1}{4}G^a_{\mu\nu}G^a_{\mu\nu} + \sum_{f=1}^{N_f} \overline{\psi}_f^{\alpha;b} \left(\gamma^\mu_{\alpha,\beta}\mathcal{D}^{bc}_\mu - m_f\delta^{bc}g_{\alpha,\beta}\right)\psi_f^{\beta;c}, \tag{1.1}$$

where $G^a_{\mu\nu}$ are the non-abelian field strength tensors, $\psi_f^{\beta;c}$ are the quark fields of flavor f ($f = u, d, s, c, b, t$), in the fundamental of $SU(3)$ with Dirac index β and color index c, and $\mathcal{D}^{bc}_\mu = \delta^{bc}\partial_\mu - ig\mathcal{A}^{bc}_\mu$ is the covariant derivative, with gluon fields $\mathcal{A}$ in the adjoint representation of $SU(3)$. The operator $\gamma^\mu\mathcal{D}_\mu$ is called the Dirac matrix, and from now on, will be expressed as $\mathcal{D}$. Any quantity of interest can be computed by taking functional derivatives of the

QCD partition function Z^{QCD}

$$\begin{aligned} Z^{QCD} &= \int DA_\mu D\overline{\psi} D\psi e^{-\int d^4x \mathcal{L}_{QCD}} \\ &= \int DA_\mu D\overline{\psi} D\psi e^{-\int d^4x \overline{\psi}(x)(\mathcal{D}+m)\psi(x) - S_{YM}} \\ &= \int DA_\mu \prod_{f=1}^{N_f} \det\left(\mathcal{D}+m_f\right) e^{-S_{YM}}. \end{aligned} \tag{1.2}$$

QCD is asymptotically free at high energies ($\Lambda > 1$ GeV), and is accurately described perturbatively [2]. At low energies, quarks and gluons are confined in hadrons, and a perturbative treatment no longer suffices. Lattice QCD, where the path integral is studied using Monte Carlo simulations, has greatly improved our knowledge of QCD at low energies [3]. However, for a clearer picture of the relevant degrees of freedom, effective models are advantageous. Building effective models requires an analysis of QCD's global symmetries.

To study the global flavor symmetries of QCD, equation (1.1) is rewritten in a chiral basis using left and right handed projection operators $P_L = \frac{1}{2}(1-\gamma_5)$ and $P_R = \frac{1}{2}(1+\gamma_5)$.

$$\begin{aligned} \mathcal{L}_{QCD} = &-\frac{1}{4} G^a_{\mu\nu} G^a_{\mu\nu} + \sum_f \left(\overline{\psi}_{R,f} i\mathcal{D}\psi_{R,f} + \overline{\psi}_{L,f} i\mathcal{D}\psi_{L,f}\right) \\ &+ \sum_{f,j} \left(\overline{\psi}_{R,f} M_{fj} \psi_{L,j} + \overline{\psi}_{L,f} M_{fj} \psi_{R,j}\right) \end{aligned} \tag{1.3}$$

From equation (1.3), it is clear that in the chiral limit ($M \to 0$), $\mathcal{L}_{QCD}$ is invariant under independent, unitary transformations of both the right, and left handed quark fields

$$\psi_{L,f} \to \psi'_{L,f} = U^L_{f,j} \psi_{L,j} \tag{1.4}$$

$$\psi_{R,f} \to \psi'_{R,f} = U^R_{f,j} \psi_{R,j} \tag{1.5}$$

Where L and R indicate whether it's a left, or right handed quark, and f and j are flavor indices. This is a classical $U(N_f)_L \times U(N_f)_R$ symmetry. Taking into account, only the three light quarks, (u, d, s) we have $N_f = 3$. The chiral transformations can be conveniently re-expressed as parity even and

parity odd transformations

$$U_V = U^L + U^R \tag{1.6}$$
$$U_A = U^L - U^R \tag{1.7}$$

While the classical lagrangian is invariant under the full $U(N_f)_V \times U(N_f)_A$ symmetry, the $U(1)_A$ symmetry is explicitly broken by the regulator [3], leaving a $SU(N_f)_V \times SU(N_f)_A \times U(1)_V$ symmetry.

In the chiral limit, one would naively expect for each parity even state generated by a $SU(N_f)_V$ charge operator, a corresponding state of equal energy, but negative parity created by a $SU(N_f)_A$ charge operator. Observations of the hadronic spectrum, however, contradict this claim. The octet of pseudo scalar mesons have masses much smaller than expected, the expected parity doubling is not seen, and an $SU(3)_V$ symmetry is realized. These facts suggest that the $SU(N_f)_A$ symmetry is broken spontaneously, and the pseudoscalar octet are candidates for Goldstone bosons.

Moreover, in the chiral limit, the ground state must be invariant under the vectorial symmetries [4]. Since the ground state is invariant under $SU(3)_V \times U(1)_V$, the Hamiltonian is too, and physical states of the system can be organized according to its irreducible representations.

Chiral symmetry is spontaneously broken by the quark condensate. It will now be useful to derive the famous Banks Casher Relation, which describes the relationship between the spectrum of the Dirac operator $\rho(\lambda)$, and the quark condensate $\Sigma = \left|\langle\overline{\psi}\psi\rangle\right|$. The chiral condensate is also equal to

$$\Sigma = \lim_{m\to 0}\lim_{V\to\infty}\frac{1}{V}\left|\frac{\partial \log Z_{QCD}}{\partial m}\right|. \tag{1.8}$$

Solving the partition function can be made simpler by expanding the Fermi fields $\psi(x)$ in terms of eigen functions of the Dirac operator

$$\psi(x) = \sum_n a_n u_n(x), \tag{1.9}$$

where a_n is a Grassman number, and $u_n(x)$ are the eigenfunctions of $\mathcal{D}$

$$\mathcal{D}u_n(x) = \lambda_n u_n(x). \tag{1.10}$$

The quantity Σ can also be found by taking the trace over the dirac propagator [5]

$$\Sigma = \lim_{m\to 0}\lim_{V\to\infty}\frac{1}{V}\left\langle\int d^4x S(x,x)\right\rangle_{YM} \tag{1.11}$$

$$= \lim_{m\to 0}\lim_{V\to\infty}\frac{1}{V}\left\langle\int d^4x \sum_k \frac{u_k^\dagger(x)u_k(x)}{\lambda_k + im}\right\rangle_{YM} \tag{1.12}$$

$$= \lim_{m\to 0}\lim_{V\to\infty}\sum_k \langle\frac{1}{V}\frac{1}{i\lambda_k + m}\rangle_{YM} \tag{1.13}$$

$$= \lim_{m\to 0}\lim_{V\to\infty}\frac{2m}{V}\sum_{\lambda_k\geq 0}\langle\frac{1}{\lambda_k^2 + m^2}\rangle_{YM} \tag{1.14}$$

We now define the spectral density of the Dirac operator

$$\rho(\lambda) = \langle\sum_n \delta(\lambda - \lambda_n)\rangle_{YM} \tag{1.15}$$

Rewriting equation (1.14) using the spectral density $\rho(\lambda)$

$$= \lim_{m\to 0}\lim_{V\to\infty}\frac{2m}{V}\int_0^\infty d\lambda\frac{\rho(\lambda)}{\lambda^2 + m^2} \tag{1.16}$$

Solving this integral as a contour integral in the complex plain gives

$$\langle\overline{\psi}\psi\rangle = \lim_{m\to 0}\lim_{V\to\infty}\pi\frac{\rho(im)}{V} \tag{1.17}$$

The spectral density in equation (1.15) has a normalization proportional to the volume V. Therefore, taking the limits in order, one finds that the chiral condensate Σ

$$\Sigma = \left|\langle\overline{\psi}\psi\rangle\right| = \pi\rho(0) \tag{1.18}$$

This result shows that in order for the chiral condensate to spontaneously break chiral symmetry, there must an accumulation of eigenvalues of the Dirac operator near $\lambda = 0$.

Chiral Lagrangian

An effective theory of the Goldstone bosons of chiral symmetry breaking can be constructed using the symmetries, and symmetry breaking patterns of QCD. According to Goldstone's Theorem [6], the spontaneous breaking of $SU(N_f)_L \times SU(N_f)_R \to SU(N_f)_V$ gives $N_f^2 - 1$ massless Goldstone modes. The Goldstone modes should be parameterized such that they are isomorphic with the coset $SU(N_f)_L \times SU(N_f)_R / SU(N_f)_V$, the vacuum is left invariant under $SU(N_f)_V$ transformations, and the vacuum transforms under $SU(N_f)_A$. The Goldstone modes should also take on the properties of the broken group they correspond to. Therefore, they should be pseudoscalars. The $SU(N)$ matrix

$$U = U_R U_L^\dagger = \exp\left(i\frac{\lambda_a \phi_a(x)}{F}\right), \tag{1.19}$$

where fields, ϕ_a are the Goldstone modes, and matrices λ_a are generators of $SU(N_f)$, has the transformation properties needed.

Under an $SU(N_f)_L \times SU(N_f)_R$ transformation, U becomes

$$U \to U' = U_R U U_L^\dagger \tag{1.20}$$

To lowest order in momentum, in the chiral limit, the lagrangian should be invariant under a chiral transformation. The kinetic term is

$$\mathcal{L} = \frac{F^2}{4} Tr\left(\partial_\mu U \partial^\mu U^\dagger\right), \tag{1.21}$$

where F is the pion decay constant.

Quark mass terms explicitly break chiral symmetry,

$$\mathcal{L}_m = -\,\overline{q}_R M q_L - \overline{q}_L M q_R. \tag{1.22}$$

If, however, M transforms under $SU(N_f)_L \times SU(N_f)_R$ as a member of the $(3*, 3)$ representation, i.e.

$$M \to U_R M U_L^\dagger, \tag{1.23}$$

chiral symmetry in equation (1.22) would be preserved. Constructing the most general lagrangian, invariant under equations (1.20) and (1.23), at lowest order, one finds

$$\mathcal{L} = \frac{F^2}{4} Tr\left(\partial_\mu U \partial^\mu U^\dagger\right) - \frac{\Sigma}{2} Tr\left(MU^\dagger + UM^\dagger\right), \tag{1.24}$$

where $\Sigma = \frac{\partial}{\partial m_q} Z_{QCD}$ is the chiral condensate.

Studying the chiral lagrangian in a box of size L^4 allows for a connection with random matrix theory. The chiral lagrangian is valid in when

$$\frac{1}{\Lambda} << L \tag{1.25}$$

Where Λ is the mass of a particle heavier than the pion.

Expanding the field U in momentum modes, and comparing the two terms in equation (1.24), one finds the zero modes become the dominant contribution to the path integral when

$$\frac{\Sigma M}{F^2} << \frac{1}{L^2} \tag{1.26}$$

This implies that when pion compton wavelength is much larger than the size of the box, the particles do not propagate, and the zero modes are the dominant contribution. This is called the ϵ-regime. In the ϵ-regime, the partition function becomes

$$Z \propto \int_{U \in SU(N_f)} DU e^{V \Sigma Re Tr M U^\dagger} \tag{1.27}$$

Random Matrix Theory

Random matrices made their first appearance in physics, in the modeling of highly excited nuclear resonances. Rather than attempting to describe the complex dynamics of each state, Wigner took a statistical approach [7, 8]. By exploiting similarities between nuclear interactions, and random matrices with the same global symmetry, Wigner constructed ensembles of Hamiltonians, each Hamiltonian having the same global symmetries.

The approach used by Wigner has, time and time again, provided accurate descriptions for complicated systems across many physical fields. Random matrix theory's success does not lie in its ability to describe a system's specific dynamical properties, but rather its simplistic, and accurate calculations

of the observables of a system, determined solely by symmetry. The recipe for modeling using random matrices is to generate an ensemble of matrices, with random entries, and the same symmetry structure as the system of interest. The then sought after physical observables, are the universal properties, common to all members of the ensemble, and depending only on the symmetries of the system.

Several generic random matrix ensembles exist, each determined by their probability density functions, their hermiticity, and symmetry properties. The ensemble of interest, encoding the global symmetry properties of QCD is called the chiral ensemble [9, 10]. The chiral ensemble consists of matrices $\mathcal{D}$ with the structure

$$\mathcal{D} = \begin{pmatrix} 0 & iW \\ iW^\dagger & 0 \end{pmatrix}, \tag{1.28}$$

where W is an $n \times m$ $(n \geq m)$ random matrix, chosen to have gaussian distributed random entries

$$P_\beta(W) = e^{-\frac{N\beta}{4}\mathrm{Tr}(W^\dagger W)}, \tag{1.29}$$

where β is the dyson index, and $N = n + m$ is the number of modes.

Equation (1.3) shows that in the massless limit the QCD lagrangian is invariant under chiral transformations. Equivalently, one can show that for a chirally symmetric lagrangian, the QCD Dirac operator $\mathcal{D}$ anticommutes with γ_5

$$\{\gamma_5, \mathcal{D}\} = 0. \tag{1.30}$$

In the chiral basis where

$$\gamma_5 = \begin{pmatrix} -\mathbf{1} & 0 \\ 0 & \mathbf{1} \end{pmatrix}, \tag{1.31}$$

the matrix in equation (1.28) and γ_5 anticommute. Because of this anticommutation relation, for each eigenvector ψ_i of $\mathcal{D}$ with nonzero eigenvalue λ_i, there is an eigen vector $\gamma_5\psi_i$ of $\mathcal{D}$ with eigenvalue $-\lambda_i$. Since both the Dirac operator, and equation (1.28) anticommute with γ_5, the eigenvalue structure of the matrix will have this property, where nonzero eigenvalues come in pairs of $\pm\lambda_i$ as well. This is characteristic of the $U(1)_A$ symmetry.

Eigenvectors ψ of $\mathcal{D}$ are composed of a left handed spinor χ, and a right handed spinor $\xi^\dagger$

$$\mathcal{D}\psi_i = \begin{pmatrix} 0 & iW \\ iW^\dagger & 0 \end{pmatrix} \begin{pmatrix} \chi \\ \xi^\dagger \end{pmatrix} \tag{1.32}$$

$$= \begin{pmatrix} iW\xi^\dagger \\ iW^\dagger\chi \end{pmatrix} = \lambda_i \begin{pmatrix} \chi \\ \xi^\dagger \end{pmatrix} \tag{1.33}$$

We therefore see that

$$WW^\dagger\chi_i = \lambda_i^2\chi_i \tag{1.34}$$

Where the index i runs from 1 to n. However, the matrix $WW^\dagger$ is of rank m, and therefore, $\nu \equiv n - m$ of the eigenvalues must be equal to 0. The m nonzero eigenvalues of $WW^\dagger$ are the same as the m eigenvalues of $W^\dagger W$. This is just the Atiyah-Singer index theorem, which, in QCD is the statement that the difference between states of definite positive, and negative chirality is a conserved topological charge, and is equal to the number of zero modes of the QCD Dirac operator. Therefore, encoded in this matrix are the topological properties of the Dirac operator.

To construct a more accurate random matrix model of the Dirac operator, one must understand transformation properties of the Dirac operator under an anti-unitary operator. There are three different non-trivial QCD theories to be studied, each differing by their transformation properties under some anti-unitary operator UK, where U is some unitary operator, and K is the complex conjugation operator.

1. The first interesting QCD scenario gives rise to a random matrix theory with dyson index $\beta = 1$, and real random variables as entries in in the matrices W. This corresponds to QCD with two colors, and fermions in the fundamental representation. With two colors, the Dirac operator is

$$\mathcal{D} = \gamma_\mu(\partial_\mu + iA_\mu^a\tau^a/2), \tag{1.35}$$

   where τ are the pauli matrices. In this case, the Dirac operator commutes with the anti-unitary operator $\gamma_2\gamma_4\tau_2 K$. The flavor symmetry resulting from a QCD lagrangian, invariant under this is $SU(2N_f)$.

The chiral condensate, however, spontaneously breaks this symmetry to $Sp(2N_f)$. Since

$$(\gamma_2\gamma_4\tau_2 C)^2 = 1, \tag{1.36}$$

the matrices W have real entries, and the dyson index is $\beta = 1$. Therefore, the flavor symmetry, and antiunitary symmetry are properties of W having real entries.

2. The second case corresponds to a dyson index $\beta = 4$. In this case, fermions are in the adjoint representation, and there can be any number of colors. The Dirac operator is

$$\mathcal{D}_{ab} = \gamma_\mu(\partial_\mu\delta_{ab} + f_{abc}A^c_\mu) \tag{1.37}$$

In this case, $[\mathcal{D}, \gamma_2\gamma_4 K] = 0$, and

$$(\gamma_2\gamma_4 C)^2 = -1. \tag{1.38}$$

The lagrangian in this case is invariant under an $SU(N_f)$ flavor symmetry for even N_f, and majorana fermions, and the chiral condensate breaks this symmetry into $O(N_f)$. The matrices W, corresponding to this antiunitary symmetry and flavor symmetry have real quaternion entries.

3. The third scenario has dyson index $\beta = 2$, and corresponds to QCD with three colors, and fermions in the fundamental representation. In this scenario, no anti-unitary operator exists that commutes with the Dirac operator. This corresponds to matrices W, with complex entries, and the flavor symmetry, $SU(N_f) \times SU(N_f)$ broken to $SU(N_f)$, as discussed above.

The partition function for the chiral random matrix thory, with N_f flavors, in the sector of topological charge ν, is

$$Z^{\beta=2}_{N_f,\nu}(m_1, m_2, \ldots, m_{N_f}) = \int DW \prod_{f=1}^{N_f} \det(\mathcal{D} + m_f) e^{-\frac{N}{2}\mathrm{Tr}(W^\dagger W)}. \tag{1.39}$$

This can be solved by expressing the determinant as an integral over grassman variables

$$Z^{\beta=2}_{N_f,\nu}(\{m_i\}) = \int DW \prod_f D\psi^f D\phi^f \exp\left\{ \sum_f \begin{pmatrix} \psi^{f*} & \phi^{f*} \end{pmatrix} \begin{pmatrix} m_f & iW \\ iW^\dagger & m_f \end{pmatrix} \begin{pmatrix} \psi^f \\ \phi^f \end{pmatrix} - \frac{N}{2} Tr W^\dagger W \right\} \tag{1.40}$$

where $D\psi^f = \prod_i d\psi_i d\psi_i^*$, and the complex conjugate convention of $\psi^{**} = -\psi$ is being used. Completing the square in W, and performing the gaussian integral leaves an irrelevant overall constant, and a four fermion term.

$$Z^{\beta=2}_{N_f,\nu}(\{m_i\}) = \int \prod_f D\psi^f D\phi^f \exp\left\{ \psi^{f*} m_f \psi^f + \phi^{f*} m_f \phi^f + \frac{2}{N} \psi_i^{f*} \psi_i^g \phi_j^{g*} \phi_j^f \right\} \tag{1.41}$$

$$= \int \prod_f D\psi^f D\phi^f \exp\left\{ \psi^{f*} m_f \psi^f + \phi^{f*} m_f \phi^f + \frac{\Sigma^2}{2N} \left((\psi_i^{f*}\psi_i^g + \phi_i^{f*}\phi_i^g)(\psi_j^{g^*}\psi_j^f + \phi_j^{g*}\phi_j^f) - (\psi_i^{f*}\psi_i^g - \phi_i^{f*}\phi_i^g)(\psi_j^{g*}\psi_j^f - \phi_j^{g^*}\phi_j^f) \right) \right\} \tag{1.42}$$

In the last line, the four fermion term was expressed as the sum of two quadratic terms. Using a hubbard stratonovich transformation, the fermionic variables can now be made quadratic, at the expense of adding a new integration variable

$$Z^{\beta=2}_{N_f,\nu}(\{m_i\}) = \int \prod_f D\psi^f D\phi^f \int D\sigma D\overline{\sigma} \exp\left\{ \psi^{f*} m_f \psi^f + \phi^{f*} m_f \phi^f - \frac{N}{2\Sigma^2} Tr(\sigma\sigma + \overline{\sigma}\overline{\sigma}) + (\psi_i^{f*}\psi_i^g + \phi_i^{f*}\phi_i^g)\sigma^{fg} + (\psi_i^{f*}\psi_i^g - \phi_i^{f*}\phi_i^g) i\overline{\sigma}^{fg} \right\} \tag{1.43}$$

$$= \int D\sigma D\overline{\sigma} \prod_f D\psi^f D\phi^f \exp\left\{ -\frac{N}{2\Sigma^2} Tr(\sigma + i\overline{\sigma})(\sigma - i\overline{\sigma}) + \psi_i^{f*}(\sigma^{fg} + i\overline{\sigma}^{fg} + m_f\delta^{fg})\psi_i^g + \phi_i^{f*}(\sigma^{fg} - i\overline{\sigma}^{fg} + m_f\delta^{fg})\phi_i^g \right\}. \tag{1.44}$$

The integrals over the grassman variables are now gaussian integrals. For real, and degenerate quark masses, this simplifies to

$$= \int D\sigma D\overline{\sigma} e^{-\frac{N}{2\Sigma^2} Tr(\sigma+i\overline{\sigma})(\sigma-i\overline{\sigma})} \det{}^{\nu}\left(\sigma + i\overline{\sigma} + m_f\right) \det{}^{n}\left[(\sigma + i\overline{\sigma} + m_f)(\sigma - i\overline{\sigma} + m_f)\right] \tag{1.45}$$

The variables $\sigma + i\overline{\sigma}$ can be decomposed into polar coordinates, $U\Lambda V^{-1}$, where Λ is diagonal, and U and V are unitary matrices. The integral can now be separated into massive modes, and massless Goldstone modes. As $n \to \infty$, performing the integral over Λ by a saddlepoint approximation, and keeping only the integrals over the Goldstone manifold results in

$$Z_\nu(m) = \int_{U \in U(N_f)} DU \det{}^{\nu} U e^{n\Sigma Tr(MU + M^\dagger U^{-1})}, \tag{1.46}$$

which is just the ϵ regime, finite volume partition function [11].

Resolvent Methods and Bosonic Partition Functions

There are several methods for computing the spectral density. Those methods, and their connections to bosonic partition functions are briefly reviewed.

As shown in equation (1.15), the spectral density for the Dirac operator is

$$\rho(\lambda) = \langle \sum_n \delta(\lambda - \lambda_n) \rangle, \tag{1.47}$$

where the average is over the guage fields, and the weight is the euclidean action. Using the identity

$$\delta(x) = \frac{1}{2\pi i}\left(\frac{1}{x - i\epsilon} - \frac{1}{x + i\epsilon}\right), \tag{1.48}$$

the spectral density becomes

$$\rho(\lambda) = \frac{1}{2\pi i}\left\langle Tr \frac{1}{\lambda - \mathcal{D} - i\epsilon} - Tr \frac{1}{\lambda - D + i\epsilon} \right\rangle \tag{1.49}$$

$$\frac{\rho(\lambda)}{V} = \lim_{\epsilon \to 0} \frac{1}{2\pi} \left(\Sigma(i\lambda + \epsilon) - \Sigma(i\lambda - \epsilon)\right). \tag{1.50}$$

$\Sigma(z)$ is an object called the resolvent, and is defined to be the averaged trace of the inverse Dirac operator.

$$\Sigma(z) = \left\langle \frac{1}{V} Tr \frac{1}{\mathcal{D} + z} \right\rangle . \tag{1.51}$$

Therefore, the spectral density can easily be computed by finding the discontinuity across the imaginary axis of the resolvent. In this section, two methods for computing the resolvent will be discussed. The first is called the supersymmetric method. The supersymmetric method is defined by the following generating functional for the resolvent

$$Z_S = \left\langle \det{}^{N_f} (\mathcal{D} + m) \frac{\det (\mathcal{D} + z + j)}{\det (\mathcal{D} + z)} \right\rangle_{YM}, \tag{1.52}$$

where the resolvent is found by taking derivatives of the generating functional.

$$\Sigma(z) = \frac{1}{V} \frac{\partial Z_S}{\partial j} \bigg|_{j=0} \tag{1.53}$$

The partition function in equation (1.52) can be expressed as a functional integral over both bosonic and fermionic variables, and for $j = 0$, the original QCD partition function is restored.

For an arbitrary random matrix theory with system represented by the random matrix H, source term J, defined by the determinant

$$\det(z - H) = \int D\overline{\psi} D\psi e^{i\overline{\psi}(z-H)\psi}, \tag{1.54}$$

The resolvent is given by

$$\Sigma(z) = \frac{\partial}{\partial z} \log \det(z - H). \tag{1.55}$$

Using the identity

$$\log X = \lim_{n \to 0} \frac{X^n - 1}{n}, \tag{1.56}$$

The resolvent can be rewritten without any denominator as

$$\Sigma(z) = \lim_{n \to 0} \frac{1}{n} \frac{\partial}{\partial z} \det{}^n (z - H) \tag{1.57}$$

The replica trick for a chiral random matrix theory with N_f flavors of mass m is defined by the generating the following generating functional for the resolvent

$$Z_{RT}(N_f, m, n) = \left\langle \det{}^{N_f}(\mathcal{D}+m) \det{}^{n}(\mathcal{D}+z) \right\rangle_{YM}, \tag{1.58}$$

where n replicas of the original fermion determinant are made, with spectral mass z. The resolvent can be computed from Z_{RT} by

$$\Sigma(z) = \lim_{n\to 0} \frac{1}{n} \frac{\partial}{\partial z} Z_{RT} \tag{1.59}$$

When computing the generating functional Z_{RT}, n is assumed to be either a positive (fermionic replicas), or negative (bosonic replicas) integer, and when computing the resolvent (or higher point functions), the limit of $n \to 0$ is taken.

Bosonic partition functions appear in both the supersymmetric and replica generating functionals as an inverse determinant.

$$\frac{1}{\det(\mathcal{D}+z)} = \int D\phi D\phi^\dagger e^{-\phi^\dagger(\mathcal{D}+z)\phi}, \tag{1.60}$$

where ϕ, is a vector of 2 commuting variables $\phi = (\phi_1, \phi_2)^T$. The action in equation (1.60) is invariant under the transformations

$$\phi \to \phi' = U\phi \tag{1.61}$$
$$U = e^{s\sigma_3} V \tag{1.62}$$

where V is unitary, and represents the vector symmetry, and the axial transformations are represented by matrices, $e^{s\sigma_3}$ where $s \in \{-\infty, \infty\}$, in the non-compact coset $Gl(1)/U(1)$. For an additional N_f bosonic flavors, the coset becomes $Gl(N_f)/U(N_f)$.

For a single bosonic replica of the quenched ($N_f = 0$) replica generating functional in topological sector ν, Z_{RT} was solved in [12], and found to be

$$Z_\nu(0, z, -1) = 2K_\nu(z) \tag{1.63}$$

While the replica generating functional may seem innocuous, it can only be solved for an integer number of replicas ($n \in \mathcal{Z}^+$). However, the resolvent is obtained in the limit of n close to 0. This limit involves analytically continuing from the set of positive integers ($\mathcal{Z}^+$) to the set of real numbers ($\mathcal{R}$).

This continuation presents difficulties. To study the validity of the replica generating functional, fermionic and bosonic partition functions were computed, and compared with one another [13]. It was found that, not only did the bosonic and fermionic replicas disagree, but both provided the incorrect result. The validity of the replica generating functional, and relationships between bosonic and fermionic partition functions were further explored in [14, 15], where the replica generating functionals were computed as solutions to the toda lattice equation and the Painleve IV equation, and the replica number n, served an index parameter. In was found that exact results could be obtained in the replica limits of these integrable systems.

Finite Chemical Potential Partition Functions

The partition function for a system characterized by Hamiltonian H with conserved charges $\hat{N}_i$ is

$$Z = Tr e^{-\beta(H-\mu_i \hat{N}_i)}. \tag{1.64}$$

For QCD at finite temperature, and chemical potential, the partition function becomes

$$\begin{aligned} Z &= \int DAD\overline{\psi}D\psi DCD\overline{C} \exp\left[\int_0^\beta d\tau \int d^3x \sum_f^{N_f} \overline{\psi}\left(\mathcal{D} + m_f + \mu\gamma_0\right)\psi + S_{YM} + S_{gf} + S_{ghost}\right]. \\ &= \left\langle \prod_f \det\left(\mathcal{D} + m_f + \mu\gamma_0\right)\right\rangle_{YM} \end{aligned} \tag{1.65}$$

The addition of the γ_5 anti-hermitian chemical potential term, $\mu\gamma_0$, to the γ_5 hermitian Dirac operator $\mathcal{D}$, removes any hermiticiy properties and causes the fermion determinant at finite density to have a complex phase. Given that probabilities must be real, positive numbers, this complex phase prohibits the interpretation of the fermion determinant and Yang-Mills action as a probability density, making Monte-Carlo simulations impossible. This is known as the sign problem [16, 17]. Random matrix theories at finite chemical potential have helped with our understanding of the sign problem [18], and QCD at finite density.

In this chapter, chiral random matrix theory was introduced, and the role it plays as an effective model of QCD was described. Chapter 2 will

describe two different random matrix models at finite density, and several different bosonic and fermionic generating functionals will be evaluated, and compared.

Chapter 2

Random Matrix Theories at Nonzero Chemical Potential

Random Matrix Models

We consider two different random matrix theories for QCD at nonzero chemical potential,

$$D_1 = \begin{pmatrix} m\mathbf{1} & C+\mu\mathbf{1} \\ -C^\dagger+\mu\mathbf{1} & m\mathbf{1} \end{pmatrix}, \tag{2.1}$$

$$D_2 = \begin{pmatrix} m\mathbf{1} & C+\mu D \\ -C^\dagger+\mu D^\dagger & m\mathbf{1} \end{pmatrix} \tag{2.2}$$

with complex $n \times n$ matrices C and D distributed according to

$$P(C) = e^{-n\Sigma^2 \mathrm{Tr} CC^\dagger}. \tag{2.3}$$

The ensemble D_1 was introduced in [19] for imaginary chemical potential and in [20] for real chemical potential. D_1 is constructed by observing in equation (1.65), that the temporal component of $\mathcal{D}$, $(\partial_0 - igA_0)$ is added to the chemical potential. The ensemble D_2 was introduced in [21] by choosing the elements of γ_0 to be random matrices D. For each of the ensembles we consider the bosonic and fermionic one-flavor and two-flavor phase-quenched

partition functions,

$$Z_{N_f=1} = \langle \mathcal{N} \det(D+m) \rangle, \tag{2.4}$$

$$Z_{N_f=-1} = \left\langle \frac{1}{\mathcal{N} \det(D+m)} \right\rangle, \tag{2.5}$$

$$Z_{1+1^*} = \langle |\mathcal{N} \det(D+m)|^2 \rangle, \tag{2.6}$$

$$Z_{0/1+1^*} = \mathcal{N} \left\langle \frac{1}{|\mathcal{N} \det(D+m)|^2} \right\rangle, \tag{2.7}$$

The normalization factor is chosen such that the free energy is μ independent for small μ and $m \to 0$. It turns out that this factor is given by

$$\mathcal{N} = e^{n\Sigma^2\mu^2}. \tag{2.8}$$

In the microscopic domain, $m \sim 1/V$ and $\mu^2 \sim 1/V$, the mass and chemical potential dependence of the partition functions is universal and coincides with that of the QCD partition function. In this limit, the random matrix ensembles D_1 and D_2 give the same results which can also be derived from the corresponding chiral Lagrangian. In particular, the one-flavor partition function does not depend on the chemical potential in this domain. Since the chemical potential of the phase quenched fermionic partition function can be interpreted as an isospin chemical potential [22, 23] this partition function is μ-independent only up to $\mu = m_\pi/2$ at which point a phase transition to a pion condensation phase occurs. The phase quenched bosonic partition function does not have a phase transition as a function of μ [24] as will be discussed in more detail in the next section. An imaginary chemical potential does not change the hermiticity properties of the Dirac operator and in the microscopic domain the partition function does not depend on it.

The ensemble D_2 does not have any other phase transitions in the nonuniversal domain. On the other hand, the ensemble D_1 has nonuniversal phase transition. For $\mu = i\mu_i$ purely imaginary it has a second order phase transition to a chirally restored phase at $\mu_i = 1$ [19], whereas for real μ it has a first order transition at $\mu = 0.527$ [20]. This phase transition resembles the QCD phase transition to a phase of nonzero baryon density which is why this model is particularly interesting. One of the main questions of this paper is the fate of this phase transition for the bosonic partition function.

The random matrix partition functions of both ensembles can be evaluated by a variety of methods such as the supersymmetric method, the

replica trick, resolvent expansion technique, the Toda lattice equation, chiral Lagrangians etc. . However, only the partition functions of the of the two-matrix ensemble D_2 can be evaluated analytically at finite n using orthogonal polynomial methods [21, 25, 24, 26]. The fermionic as well as phase quenched partition functions of the ensemble D_1 have been evaluated both for real [20, 27] and imaginary chemical potential [19, 28]. Both exact results in terms of one-dimensional integrals [27] and mean field results [20, 29] have been obtained. The bosonic partition function of the ensemble D_1 has not been studied in the literature, and we will evaluate it both for imaginary chemical potential at nonzero quark mass and real chemical potential at zero quark mass.

Phase Quenched QCD

The phase quenched fermionic partition function [22] can be rewritten as

$$
\begin{aligned}
Z_{1+1^*} &= \langle|\mathcal{N}\det(D+\mu\gamma_0+m)|^2\rangle, && (2.9)\\
&= \left\langle \mathcal{N}\det\begin{pmatrix} D+\mu\gamma_0+m & 0 \\ 0 & D^\dagger+\mu\gamma_0+m \end{pmatrix}\right\rangle && (2.10)\\
&= \left\langle \mathcal{N}\det\begin{pmatrix} D+\mu\gamma_0+m & 0 \\ 0 & \gamma_5 D\gamma_5+\mu\gamma_0+m \end{pmatrix}\right\rangle && (2.11)\\
&= \langle \mathcal{N}\det(D+\mu\gamma_0+m)\det(D-\mu\gamma_0+m)\rangle. && (2.12)
\end{aligned}
$$

Going from line 2.9 to 2.10 can be interpreted as rewriting the quenched determinant in flavor space, and is therefore the two-flavor partition function at nonzero isospin chemical potential. It has a phase transition to a Bose condensed phase at $\mu = m_\pi/2$. This transition coincides with the point where the quark mass enters the cloud of eigenvalues [30].

The phase quenched bosonic partition function (2.7) can be evaluated simply by writing it as an integral over the joint probability distribution [24]

$$
Z_{0/1+1^*}(z,z^*,\mu) = \int \prod_{k=1}^{n} \frac{d^2 z_k w(z_k,z_k^*;\mu)}{(z^2-z_k^2)(z^{*2}-z_k^{*2})}|\Delta(z_k^2)|^2, \qquad (2.13)
$$

where [21]

$$
w(z_k,z_k^*;\mu) = |z|^{2\nu+2} e^{n(1-\mu^2)(z^2+z^{*2})/4\mu^2} K_\nu\left(\frac{n(1+\mu^2)|z^2|}{2\mu^2}\right). \qquad (2.14)
$$

The integral diverges logarithmically when one of the eigenvalues is close to z. While the divergent term dominates the partition function, the divergence can be absorbed into the normalization. Then the bosonic determinant cancels against the same factor from the Vandermonde determinant and the partition function reduces to [25, 24]

$$Z_{0/1+1^*}(z, z^*, \mu) \sim w(z, z^*; \mu) \log(\epsilon). \tag{2.15}$$

This gives rise to a baryon density and a chiral condensate that depend smoothly on the chemical potential and the phase transition of the fermionic theory at $\mu = m_\pi/2$ does not take place.

The logarithmic singularity is a generic feature of the bosonic partition function which can also be understood starting from a chiral Lagrangian. The Dirac operator in the phase quenched bosonic partition function has to be regularized as [31]

$$D^{\text{reg}} = \begin{pmatrix} \hat{D} + \mu\gamma_0 & \epsilon \\ -\epsilon & -\hat{D} + \mu\gamma_0 \end{pmatrix} \tag{2.16}$$

with the chiral block structure of the Dirac operator $\hat{D}$ given by

$$\hat{D} = \begin{pmatrix} m & id \\ id^\dagger & m \end{pmatrix}. \tag{2.17}$$

The determinant of this two-flavor Dirac operator can be rewritten as

$$\det((\hat{D} + \mu\gamma_0)^\dagger(\hat{D} + \mu\gamma_0) + \epsilon^2) = \det(\hat{D}\mathbf{1} + \mu\gamma_0\tau_3 + \epsilon\gamma_5 i\tau_2), \tag{2.18}$$

so that, physically, ϵ is the source term for the isospin condensate. By permutation of rows and columns, the regularized determinant operator can be written as

$$\det \tilde{D}^{\text{reg}} \tag{2.19}$$

with

$$\tilde{D}^{\text{reg}} = \begin{pmatrix} \epsilon + im\tau_2 & id\tau_1 + \mu i\tau_2 \\ id^\dagger\tau_1 + \mu i\tau_2 & \epsilon + im\tau_2 \end{pmatrix}, \tag{2.20}$$

which makes it possible to express the bosonic partition function as a convergent Gaussian integral

$$Z_{0/1+1^*} = \left\langle \int \prod_k d\phi_k d\phi_k^* \exp\left[- \begin{pmatrix} \phi_1^* \\ \phi_2^* \end{pmatrix}^T \begin{pmatrix} \epsilon + im\tau_2 & id\tau_1 + \mu i\tau_2 \\ id^\dagger\tau_1 + \mu i\tau_2 & \epsilon + im\tau_2 \end{pmatrix} \begin{pmatrix} \phi_1 \\ \phi_2 \end{pmatrix} \right] \right\rangle \tag{2.21}$$

The pion condensate is given by the expectation value

$$\frac{1}{n}\langle \phi_1^* \cdot \phi_1 + \phi_2^* \cdot \phi_2 \rangle, \tag{2.22}$$

which follows by differentiation with respect to the source term. A nonzero value of this condensate spontaneously breaks the symmetry the Gl(1)/U(1) symmetry

$$\begin{pmatrix} \phi_1 \\ \phi_2 \end{pmatrix} \to \exp(s\tau_3) \begin{pmatrix} \phi_1 \\ \phi_2 \end{pmatrix}, \qquad \begin{pmatrix} \phi_1^* \\ \phi_2^* \end{pmatrix}^T \to \begin{pmatrix} \phi_1^* \\ \phi_2^* \end{pmatrix}^T \exp(s\tau_3), \tag{2.23}$$

of $\tilde{D}^{\rm reg}$ with s real (for $\epsilon \to 0$). Note that an imaginary part of s would violate the complex conjugation property of the integration variables and the integral would no longer be convergent. In the chiral Lagrangian, the s-degree of freedom becomes a "Goldstone mode" which for nonzero ϵ acquires a mass term

$$\sim \epsilon {\rm Tr} e^{\tau_3 s} = 2\epsilon \cosh s. \tag{2.24}$$

The integral over s gives the $\log \epsilon$-divergence of the partition function found earlier in this section. This is a general argument that applies both to the ensemble D_1 and the ensemble D_2 and applies as long as the above Gl(1)/U(1) symmetry is spontaneously broken.

The source term for the chiral condensate is the quark mass, and it is thus given by

$$\frac{1}{n}\langle \phi_1^* i\tau_2 \phi_1 + \phi_2^* i\tau_2 \phi_2 \rangle. \tag{2.25}$$

The corresponding Goldstone manifold for the noncompact symmetry is thus given by

$$e^{s\tau_3} \Sigma_c e^{s\tau_3} \tag{2.26}$$

with $\Sigma_c = i\tau_2$. The s degree of freedom drops out of the Goldstone manifold, and it is not possible to regularize the partition function by introducing a regulator mass in this source term. If the partition function has to make sense we necessarily need a nonzero pion condensate for which the Gl(1)/U(1) symmetry is spontaneously broken, and the Goldstone degree of freedom s acquires the mass term (2.24).

Let m_c be the critical mass such that for $m < m_c$, m is inside the support of the spectrum of $\hat{D}$, while for $m > m_c$ it is outside of this region. Then it is clear that the anti-Hermitian Dirac operator (2.20) does not have a gap for $m < m_c$ (as a function of ϵ), and the symmetry (2.23) is spontaneously broken. For $m > m_c$, although the spectrum of the matrix in (2.20) acquires a gap, the pion condensate (2.22) remains nonzero. The reason is that the contribution of single eigenvalue of $\hat{D} + \mu\gamma_0$ close to the mass diverges as $\log \epsilon$ in the regularized partition function. This follows by writing the phase quenched bosonic partition function in terms of the eigenvalues of the Dirac operator $\hat{D} + \mu\gamma_0$ as

$$\begin{aligned} Z &= \int \frac{\rho(\lambda_1, \cdots \lambda_n)}{\prod_{k=1}^n |m^2 - \lambda_k^2|^2} \prod_{k=1}^n d\lambda_k d\lambda_k^* \\ &\sim \frac{n \log \epsilon}{4m^2} \int \frac{\rho(\lambda_1, \cdots \lambda_{n-1}, \pm m)}{\prod_{k=1}^{n-1} |m^2 - \lambda_k^2|^2} \prod_{k=1}^{n-1} d\lambda_k d\lambda_k^*. \end{aligned} \tag{2.27}$$

For the partition function D_2 the bosonic determinant cancels against the Vandermonde determinant, and we find that the chiral condensate is given by m/μ^2. For the partition function D_1 it is not possible to further simplify (2.27), but we expect that the chiral condensate remains continuous at $m = m_c$. Indeed, for the random matrix ensemble D_1, the partition function is still dominated by the logarithmic singularity due to a single eigenvalue close to the quark mass, and because of eigenvalue repulsion, there are no other eigenvalues close to m. In particular, the joint eigenvalue density $\rho(\lambda_1, \cdots \lambda_{n-1}, \pm m)$ vanishes linearly for any of the $\lambda_1, \cdots, \lambda_{n-1}$ close to $\pm m$. However, we no longer have the exact cancellation of the bosonic determinant against the Vandermonde determinant.

The chiral Lagrangian for the phase quenched partition function of D_1 was derived in [32]. The mean field limit of the corresponding partition function given by (in units where $\Sigma = 1$)

$$Z(m, \mu) = e^{-4n\mu^2 - nm^2/\mu^2} \tag{2.28}$$

results in the chiral condensate

$$\Sigma(m, \mu) = -\frac{1}{2n} \frac{d}{dm} \log Z(m, \mu) = \frac{m}{\mu^2}, \tag{2.29}$$

and the baryon density

$$n_B(\mu) - \frac{1}{2n}\frac{d}{d\mu}\log Z(m,\mu) = 4\mu - \frac{m^2}{\mu^3}. \tag{2.30}$$

In the Bose-condensed phase the mean field limit of the fermionic phase quenched partition function is given by

$$Z_{1+1^*/0}(m,\mu) = e^{4n\mu^2 + nm^2/\mu^2} \tag{2.31}$$

resulting in the same chiral condensate and baryon density as obtained for the bosonic partition function. In the normal phase ($m > 2\mu^2$) the mean-field limit of the phase quenched partition function is given by

$$Z_{1+1^*/0}(m,\mu) = e^{4nm}. \tag{2.32}$$

This phase is not present in the bosonic partition function.

What we learn from this example is that in order to obtain the $\log\epsilon$ dependence, the noncompact flavor symmetry of the bosonic partition function has to be broken spontaneously. If it would not be broken, the noncompact degree of freedom could not be regularized and the regularization that works for the fundamental theory, would fail for the effective theory.

One Flavor Partition Function at Imaginary Chemical Potential

The fermionic one-flavor partition function of the random matrix theory D_1 was analyzed in [19, 28] for imaginary chemical potential and in [20, 27] for real chemical potential. Some of the relevant results for the fermionic partition function will be reviewed in the next subsection, while the bulk of this section is devoted to the derivation of an analytical expression for the bosonic partition function, and a comparison of observables for the two partition functions.

The Fermionic Partition Function at Nonzero (Imaginary) Chemical Potential

The fermionic one-flavor partition function can be evaluated by writing the determinant as a Grassmann integral and performing a Hubbard-Stratonovitch

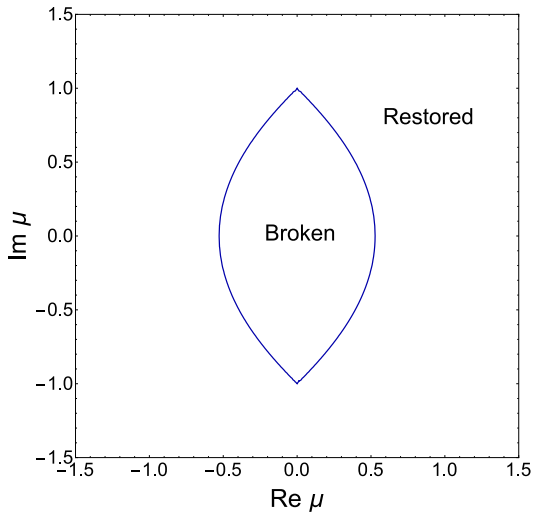

Figure 2.1: Phase diagram of the random matrix partition function in the complex μ plane in units where the chiral condensate is equal to 1.

transformation after averaging over the randomness, or alternatively by superbosonization [33, 34, 35, 36, 37]. The exact result for finite n in the sector of topological charge ν is given by [19, 27]

$$Z^{\nu}(m,\mu) = \int_0^{\infty} dss^{\nu+1} I_{\nu}(2mns\Sigma)(s^2-\mu^2)^n e^{-n\Sigma^2(s^2-\mu^2+m^2)}. \tag{2.33}$$

This result is valid both for arbitrary complex chemical potential, and in particular for real or purely imaginary chemical potential. It has two phases, a chirally broken phase and a phase with restored chiral symmetry. In units where $\Sigma = 1$, the critical curve is given by [19, 20, 27]

$$Re(1+\mu^2+\log\mu^2) = 0. \tag{2.34}$$

In Fig. 1 we show this curve in the complex μ-plane. The first order lines end at $\mu = \pm i$ where the transition is of second order.

An alternative expression for the fermionic partition function can be obtained by means of the superbosonization technique. The result can be ex-

pressed as (see Appendix .1)

$$Z^{\nu}(m,\mu)=\frac{(n+1)!e^{n\Sigma^2\mu^2}}{(n+1-\nu)!}\int_{-\pi}^{\pi}d\beta\int_{-1}^{1}xdxe^{-i\beta(2n+\nu)}x^{\nu}I_{\nu}(2me^{i\beta}x)J_0(2\mu e^{i\beta}\sqrt{1-x^2})e^{e^{2i\beta}x^2/n\Sigma^2}. \tag{2.35}$$

The integrals over x and β can be performed analytically resulting in a finite sum that can easily be evaluated numerically.

The Bosonic Partition Function

After averaging over the chiral random matrix ensemble, the one-flavor bosonic partition function for $\nu=0$ and imaginary chemical potential is given by [38]

$$Z(m,i\mu_i)=e^{\bar{n}\Sigma^2\mu_i^2}\int d\phi_1^*d\phi_1d\phi_2^*d\phi_2\exp\left[i\begin{pmatrix}\phi_1^*\\ \phi_2^*\end{pmatrix}\begin{pmatrix}im & \mu_i\\ \mu_i & im\end{pmatrix}\begin{pmatrix}\phi_1\\ \phi_2\end{pmatrix}-\frac{\phi_1^*\cdot\phi_1\phi_2^*\cdot\phi_2}{\bar{n}\Sigma^2}\right] \tag{2.36}$$

where the normalization factor $\exp\bar{n}\Sigma^2\mu^2$ is chosen to give a μ-independent partition function in the chiral limit below the critical point. We distinguish $\bar{n}$ appearing in the probability distribution and the number of components n of the vector ϕ_1. Instead of using a Hubbard-Stratonovitch transformation to linearize the quartic term, we use the bosonic part of the superbosonization transformation to evaluate the integral. The starting point is to insert the δ -function

$$\delta(\Phi-S) \tag{2.37}$$

in the partition function with S a positive definite Hermitian matrix and

$$\Phi=\begin{pmatrix}\phi_1^*\cdot\phi_1 & \phi_1^*\cdot\phi_2\\ \phi_2^*\cdot\phi_1 & \phi_2^*\cdot\phi_2\end{pmatrix}. \tag{2.38}$$

The partition function can then be rewritten as

$$Z(m,i\mu_i)=e^{\bar{n}\Sigma^2\mu_i^2}\int dSd\Phi\delta(S-\Phi)e^{-m\mathrm{Tr}\Phi+i\mu_i\mathrm{Tr}\sigma_1\Phi-S_{11}S_{22}/\bar{n}\Sigma^2}, \tag{2.39}$$

where the integral is over Hermitian matrices S. The δ-function can be expressed as [39]

$$\delta(S-\Phi)=\int dFe^{i\mathrm{Tr}F(S-\Phi-i\epsilon)} \tag{2.40}$$

resulting in the partition function

$$Z(m,i\mu_i) = e^{\bar{n}\Sigma^2\mu_i^2}\int dSddΦdFe^{iFS}e^{-m\mathrm{Tr}\Phi+i\mu_i\mathrm{Tr}\sigma_1\Phi-i\mathrm{Tr}F\Phi-S_{11}S_{22}/\bar{n}\Sigma^2}. \quad (2.41)$$

The integral over Φ evaluates to

$$Z(m,i\mu_i) = e^{n\mu_i^2}\int dSdFe^{i\mathrm{Tr}FS}\frac{1}{\det^n[F-im-\sigma_1\mu_i]}e^{-S_{11}S_{22}/n\Sigma^2}. \quad (2.42)$$

The integral over F is an Ingham-Siegel integral [40, 41, 39, 32] which is known analytically,

$$\int dF\det{}^{-n}(F-i\epsilon)e^{i\mathrm{Tr}SF} = \theta(S)\det{}^{n-2}Se^{-\epsilon\mathrm{Tr}S}, \quad (2.43)$$

where $\theta(S)$ indicates that S is positive definite. We thus find

$$Z(m,\mu_i) = e^{\bar{n}\Sigma^2\mu_i^2}\int_{S>0} dS\det{}^{n-2}Se^{-m(S_{11}+S_{22})+i\mu_i(s_{12}+s_{21})-S_{11}S_{22}/\bar{n}\Sigma^2}. \quad (2.44)$$

For $\nu \neq 0$, we choose ϕ_1 to be of length $n+\nu$ and ϕ_2 of length n. When comparing different topological sectors [42], we will put $\bar{n} = n+\nu/2$ and keep $\bar{n}$ fixed so that the number of eigenvalues of the Dirac matrix is the same for different ν. In Eq. (2.42) this results in an extra factor $1/(F_{11}-iz)^\nu$,

$$Z^\nu(m,i\mu_i) = e^{\bar{n}\Sigma^2\mu_i^2}\int dSe^{i\mathrm{Tr}FS}\frac{1}{\det^n[F-im-\sigma_1\mu_i](F_{11}-im)^\nu}e^{-S_{11}S_{22}/\bar{n}\Sigma^2} \quad (2.45)$$

and after shifting the diagonal matrix elements of F by im, we need to evaluate the integral

$$\int dF\det{}^{-n}(F-i\epsilon)(F_{11}-i\epsilon)^{-\nu}e^{i\mathrm{Tr}SF}. \quad (2.46)$$

To calculate this integral we rewrite the determinant to obtain

$$\int dF(F_{22}-i\epsilon-F_{21}F_{12}/(F_{11}-i\epsilon))^{-n}(F_{11}-i\epsilon)^{-\nu-n}e^{i\mathrm{Tr}SF}. \quad (2.47)$$

The integral over F_{22} can be performed by a contour integration resulting in

$$\frac{2\pi i^n}{(n-1)!}S_{22}^{n-1}\theta(S_{22})\int dFs(F_{11}-i\epsilon)^{-\nu-n}e^{i\mathrm{Tr}S_{22}\frac{F_{21}F_{12}}{F_{11}-i\epsilon}+iS_{11}F_{11}+iS_{12}F_{21}+iS_{21}F_{12}}. \quad (2.48)$$

The integral over F_{12} and $F_{21} = F_{12}^*$ is a Gaussian integral which can be easily evaluated. We find

$$\frac{2\pi i^n}{(n-1)!} S_{22}^{n-1} \frac{\pi i}{S_{22}} \theta(S_{22}) \int dF (F_{11} - i\epsilon)^{-\nu-n+1} e^{-i\mathrm{Tr} S_{12} S_{21} F_{11}/S_{22} + i S_{11} F_{11}}. \quad (2.49)$$

Also the integral over F_{11} can be performed by a contour integration so that we finally obtain for the integral (2.46)

$$\begin{aligned} & -\frac{2\pi(-i)^{\nu+1}}{(n-1)!} S_{22}^{n-2} \pi \frac{2\pi}{(n+\nu-2)!} (S_{11} - S_{12}S_{21}/S_{22})^{n+\nu-2} \theta(S_{22}) \theta(S_{11} - S_{12}S_{21}/S_{22}) \\ = & -\frac{4(\pi(-i))^{nu+1}}{(n-1)!(n+\nu-2)!} \det{}^{n-2} S [\det S/S_{22}]^{\nu} \theta(S), \end{aligned} \quad (2.50)$$

where $\theta(S)$ denotes that S is positive definite.

The integration over positive definite matrices S can be performed by using the parameterization

$$S = e^v \begin{pmatrix} e^u \cosh s & i e^{i\phi} \sinh s \\ -i e^{-i\phi} \sinh s & e^{-u} \cosh s \end{pmatrix}. \quad (2.51)$$

The integration measure is given by

$$dS = 4 e^{4v} \cosh s \sinh s. \quad (2.52)$$

This results in the partition function

$$\begin{aligned} Z^{\nu}(m, i\mu_i) &= \frac{e^{\bar{n}\Sigma^2 \mu_i^2}}{(n-1)!(n+\nu-2)!} \int dv du ds d\phi \cosh s \sinh s e^{2nv} \left[\frac{e^{u+v}}{\cosh s} \right]^{\nu} \\ & \times e^{-2me^v \cosh s \cosh u - 2i\mu_i e^v \sinh s \sin\phi - e^{2v} \cosh^2 s/\bar{n}\Sigma^2}. \end{aligned} \quad (2.53)$$

The integrals over u and ϕ can be expressed in terms of Bessel functions

$$\begin{aligned} Z^{\nu}(m, i\mu_i) &= \frac{e^{\bar{n}\Sigma^2 \mu_i^2}}{(n-1)!(n+\nu-2)!} \int dv ds \frac{\cosh s \sinh s}{\cosh^{\nu} s} e^{(2n+\nu)v} K_{\nu}(2me^v \cosh s) J_0(2\mu_i e^v \sinh s) \\ & \times e^{-e^{2v} \cosh^2 s/\bar{n}\Sigma^2}. \end{aligned} \quad (2.54)$$

After shifting the v-integration by $\log\cosh s$ and choosing $x = \exp v$ as a new integration variable we obtain

$$Z^{\nu}(m, i\mu_i) = \frac{e^{\bar{n}\Sigma^2 \mu_i^2}}{(n-1)!(n+\nu-2)!} \int dx ds \frac{\cosh s \sinh s}{\cosh^{2n+2\nu} s} x^{2n+\nu-1} K_{\nu}(2mx) J_0(2\mu_i x \tanh s) e^{-x^2/\bar{n}\Sigma^2}. \quad (2.55)$$

The integral over y can be evaluated as a Bessel function resulting in the expression

$$Z^\nu(m,i\mu_i) = \frac{1}{2}e^{\bar{n}\Sigma^2\mu_i^2}\frac{\mu^{1-n-\nu}\bar{n}^{(n+1)/2}}{(n-1)!}\int_0^\infty dx x^n J_{n+\nu-1}(2\mu_i x\sqrt{\bar{n}})K_\nu(2mx\sqrt{\bar{n}})e^{-x^2/\Sigma^2} \quad (2.56)$$

where we have also rescaled the integration variable by $\sqrt{\bar{n}}$. This form can easily be evaluated numerically also for large values of n. However, because of the oscillatory nature of the integrand, it is not amenable to mean field estimates.

Next we derive an expression for the partition function in terms of a positive definite integrand. This result can be obtained if we insert the following representation for the K_ν function

$$K_\nu(x) = \frac{1}{2}\frac{x^\nu}{2^\nu}\int_0^\infty \frac{ds}{s^{\nu+1}}e^{-s-x^2/4s} \quad (2.57)$$

resulting in

$$\begin{aligned} Z^\nu(m,i\mu_i) &= \frac{1}{4}e^{\bar{n}\Sigma^2\mu_i^2}\frac{\mu_i^{1-n-\nu}\bar{n}^{(n+1)/2}}{(n-1)!}\int_0^\infty ds\frac{(xm\sqrt{\bar{n}})^\nu}{s^{\nu+1}}\int_0^\infty dx x^n J_{n+\nu-1}(2\mu_i x\sqrt{\bar{n}}) \\ &\quad \times e^{-s-m^2x^2\bar{n}/s-x^2/\Sigma^2}. \end{aligned} \quad (2.58)$$

The integral over x is known analytically [43]

$$\int_0^\infty dx x^{n+\nu}J_{n+\nu-1}(\beta x)e^{-\alpha x^2} = \frac{\beta^{n+\nu-1}}{(2\alpha)^{n+\nu}}e^{-\beta^2/4\alpha}. \quad (2.59)$$

After changing the integration variable be $s \to s\bar{n}m^2$ we find

$$\begin{aligned} Z^\nu(m,i\mu_i) &= \frac{\bar{n}^n e^{\bar{n}\Sigma^2\mu_i^2}}{8(n-1)!}m^{-\nu}\int_0^\infty \frac{ds}{s^{\nu+1}}e^{-s\bar{n}m^2}\frac{1}{(1/s+1/\Sigma^2)^{n+\nu}}e^{-\bar{n}\mu_i^2/(1/s+1/\Sigma^2)} \\ &= \frac{\bar{n}e^{n\Sigma^2\mu_i^2}}{8}m^{-\nu}\int_0^\infty s^\nu\frac{ds}{s}e^{-\bar{n}m^2/s}\frac{1}{(s+1/\Sigma^2)^{n+\nu}}e^{-\bar{n}\mu_i^2/(s+1/\Sigma^2)} \end{aligned} \quad (2.60)$$

where we also changed $s \to 1/s$ in the last line.

Limiting Cases

In this subsection, we derive three limiting cases of (2.60), the microscopic limit, the $\mu_i \to 0$ limit, the chiral limit and the large n-limit of the bosonic partition function.

In the microscopic limit for the mass, $m\bar{n}=$ fixed for $\bar{n}\to\infty$ and $n\to\infty$ with $n\to\bar{n}$ at fixed imaginary chemical potential the partition function simplifies to

$$\begin{aligned} Z^{\nu}(m,i\mu_i) &= \frac{e^{n\Sigma^2\mu_i^2}}{8(n-1)!}(\bar{n}\Sigma^2)^{n+\nu}m^{\nu}\int_0^{\infty}\frac{ds}{s^{\nu+1}}e^{-s}e^{-\bar{n}^2m^2\Sigma^2/s-\mu_i^2\bar{n}\Sigma^2(1-\bar{n}\Sigma^2m^2/s)} \\ &= \frac{e^{n\Sigma^2\mu_i^2}}{8(n-1)!}(\bar{n}\Sigma^2)^{n+\nu}m^{\nu}2(\bar{n}m\Sigma\sqrt{1-\mu_i^2\Sigma^2})^{-\nu}e^{-\mu_i^2\bar{n}\Sigma^2}K_{\nu}(2\bar{n}m\Sigma\sqrt{1-\mu_i^2\Sigma^2}) \\ &= \frac{e^{n\Sigma^2\mu_i^2}}{8(n-1)!}\frac{\bar{n}^n\Sigma^{2n+\nu}}{(1-\mu_i^2\Sigma^2)^{\nu/2}}e^{-\mu^2n\Sigma^2}K_{\nu}(2\bar{n}m\Sigma\sqrt{1-\mu_i^2\Sigma^2}), \end{aligned} \tag{2.61}$$

which is consistent with the result obtained in [38].

For $\mu_i=0$ the partition function (2.54) can be written as

$$Z^{\nu}(m,i\mu_i=0)=\int_0^{\infty}dxdsx^{2n+\nu-1}\cosh s\sinh sK_0(2mx\cosh s)e^{-x^2\cosh^2 s/\bar{n}\Sigma^2} \tag{2.62}$$

After rescaling x by $\cosh s$, the s integral gives an overall constant so that the partition function simplifies to

$$Z^{\nu}(m,i\mu_i=0)=\int_0^{\infty}dxx^{2n+\nu-1}K_{\nu}(2mx)e^{-x^2/\bar{n}\Sigma^2}. \tag{2.63}$$

This is indeed the Cauchy transform of a Laguerre polynomial [44], which is the correct finite n result for the chiral random matrix partition function.

For $m\to 0$ we have that

$$\begin{aligned} K_{\nu}(2mx\sqrt{\bar{n}}) &\sim \frac{1}{2}(mx\sqrt{n}b)^{-\nu} \qquad \text{for} \quad \nu\neq 0, \\ K_0(2mx\sqrt{\bar{n}}) &\sim -\log m \qquad \text{for} \quad \nu=0. \end{aligned} \tag{2.64}$$

For $\nu=0$, the chiral limit can be worked out analytically

$$Z^{\nu=0}(m\to 0,i\mu_i)=-\frac{1}{2}e^{n\Sigma^2\mu_i^2}\frac{\mu^{1-n}\bar{n}^{(n+1)/2}}{(n-1)!}\log m\int_0^{\infty}dxx^nJ_{n-1}(2\mu_ix\sqrt{\bar{n}})e^{-x^2/\Sigma^2} \tag{2.65}$$

This integral is known analytically [43] resulting in

$$Z^{\nu=0}(m\to 0,i\mu_i)=-\frac{\bar{n}^n2^{2n-2}}{(n-1)!\Sigma^{2n}}\log m. \tag{2.66}$$

In the chiral limit, the partition function is dominated by the logarithmic singularity which does not depend on the imaginary chemical potential. Contrary to the fermionic partition function, it is always in a phase with zero "baryon density".

For large n the partition function can be evaluated by a saddle point approximation. The saddle point equation for the expression in the second line of (2.60) reads

$$-\frac{m^2}{s^2}+\frac{1}{1+s}-\frac{\mu^2}{(1+s)^2}=0. \tag{2.67}$$

To leading order in m the solution is given by

$$\bar{s}=\begin{cases}\dfrac{m}{\sqrt{1-\mu_i^2}}, & \mu_i<1,\\ \mu_i^2-1, & \mu_i>1,\end{cases} \tag{2.68}$$

resulting in the free energy ($\bar{F}=(\log Z)/n$)

$$\bar{F}=\begin{cases}2m\sqrt{1-\mu_i^2}, & \mu_i<1,\\ 1-\mu_i^2+\log\mu_i^2+\dfrac{m^2}{\mu_i^2-1}, & \mu_i>1.\end{cases} \tag{2.69}$$

The chiral condensate is given by

$$-\frac{1}{2n}\frac{d\log Z}{dm}=\begin{cases}\sqrt{1-\mu_i^2}, & \mu_i<1,\\ \dfrac{m}{\mu_i^2-1}, & \mu_i>1,\end{cases} \tag{2.70}$$

and the baryon number density by

$$-\frac{1}{2n}\frac{d\log Z}{d\mu_i}=\begin{cases}0, & \mu_i<1,\\ -\dfrac{1}{\mu_i}+\mu_i, & \mu_i>1.\end{cases} \tag{2.71}$$

The baryon number susceptibility at imaginary chemical potential is defined by

$$\chi_B=-\frac{1}{2n}\frac{d^2\log Z}{d\mu_i^2}=\begin{cases}0, & \mu_i<1,\\ \dfrac{1}{\mu_i^2}+1, & \mu_i>1.\end{cases} \tag{2.72}$$

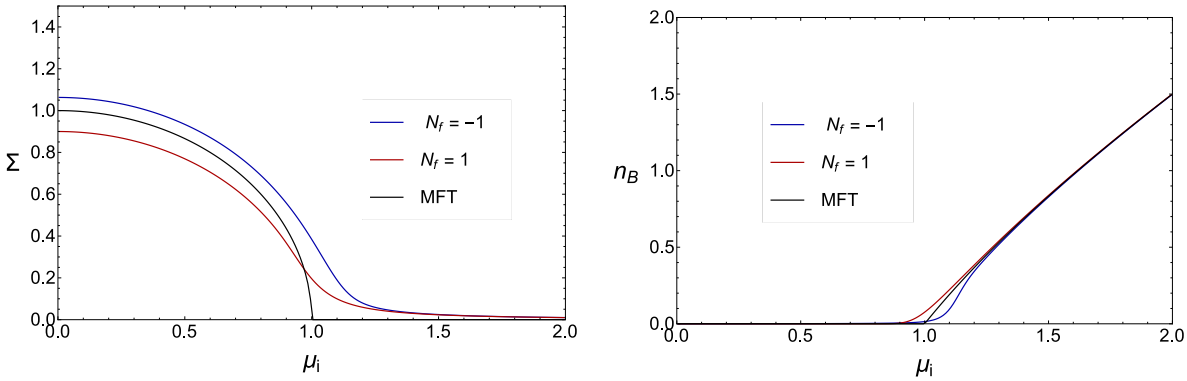

Figure 2.2: The chiral condensate (left) and the baryon density (right) as a function of the imaginary chemical potential. We show the result for the one-flavor bosonic partition function (blue), the one flavor fermionic partition function (red) and the mean field result (black).

In Fig. 2 we show the chiral condensate (left) and the baryon number (right) as a function of the imaginary chemical potential. The results are for $n = 100$, $m = 3/100$ in case of the chiral condensate and $n = 100$, $m = 3/10000$ in case of the baryon number all in units with $\Sigma = 1$ in the partition function. Both the results for the fermionic partition function (blue) and the bosonic partition function (red) are close to the mean field result (black) which has been obtained for $n \to \infty$ in the chiral limit.

The baryon number susceptibility defined in Eq. (2.72) is shown in Fig. 2.3 as a function of the imaginary chemical potential for $n = 100$ and $m = 3/10000$. Again the bosonic and fermionic susceptibility are close to the mean field result, but the deviation near the critical point is much larger than in case of the baryon number density (see Fig. 2.2). The convergence of the susceptibility to the thermodynamic limit is non-uniform in m.

Bosonic Partition Function for Real Chemical Potential

In this section we consider the massless bosonic chiral random matrix partition function for real chemical potential. In this case, the partition function can be expressed in terms of the joint probability distribution of the Ginibre ensemble, which allows us to obtain exact analytical results. We start with a heuristic derivation of the mean field results for the chemical potential dependence of the partition function, and in the second subsection we reduce this partition function to a two-dimensional integral. Everywhere in this section we work in units where $\Sigma = 1$ and in the sector of zero topological charge.

Heuristic Derivation of the Mean Field Result

In units where $\Sigma = 1$ and $\nu = 0$, the massless bosonic partition function can be expressed as

$$Z_{0/1}(\mu) = e^{-n\mu^2} \left\langle \det \frac{1}{D(\mu)} \right\rangle \tag{2.73}$$

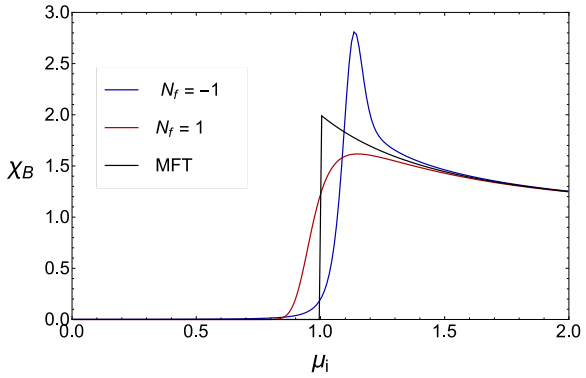

Figure 2.3: The baryon number susceptibility as a function of the imaginary chemical potential, μ_i for $n = 100$ and $m = 3/10000$. Results are shown for the fermionic partition function (red), the bosonic partition function (blue), and the mean field limit of these partition functions.

with $D(\mu)$ given by

$$D(\mu) = \begin{pmatrix} 0 & id + \mu \\ -id^\dagger + \mu & 0 \end{pmatrix}, \tag{2.74}$$

and the normalization factor $\exp(-n\mu^2)$ has been included to give the correct μ dependence for small μ. If μ is inside the domain of eigenvalues, the partition function has to be regularized. This can be done in the same way as for the phase quenched bosonic partition function,

$$Z_{0/1}(\mu) = \left\langle \frac{\det{}^* D(\mu)}{\det(D(\mu)D(\mu)^\dagger + \epsilon^2)} \right\rangle, \tag{2.75}$$

where the limit $\epsilon \to 0$ has to be taken at the end of the calculation. Contrary to the partition function with a pair of conjugate bosonic quarks at nonzero chemical potential, this partition function, because of the extra fermionic determinant, is finite for $\epsilon \to 0$. At the mean field level we expect that this partition function is given by the ratio of two fermionic partition functions,

$$Z_{0/1}^{\rm MFT}(\mu) = \frac{Z_{N_f=1}(\mu)}{Z_{N_f=1+1^*}(\mu)}, \tag{2.76}$$

where $Z_{N_f=1+1^*}(\mu)$ is the phase quenched partition function, or equivalently, the product of the same one flavor partition function and the bosonic phase quenched partition function (see Eq. (2.28)). The baryon density is thus given by

$$\begin{aligned} n_B &= -\frac{1}{2n}\frac{d}{d\mu}\log Z_{0/1}(\mu) \\ &\quad \frac{1}{2n}\frac{d}{d\mu}\log Z_{1+1^*}(\mu) - \frac{d}{d\mu}\log Z_1(\mu). \end{aligned} \tag{2.77}$$

The μ dependence of both partition functions is well known [32, 20] and is given by

$$\begin{aligned} \frac{1}{2n}\frac{d}{d\mu}\log Z_{1+1^*}(\mu) &= \theta(1-\mu)4\mu + \theta(\mu-1)(2\mu + \frac{2}{\mu}) \\ \frac{1}{2n}\frac{d}{d\mu}\log Z_1(\mu) &= \theta(\mu-\mu_c)(\mu + \frac{1}{\mu}). \end{aligned} \tag{2.78}$$

where $\mu_c = 0.527$. In Fig. 2.4, the black curve represents the mean field re-

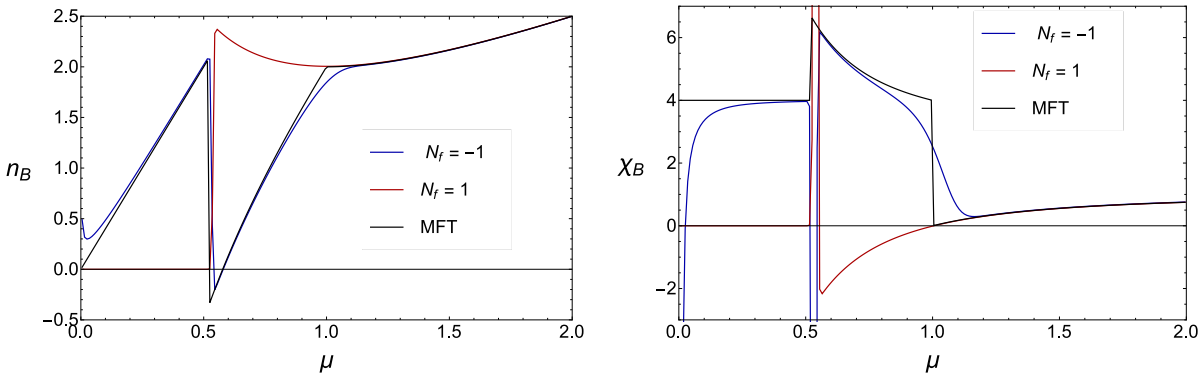

Figure 2.4: The baryon number density (left) and baryon number susceptibility (right) as a function of the chemical potential, μ for $n = 100$ and $m = 0$. Results are give for the fermionic partition function (red), the bosonic partition function (blue), and the mean field limit of the bosonic partition function.

sult for the baryon density. In the same figure we have plotted the analytical for finite n (blue curve), which will be derived in the next subsection, and the finite n result for the baryon density of the fermionic partition function (red curve). When μ is outside the domain of eigenvalues, the fermionic and bosonic results become equal in the thermodynamic limit.

The Finite n Massless Bosonic Partition Function at Nonzero Chemical Potential

In this section we evaluate the massless bosonic random matrix partition function as a function of the real baryon chemical potential. This partition function can be written as (the equality only holds for even n) [45]

$$\left\langle \frac{1}{\det(d+\mu)\det(-d^\dagger+\mu)} \right\rangle = \left\langle \frac{1}{\det(d+\mu)\det(d^\dagger-\mu)} \right\rangle, \tag{2.79}$$

where the matrix elements of the complex $n \times n$ matrix d are distributed according to

$$p(d) = e^{-\bar{n}\mathrm{Tr}d^\dagger d}. \tag{2.80}$$

The quenched matrix ensemble with this distribution, known as the Ginibre ensemble, has the joint eigenvalue density

$$P(z_k) = \Delta(\lambda_k)\Delta(\lambda_k^*)\prod_k e^{-\bar{n}\lambda_k^*\lambda_k}, \tag{2.81}$$

where $\Delta(\lambda_k)$ is the Vandermonde determinant. The corresponding monic orthogonal polynomials and their normalization are equal to

$$p_n(z) = z^n, \quad \text{with} \quad h_n = \int dz dz^* p_n^*(z) p_m(z) = \delta_{nm}\frac{n!}{\bar{n}^{n+1}}. \tag{2.82}$$

The partition function of the Ginibre ensemble, defined as the integral over the probability distribution, can be obtained by expressing the Vandermonde determinants in terms of these orthogonal polynomials. Performing the integrals by means of orthogonality relations we obtain

$$Z_n^{\mathrm{G}} = n!\prod_{k=0}^{n-1} h_k. \tag{2.83}$$

In terms of the eigenvalues of d, the bosonic partition function can be written as

$$Z_{0/1}(\mu) = \frac{e^{-n\mu^2}}{Z_n^{\mathrm{G}}}\int\prod_k d\lambda_k d\lambda_k^* \frac{e^{-\bar{n}\lambda_k^*\lambda_k}}{(\lambda_k+\mu)(\lambda_k^*+\mu)}|\Delta(\lambda_k)|^2. \tag{2.84}$$

To evaluate this partition function we need identity

$$u^{n-1}\frac{\Delta_k(\lambda_i)}{\prod_{k=1}^n(\lambda_k-u)} = \sum_{k=1}^n(-1)^{k+n}\frac{\lambda_k^{n-1}}{(\lambda_k-u)}\Delta_k'(\lambda_i), \tag{2.85}$$

where

$$\Delta_p'(z_k) = \prod_{k<l,kl\neq p}(z_k - z_l). \tag{2.86}$$

This identity can be proved by including the factors $1/(\lambda_k - u)$ in the determinant and expanding it with respect to the last row. Applying this identity to the bosonic determinant results in

$$(-1)^{n-1}\mu^{2n-2}\frac{1}{\prod_{k=1}^n(\lambda_k-u)(\lambda_k^*+u)} = \sum_{k,l=1}^n(-1)^{k+l}\frac{\lambda_k^{n-1}\lambda_l^{*n-1}}{(\lambda_k-\mu)(\lambda_l^*+\mu)}\frac{\Delta_k'(\lambda_i)\Delta_l'(\lambda_j^*)}{\Delta_k(\lambda_i)\Delta_l(\lambda_j^*)} \tag{2.87}$$

We can distinguish two types of terms, those with $k = l$, and those with $k \neq l$. All terms of each type give the same contribution to the bosonic partition function. We thus find

$$\begin{aligned} Z_{0/1}(\mu) &= e^{-n\mu^2}\frac{n(-1)^{n-1}}{Z_n^{\mathrm{G}}\mu^{2n-2}}\int\prod_k d\lambda_k d\lambda_k^* e^{-\bar{n}\lambda_k\lambda_k^*}\frac{(\lambda_1\lambda_1^*)^{n-1}}{(\lambda_1-\mu)(\lambda_1^*+\mu)}\Delta_1'(\lambda_i)\Delta_1'(\lambda_j^*) \\ &\quad -e^{-n\mu^2}\frac{n(n-1)(-1)^{n-1}}{Z_n^{\mathrm{G}}u^{2n-2}}\int d\lambda_k d\lambda_k^* e^{-\bar{n}\lambda_k\lambda_k^*}\frac{(\lambda_1\lambda_2^*)^{n-1}}{(\lambda_1-u)(\lambda_2^*+u)}\Delta_1'(\lambda_i)\Delta_2'(\lambda_j^*), \end{aligned} \tag{2.88}$$

where the partition function is normalized with respect to the Ginibre partition function (2.83). This expression can be rewritten as

$$\begin{aligned} Z_{0/1}(\mu) &= e^{-n\mu^2}\frac{n(-1)^{n-1}}{Z_n^{\mathrm{G}}\mu^{2n-2}}\int d\lambda_1 d\lambda_1^* e^{-\bar{n}\lambda_1\lambda_1^*}\frac{(\lambda_1\lambda_1^*)^{n-1}}{(\lambda_1-u)(\lambda_1^*+u)}Z_{n-1}^{\mathrm{G}} \\ &\quad +e^{-n\mu^2}\frac{n(n-1)(-1)^{n}}{Z_n^{\mathrm{G}}\mu^{2n-2}}\int d\lambda_1 d\lambda_1^* d\lambda_2 d\lambda_2^* e^{-\bar{n}(\lambda_1\lambda_1^*-\lambda_2\lambda_2^*)}\frac{(\lambda_1\lambda_2^*)^{n-1}}{(\lambda_1-\mu)(\lambda_2^*+\mu)} \\ &\quad \times\langle\pi_{n-2}(\lambda_2)\pi_{n-2}(\lambda_1^*)\rangle Z_{n-2}^{\mathrm{G}}. \end{aligned} \tag{2.89}$$

where the average of two characteristic polynomials is defined by

$$\langle\pi_{n-2}(u)\pi_{n-2}(v^*)\rangle = \frac{1}{Z_{n-2}^G}\int\prod_{k=1}^{n-2}\frac{d\lambda_k d\lambda_l^*}{\pi}\prod_{k=1}^{n-2}(u-\lambda_k)(v^*-\lambda_k^*)e^{-\bar{n}\lambda_k\lambda_k^*}|\Delta(\lambda_1,\cdots,\lambda_{n-2})|^2. \tag{2.90}$$

This average can be expressed in terms of the two-point kernel of the Ginibre ensemble [46]

$$\langle\pi_{n-2}(u)\pi_{n-2}(v^*)\rangle = h_{n-2}\sum_{k=0}^{n-2}\frac{(uv^*)^k}{h_k}. \tag{2.91}$$

This results in the partition function

$$\begin{aligned} Z_{0/1}(\mu) &= \frac{(-1)^{n-1}e^{-n\mu^2}}{h_n\mu^{2n-2}}\int d\lambda_1 d\lambda_1^* e^{-\bar{n}\lambda_1\lambda_1^*}\frac{(\lambda_1\lambda_1^*)^{n-1}}{(\lambda_1-\mu)(\lambda_1^*+\mu)} \\ &\quad -\frac{(-1)^{n-1}e^{-n\mu^2}}{h_{n-1}\mu^{2n-2}}\int d\lambda_1 d\lambda_1^* d\lambda_2 d\lambda_2^* e^{-\bar{n}\lambda_1\lambda_1^*-\bar{n}\lambda_2\lambda_2^*}\frac{(\lambda_1\lambda_2^*)^{n-1}}{(\lambda_1-\mu)(\lambda_2^*+\mu)}\sum_{k=0}^{n-2}\frac{(\lambda_2\lambda_1^*)^k}{h_k}. \end{aligned} \tag{2.92}$$

This derivation is also valid for complex values of μ. The first integral in Eq. (2.93) is logarithmically divergent for purely imaginary μ and has to be regularized which can be done by including a mass term. The resulting logarithmically divergent part of the partition function is μ independent, which agrees with the result for the chiral limit of the bosonic partition function at imaginary chemical potential which diverges as $\log m$ for $\nu = 0$ (see Eq. (2.66)).

The integrals can be calculated using polar coordinates and converting the angular integral to a contour integral,

$$\begin{aligned} Z_{0/1}(\mu) &= \frac{(-1)^{n-1}e^{-n\mu^2}}{h_{n-1}\mu^{2n-2}\pi}\int d\lambda d\phi e^{-\bar{n}\lambda^2}\frac{\lambda^{2n-2}}{(\lambda e^{i\phi}-\mu)(\lambda e^{-i\phi}+\mu)} \\ &\quad -\frac{(-1)^{n-1}e^{-n\mu^2}}{h_{n-1}\mu^{2n-2}\pi^2}\sum_{k=0}^{n-2}\frac{(-1)^{k+n}}{h_k}\left[\int d\lambda d\phi e^{-\bar{n}\lambda^2}\frac{\lambda^{n+k}e^{i\phi(n-1-k)}}{(\lambda e^{i\phi}-\mu)}\right]^2 \\ &= \frac{2(-1)^{n-1}e^{-n\mu^2}}{h_{n-1}\mu^{2n-2}}\left[-\int_0^{|\mu|}d\lambda e^{-\bar{n}\lambda^2}\frac{\lambda^{2n-1}}{\mu^2+\lambda^2}+\int_{|\mu|}^{\infty}d\lambda e^{-\bar{n}\lambda^2}\frac{\lambda^{2n-1}}{\mu^2+\lambda^2}\right] \\ &\quad -\frac{4(-1)^{n-1}e^{-n\mu^2}}{h_{n-1}\mu^{2n-2}}\sum_{k=0}^{n-2}\frac{(-1)^{k+n}}{h_k}\left[\int_{|\mu|}^{\infty}d\lambda e^{-\bar{n}\lambda^2}\lambda^{2k+1}\mu^{n-2-k}\right]^2 \end{aligned} \tag{2.93}$$

Note that this partition function is not an analytic function of μ which was also the case for the bosonic partition function of model (2.2) [24]. Because of large cancellations this form of the partition function is not amenable to a mean field analysis. In Appendix .2 we derive a form where these cancellations have been taken care of analytically. It is given by (for $\mu > 0$)

$$\begin{aligned} Z_{0/1}(u) &= \frac{e^{-n\mu^2}}{h_{n-1}}\left[\int_0^{\infty}dx\frac{e^{-\bar{n}\mu^2(2x+1)}}{x+1}-\int_0^1 dx\frac{e^{-\bar{n}\mu^2(2x+1)}}{x+1}\left(\frac{\Gamma(n-1,-\bar{n}\mu^2x)}{\Gamma(n-1)}\right)\right. \\ &\quad \left.+\int_0^1 dx\frac{e^{-\bar{n}\mu^2(x+y)}}{x+1}(-x)^n\left(1-\frac{\Gamma(n-1,\bar{n}\mu^2}{\Gamma(n-1)}\right)\right]. \end{aligned} \tag{2.94}$$

We have checked that this result agrees with a direct evaluation of the partition function for $n = 2$ and $n = 3$. See Appendix .3 for the brute force expressions for $n = 2$ and $n = 3$.

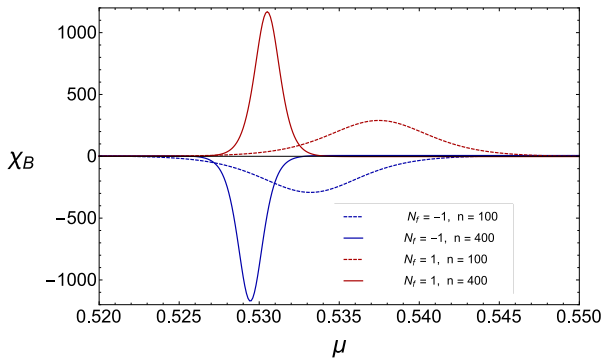

Figure 2.5: The baryon number susceptibility near the critical point for $\bar{n} = n = 100$ (dashed) and $\bar{n} = n = 400$ (solid) both for the bosonic 9 (blue) and the fermionic partition function. Up to a minus sign, which could have been absorbed by the definition of the bosonic baryon number susceptibility, the result are similar.

Large n Limit of the Bosonic Partition Function

In the large n limit, where we take $\bar{n} = n$, the first term of Eq. (2.94) is given by

$$\frac{1}{h_{n-1}} \frac{1}{4nu^2} e^{-4n\mu^2} \sim \frac{e^{-n(4\mu^2-1)}}{4\mu^2\sqrt{2\pi n}}, \tag{2.95}$$

and the second term by

$$\begin{cases} \dfrac{1}{h_{n-1}\Gamma(n-1)} \dfrac{e^{-3n\mu^2}(-n\mu^2)^{n-3}}{2n\mu^2(1+1/\mu^2)(1/\mu^2-1)} \sim \dfrac{(-1)^n e^{-n(3\mu^2-\log\mu^2-2)}}{4\pi n^2\mu^2(1+\mu^2)(1-\mu^2)}, & \text{for} \quad \mu < 1 \\ \dfrac{1}{h_{n-1}} \dfrac{e^{-2n\mu^2}}{2nu^2(1+1/\mu^2)} \sim \dfrac{e^{-n(1+2\mu^2)}}{\sqrt{2\pi n}2n(1+\mu^2)} & \text{for} \quad \mu > 1 \end{cases} \tag{2.96}$$

The last term factorizes into the product of two integrals. For large n it can be approximated by

$$\begin{cases} \dfrac{\Gamma(n-1)}{h_{n-1}} \dfrac{(-1)^n e^{-n\mu^2}}{(n\mu^2)^n(1+1/\mu^2)} \sim \dfrac{(-1)^n \mu^2 e^{-n\log\mu^2} - n\mu^2}{1+\mu^2} & \text{for} \quad u > 1 \\ \dfrac{1}{h_{n-1}\Gamma(n-1)} \dfrac{(-1)^n e^{-3n\mu^2}(-n\mu^2)^{n-3}}{2(1-1/\mu^2)^2} \sim \dfrac{(-1)^n e^{-n(3\mu^2-\log\mu^2-2)}}{4\pi n\mu^2(1-\mu^2)^2} & \text{for} \quad \mu < 1 \end{cases} \tag{2.97}$$

This result agrees with the heuristic estimate of section 2.4.1.

In Fig. 2.4 we show the baryon number density and the baryon number susceptibility as a function of the chemical potential for $n = 100$ and $m = 0$. Results are given for fermionic partition function (red), the bosonic partition function (blue) and the mean field limit of the bosonic partition function. The susceptibility diverges at $\mu = \mu_c = 0.523$ as $\sim n$ in the thermodynamic limit, see Fig. 2.5. This reflects that the slope

$$\left.\frac{dn_B}{d\mu}\right|_{\mu=\mu_c} \sim n. \tag{2.98}$$

Note that we could have defined the baryon number susceptibility with the opposite sign.

Conclusions

We have studied bosonic random matrix partition functions (averages of inverse determinants) and compared them to fermionic random matrix partition functions (averages of a determinants) for the same value of the external parameters. In particular, we consider the dependence of the chiral condensate, the baryon density and the baryon number susceptibility on the (imaginary) chemical potential and the quark mass. For imaginary chemical potential, μ_i, and nonzero quark mass, these observables approach the same limit for $n \to \infty$, where the μ_i-dependence is given by the mean field result of the effective partition function. In the chiral limit, the bosonic partition function diverges as $\log m$ whereas the fermionic partition function remains finite.

We have seen two cases where the bosonic partition is always in the broken phase while the fermionic partition function undergoes a phase transition to the restored phase. The first case is the phase quenched partition function, where the pion condensate of the bosonic partition function is nonvanishing for all μ while it is becomes zero for $\mu < m_\pi/2$ in case of the fermionic partition function. The second case is the chiral limit of the one flavor partition function as a function of imaginary chemical potential. In this case the fermionic partition function has as phase transition to the restored phase at $\mu_i = 1$ while the bosonic partition diverges as $\log m$ and is in the same phase for all values of μ_i. As a side remark we note that this gives us two more examples where the replica trick is doomed to fail [47].

The spontaneous breaking of noncompact symmetries has also been studied for hyperbolic spin models in one and two dimensions. The conclusion of this work is that a noncompact symmetry is always broken spontaneously, even in one and two dimensions, if the partition function diverges for vanishing symmetry breaking term. Our work supports this conclusion for a different class of models.

Appendices

Derivation of the Fermionic Partition Function Using Superbosonization

Superbosonization was developed as an alternative to the Hubbard-Stratonovitch transformation [33, 34, 35, 36, 37] in order to be able to deal with non-Gaussian probability distributions. Below we only use the fermion-fermion part of the superbosonization transformation. The fermionic partition function is given by

$$Z^{\nu}(z,\mu) = e^{n\Sigma^2\mu^2}\int d\chi_1^* d\chi_1 d\chi_2^* d\chi_2 \exp\left[\begin{pmatrix}\chi_1^* \\ \chi_2^*\end{pmatrix}\begin{pmatrix} z & \mu \\ \mu & z\end{pmatrix}\begin{pmatrix}\chi_1 \\ \chi_2\end{pmatrix} + \frac{1}{n\Sigma^2}\chi_1^*\cdot\chi_1\chi_2^*\cdot\chi_2\right], \quad (99)$$

where the vector χ_1 is of length $n+\nu$ and the length of the vector χ_2 is of length n. To linearize the four-fermion term, we use the fermion-fermion part of the superbosonization transformation by inserting the δ-function

$$\delta(G-Y) = \int dF e^{i\mathrm{Tr}F(G-Y)} \quad (100)$$

with

$$G = \begin{pmatrix}\chi_1^*\chi_1 & \chi_1^*\chi_2 \\ \chi_2^*\chi_1 & \chi_2^*\chi_2\end{pmatrix}, \quad (101)$$

and $Y^{\dagger} = Y$. After integration of the χ-variables, this results in the partition function,

$$Z^{\nu}(z,\mu) = e^{n\Sigma^2\mu^2}\int dY dF F_{11}^{\nu}\det{}^n F \exp\left[z(Y_{11}+Y_{22}) + \mu(Y_{12}+Y_{21}) + \frac{Y_{11}Y_{22}}{n\Sigma^2} - i\mathrm{Tr}FY\right]. \quad (102)$$

The integral over F can be evaluated by means of an Itzykson-Zuber integral as

$$[i\partial_{Y_{11}}]^{\nu}\int dF \det{}^n F e^{-i\mathrm{Tr}FY} \quad (103)$$

with

$$\begin{aligned}\int dF \det{}^n F e^{-i\mathrm{Tr}FY} &= \int\prod df_k \Delta^2(\{f_k\})\prod f_k^n \frac{\det e^{if_k y_l}}{\Delta(\{f_k\})\Delta(\{y_l\})} \\ &= \frac{\det\delta^{(n+k-1)}(y_l)}{\Delta(\{y_l\})} \end{aligned} \quad (104)$$

where $\delta^{(p)}(y)$ is the p-th derivative of a δ-function. Acting on a regular test function $F(Y)$, it has the property [36]

$$\begin{aligned}
\int DY \frac{\det \delta^{(n+k-1)}(y_l)}{\Delta(\{y_l\})} F(Y) &= \int dY \sum_\pi (-1)^{\sigma_\pi} \left. \frac{\prod_{k=1}^p \partial_{y_{\pi(k)}}^{n+k-1} F(Y)}{\Delta(\{y_l\})} \right|_{y_k=0} \\
&= \int dU \oint \prod_k dy_k 2\pi i \Delta^2(\{y_l\}) \sum_\pi (-1)^{\sigma_\pi} \frac{F(Y)}{\Delta(\{y_l\}) \prod_{k=1}^p y_{\pi(k)}^{n+k}} \\
&= \int dU \oint \prod_k \frac{dy_k}{2\pi i} \Delta^2(\{y_l\}) \sum_\pi (-1)^{\sigma_\pi} \frac{F(Y) \prod_{k=1}^p y_{\pi(k)}^{p-k}}{\Delta(\{y_l\}) \prod_{k=1}^p y_k^{n+p}} \\
&= \int_{Y \in U(p)} \frac{dY}{(2\pi)^4} \det{}^{-n-p} Y F(Y), \qquad (105)
\end{aligned}$$

where in the second last equation we have used that the last product is a Vandermonde determinant. Note the measure dY is the product over independent differentials. We thus arrive at the partition function

$$\begin{aligned}
Z^\nu(z,\mu) &= e^{n\Sigma^2\mu^2} \int_{Y\in U(2)} \frac{dY}{2\pi^4} [[i\partial_{Y_{11}}]^\nu \det{}^{-n-2} Y] \exp\left[z(Y_{11}+Y_{22}) + \mu(Y_{12}+Y_{21}) + \frac{Y_{11}Y_{22}}{n\Sigma^2} \right] \\
&= \frac{(n+\nu+1)! e^{n\Sigma^2\mu^2}}{(n+1)!} \int_{Y\in U(2)} \frac{dY}{(2\pi)^4} \frac{[-iY_{22}]^\nu}{\det{}^{n+2+\nu} Y} \qquad (106) \\
&\quad \times \exp\left[z(Y_{11}+Y_{22}) + \mu(Y_{12}+Y_{21}) + \frac{1}{n\Sigma^2} Y_{11}Y_{22} \right].
\end{aligned}$$

We parameterize Y as

$$Y = e^{i\beta} \begin{pmatrix} e^{i\alpha}\cos\theta & e^{i\phi}\sin\theta \\ -e^{-i\phi}\sin\theta & e^{-i\alpha}\cos\theta \end{pmatrix}, \qquad (107)$$

where $\beta \in [0, 2\pi]$, $\phi \in [0, 2\pi]$, $\alpha \in [0, \pi]$ and $\theta \in [0, \pi]$. The invariant measure is given by

$$\frac{dY}{(2\pi)^3 \det{}^2 Y} = \frac{\cos\theta \sin\theta d\beta d\alpha d\theta d\phi}{2\pi^3}. \qquad (108)$$

This results in the partition function

$$\begin{aligned}
Z^\nu(z,\mu) &= \frac{(n+\nu+1)! e^{n\Sigma^2\mu^2}}{2\pi(n+1)!} \int \frac{d\beta d\alpha d\theta d\phi}{(2\pi)^2} \cos\theta \sin\theta e^{-2i\beta(n+\nu)} (-i)^\nu e^{i\nu(\beta-\alpha)} \cos^\nu\theta \\
&\quad \times e^{2ze^{i\beta}\cos\theta\cos\alpha + 2i\mu e^{i\beta}\sin\theta\sin\phi + \frac{1}{n\Sigma^2} e^{2i\beta}\cos^2\theta}. \qquad (109)
\end{aligned}$$

The integral over α and ϕ gives a modified Bessel function so that we finally obtain

$$\begin{aligned} Z^{\nu}(z,\mu) &= \frac{(n+\nu+1)!e^{n\Sigma^2\mu^2}}{2\pi(n+1)!}\int\frac{d\beta d\theta}{4\pi}\cos\theta\sin\theta e^{-2i\beta n}e^{-i\beta\nu}\cos^{\nu}\theta I_{\nu}(2ze^{i\beta}\cos\theta) \\ &\times J_0(2\mu e^{i\beta}\sin\theta)e^{\frac{1}{n\Sigma^2}e^{2i\beta}\cos^2\theta}. \end{aligned} \tag{110}$$

The normalization will be fixed by the result for $\mu = 0$.

$$\begin{aligned} Z^{\nu}(z,\mu=0) &= \frac{(n+\nu+1)!}{(n+1)!}\int d\beta d\theta\cos\theta\sin\theta e^{-2i\beta n}e^{-i\beta\nu}\cos^{\nu}\theta I_{\nu}(2ze^{i\beta}\cos\theta)e^{\frac{1}{n\Sigma^2}e^{2i\beta}\cos^2\theta} \\ &= \frac{(n+\nu+1)!}{(n+1)!}\int d\beta dx x e^{-2i\beta n}e^{-i\beta\nu}x^{\nu}I_{\nu}(2ze^{i\beta}x)e^{\frac{1}{n\Sigma^2}e^{2i\beta}x^2} \\ &= \frac{(n+\nu+1)!}{(n+1)!}\int_0^1 dx x\sum_{k+l=n}(zx)^{2k+\nu}x^{\nu}(\frac{1}{n\Sigma^2}x^2)^l\frac{1}{k!(k+\nu)!l!} \\ &= \frac{1}{2}\frac{(n+\nu)!}{(n+1)!}\sum_{k=0}^{n}(z)^{2k+\nu}(n\Sigma^2)^{k-n}\frac{1}{k!(k+\nu)!(n-k)!}. \end{aligned} \tag{111}$$

The sum is exactly the expression for a Laguerre polynomial so that

$$Z(z,\mu=0) = \frac{z^{\nu}}{(n+1)!\Sigma^{2n}}L_n^{\nu}(-z^2n\Sigma^2). \tag{112}$$

In the microscopic limit this reduces to

$$Z(z,\mu=0) = \frac{1}{(n+1)!\Sigma^{2n+\nu}}I_{\nu}(2zn\Sigma). \tag{113}$$

To get the correct ν dependence we have to include an additional factor of Σ^{ν} in the partition function which was already observed in [28].

Massless one Flavor Bosonic Partition Function

The goal of this appendix to derive a form of the massless bosonic one flavor partition function where the cancellation of the leading order terms has been

take care of analytically. The starting point is in the expression in (2.93)

$$
\begin{aligned}
Z_n^{N_f=-1}(\mu) &= \frac{(-1)^{n-1}}{h_{n-1}}\left[-\int_0^1 dx e^{-\bar{n}\mu^2 x}\frac{x^{n-1}}{x+1}+\int_1^\infty dx e^{-\bar{n}\mu^2 x}\frac{x^{n-1}}{x+1}\right] \\
&\quad -\frac{(-1)^{n-1}}{h_{n-1}}\sum_{k=0}^{n-2}\frac{(-1)^{k+n}}{h_k}\left[\mu^{k+1}\int_1^\infty dx e^{-\bar{n}\mu^2 x}x^k\right]^2 .
\end{aligned}
\tag{114}
$$

The sum on the second line of this equation can be written as

$$
\begin{aligned}
&\sum_{k=0}^{n-2}\frac{(-1)^k}{h_k}\left[\mu^{k+1}\int_1^\infty dx e^{-\bar{n}\mu^2 x}x^k\right]^2 \\
&=\sum_{k=0}^{n-2}\frac{(-1)^k}{h_k}\mu^{2(+1)}\int_1^\infty dy e^{-\bar{n}\mu^2 y}y^k\Big(\int_0^\infty dx e^{-\bar{n}\mu^2 x}x^k-\int_0^1 dx e^{-\bar{n}\mu^2 x}x^k\Big) \\
&=\sum_{k=0}^{n-2}\frac{(-1)^k}{h_k}\mu^{2(k+1)}\int_1^\infty dy e^{-\bar{n}\mu^2 y}y^k\left(\frac{k!}{(\bar{n}\mu^2)^{k+1}}-\int_0^1 dx e^{-\bar{n}\mu^2 x}x^k\right) \\
&=\sum_{k=0}^{n-2}\int_1^\infty dy e^{-\bar{n}\mu^2 y}(-y)^k-\frac{\mu^{2(k+1)}}{h_k}\int_0^1 dx e^{-\bar{n}\mu^2 x}x^k\int_1^\infty dy e^{-\bar{n}\mu^2 y}(-y)^k \\
&=\int_1^\infty dy e^{-\bar{n}\mu^2 y}\frac{1-(-y)^{n-1}}{1+y}-\sum_{k=0}^{n-2}\frac{\mu^{2(k+1)}}{h_k}\int_0^1 dx e^{-\bar{n}\mu^2 x}x^k\int_1^\infty dy e^{-\bar{n}\mu^2 y}(-y)^k \\
&=(-1)^n\int_1^\infty dy\frac{y^{n-1}e^{-\bar{n}\mu^2 y}}{1+y}+\int_1^\infty dy\frac{e^{-\bar{n}\mu^2 y}}{1+y} \\
&-\sum_{k=0}^{n-2}\frac{\mu^{2(k+1)}}{h_k}\int_0^1 dx e^{-\bar{n}\mu^2 x}x^k\int_1^\infty dy e^{-\bar{n}\mu^2 x}(-y)^k \\
&=(-1)^n\int_1^\infty dy\frac{y^{n-1}e^{-\bar{n}\mu^2 y}}{1+y}+\int_1^\infty dy\frac{e^{-\bar{n}\mu^2 y}}{1+y} \\
&-\bar{n}\mu^2\int_0^1 dx\int_1^\infty dy e^{-\bar{n}\mu^2(x+y+xy)}\frac{\Gamma(n-1,-\bar{n}\mu^2 xy)}{\Gamma(n-1)}
\end{aligned}
\tag{115}
$$

Inserting this result in the partition function (114) we find

$$\begin{aligned}
Z(\mu) &= \frac{1}{h_{n-1}}\left[-(-1)^{n-1}\int_0^1 dx e^{-\bar{n}\mu^2 x}\frac{x^{n-1}}{x+1}+\int_1^\infty dx e^{-\bar{n}\mu^2 x}\frac{1}{1+x}\right.\\
&\left.-\bar{n}\mu^2\int_0^1 dx\int_1^\infty dy e^{-\bar{n}\mu^2(x+y+xy)}\frac{\Gamma(n-1,-\bar{n}\mu^2 xy)}{\Gamma(n-1)}\right]\\
&= \frac{1}{h_{n-1}}\left[(-1)^n\int_0^1 dx\frac{x^{n-1}e^{-\bar{n}\mu^2 x}}{x+1}+\int_1^\infty dx\frac{e^{-\bar{n}\mu^2 x}}{1+x}-\bar{n}\mu^2\int_0^1 dx\int_1^\infty dy e^{-\bar{n}\mu^2(x+y+xy)}\right.\\
&\left.-\bar{n}\mu^2\int_0^1 dx\int_1^\infty dy e^{-\bar{n}\mu^2(x+y+xy)}\left(\frac{\Gamma(n-1,-\bar{n}\mu^2 xy)}{\Gamma(n-1)}-1\right)\right]\\
&= \frac{1}{h_{n-1}}\left[-(-1)^{n-1}\int_0^1 dx e^{-\bar{n}\mu^2 x}\frac{x^{n-1}}{x+1}+\bar{n}\mu^2\int_1^\infty dx\int_1^\infty dy e^{-\bar{n}\mu^2(x+y+xy)}\right.\\
&\left.-\bar{n}\mu^2\int_0^1 dx\int_1^\infty dy e^{-\bar{n}\mu^2(x+y+xy)}\left(\frac{\Gamma(n-1,-\bar{n}\mu^2 xy)}{\Gamma(n-1)}-1\right)\right]. \qquad (116)
\end{aligned}$$

Next we partial integrate the last term with respect to y. This results in

$$\begin{aligned}
Z(\mu) &= \frac{1}{h_{n-1}}\left[-(-1)^{n-1}\int_0^1 dx e^{-\bar{n}\mu^2 x}\frac{x^{n-1}}{x+1}+\bar{n}\mu^2\int_1^\infty dx\int_1^\infty dy e^{-\bar{n}\mu^2(x+y+xy)}\right.\\
&-\int_0^1 dx\frac{e^{-\bar{n}\mu^2(2x+1)}}{x+1}\left(\frac{\Gamma(n-1,-\bar{n}\mu^2 x)}{\Gamma(n-1)}-1\right) \qquad (117)\\
&\left.+\frac{\bar{n}\mu^2}{\Gamma(n-1)}\int_0^1 dx\int_1^\infty dy\frac{e^{-\bar{n}\mu^2(x+y)}}{x+1}(-x)^{n-1}(y\bar{n}\mu^2)^{n-2}\right].
\end{aligned}$$

When the upper limit of the y-integral in the last term is extended to $[0,\infty]$ it is equal to $\Gamma(n-1)$ and cancels the first term. What remains is the y-integral over $[0,1]$. We thus find

$$\begin{aligned}
Z(\mu) &= \frac{1}{h_{n-1}}\left[\bar{n}\mu^2\int_1^\infty dx\int_1^\infty dy e^{-\bar{n}\mu^2(x+y+xy)}-\int_0^1 dx\frac{e^{-\bar{n}\mu^2(2x+1)}}{x+1}\left(\frac{\Gamma(n-1,-\bar{n}\mu^2 x)}{\Gamma(n-1)}-1\right)\right.\\
&\left.-\frac{\bar{n}\mu^2}{\Gamma(n-1)}\int_0^1 dx\int_0^1 dy\frac{e^{-\bar{n}\mu^2(x+y)}}{x+1}(-x)^{n-1}(y\bar{n}\mu^2)^{n-2}\right]. \qquad (118)
\end{aligned}$$

The integrals over y can be performed analytically resulting in

$$Z(u) = \frac{e^{-n\mu^2}}{h_{n-1}}\left[\int_0^\infty dx \frac{e^{-\bar{n}\mu^2(2x+1)}}{x+1} - \int_0^1 dx \frac{e^{-\bar{n}\mu^2(2x+1)}}{x+1}\left(\frac{\Gamma(n-1,-\bar{n}\mu^2 x)}{\Gamma(n-1)}\right)\right.$$
$$\left. - \int_0^1 dx \frac{e^{-\bar{n}\mu^2 x}}{x+1}(-x)^{n-1}\left(1-\frac{\Gamma(n-1,\bar{n}\mu^2}{\Gamma(n-1)}\right)\right]. \quad (119)$$

Bosonic Partition function for $n = 2$ and $n = 3$

In this appendix we evaluate the bosonic partition function without relying on the tricks used in section 2.4.2. Starting from the definition we obtain given by

$$\begin{aligned} Z_2(\mu)Z_2^{\rm G} &= \frac{1}{\pi^2}\int d\lambda_1 d\lambda_1^* d\lambda_2 d\lambda_2^* |\lambda_1-\lambda_2|^2 \prod_{k=1}^2 \frac{e^{-\bar{n}\lambda_k^*\lambda_k}}{(\lambda_k-u)(\lambda_k^*+\mu)} \\ &= \frac{2}{\pi^2}\int d\lambda_1 d\lambda_1^*(\lambda_1^*\lambda_1-\lambda_1\lambda_2^*)\prod_{k=1}^2 \frac{e^{-\bar{n}\lambda_k^*\lambda_k}}{(\lambda_k-\mu)(\lambda_k^*+\mu)} \\ &= \frac{2}{\pi^2}\int d\lambda_1 d\lambda_1^* \frac{\lambda_1^*\lambda_1 e^{-\bar{n}\lambda_1^*\lambda_1}}{(\lambda_1-\mu)(\lambda_1^*+\mu)}\int d\lambda_2 d\lambda_2^* \frac{e^{-\bar{n}\lambda_2^*\lambda_2}}{(\lambda_2-\mu)(\lambda_2^*+\mu)} \\ &\quad +2\left(\frac{1}{\pi}\int d\lambda_1 d\lambda_1^* \frac{\lambda_1 e^{-\bar{n}\lambda_1^*\lambda_1}}{(\lambda_1-\mu)(\lambda_1^*+\mu)}\right)^2 \\ &= 8\int d\lambda\lambda \frac{\lambda^2 e^{-\bar{n}\lambda^2}}{\lambda^2+\mu^2}\mathrm{sign}(\lambda-\mu)\int d\lambda\lambda \frac{e^{-\bar{n}\lambda^2}}{\lambda^2+\mu^2}\mathrm{sign}(\lambda-\mu) \\ &\quad +2\left(2\int_1^\infty d\lambda \frac{\lambda\mu e^{-\bar{n}\lambda^2}}{\lambda^2+\mu^2}+2\int_0^1 d\lambda \frac{\lambda^3 e^{-\bar{n}\lambda^2}}{\mu(\lambda^2+\mu^2)}\right)^2. \quad (120) \end{aligned}$$

Using the same steps as for $n = 2$, for $n = 3$ the partition function can be expressed in terms of three integrals

$$Z_3(\mu)Z_3^G = 6Z_0^a(\mu)Z_1^a(\mu)Z_2^a(\mu) + 6Z_0^a(\mu)(Z_1^b(\mu))^2 - 12Z_1^c(\mu)Z_1^b(\mu)Z_2^b(\mu) \quad (121)$$

where

$$
\begin{aligned}
Z_p^a(\mu) &= \mu^{2(p+1)} \int_0^\infty dx \mathrm{sign}(x-1) \frac{e^{-\bar{n}\mu^2 x} x^p}{x+1}, \\
Z_p^b(\mu) &= \mu^p \int_1^\infty dx \frac{e^{-\bar{n}\mu^2 x}}{x+1} - (-u)^p \int_0^1 dx \frac{e^{-\bar{n}\mu^2 x} x^p}{x+1}, \\
Z_p^c(\mu) &= \mu^{2p+1} \int_1^\infty dx \frac{e^{-\bar{n}\mu^2 x x^p}}{x+1} + \mu^{2p+1} \int_0^1 dx \frac{e^{-\bar{n}\mu^2 x} x^{p+1}}{x+1},
\end{aligned}
\tag{122}
$$

The $n = 2$ partition function can be rewritten in terms of the first two integrals

$$
Z_2(\mu) Z_2^G = (2 Z_0^a(\mu) Z_1^a(\mu) + 2 (Z_1^b(\mu))^2. \tag{123}
$$

Chapter 3

X-Space Renormalization of Dimension-5 Operators

Introduction

Violation of the discrete CP symmetry is a sought after ingredient for new physics, and a complete understanding of the baryon asymmetry problem. Standard model CP violating processes coming from the phase in the CKM quark mixing matrix of the electroweak sector have been observed in processes such as K decays, $K^0 - \overline{K}^0$ mixing and in $B^0 - \overline{B}^0$ mixing, which are all consistent with theoretical predictions. The dimension 4, QCD θ term is parameterized by the dimensionless θ parameter which has been constrained to be less than 10^{-10} [48] through a lack of any observations of CP violating processes. Despite the accurate predictions made by the standard model, it still does not predict enough CP violation to explain the cosmological baryon asymmetry problem. The standard model is likely, part of a larger theory that could contain new sources of CP violation. As suggested in the seminal paper by Purcell and Ramsey[49], electric dipole moments can be used as probes of CP violation.

After integrating out all standard model fields heavier than the down

quark, and performing a chiral rotation, the effective lagrangian is

$$\begin{aligned}\mathcal{L} =&\mathcal{L}_{QCD} + \mathcal{L}_{QED} \\ &- g\overline{\psi}^{(i)} \left(d_{ij}^{(gm)} \sigma_{\mu\nu} G^{\mu\nu} - d_{ij}^{(ge)} \sigma_{\mu\nu} G^{\mu\nu} \gamma_5 \right) \psi^{(j)} \\ &- e\overline{\psi}^{(i)} \left(d_{ij}^{(\gamma m)} \sigma_{\mu\nu} F^{\mu\nu} - d_{ij}^{(\gamma e)} \sigma_{\mu\nu} F^{\mu\nu} \gamma_5 \right) \psi^{(j)} \\ &+ \text{dimension 6 quark and gluon operators} \\ =&\mathcal{L}_{QCD} + \mathcal{L}_{QED} + \mathcal{L}_{dim\geq 5}, \end{aligned} \tag{3.1}$$

where i and j are flavor indices. These are the dimension 5 quark chromo-magnetic dipole moment, chromo-electric dipole moment, magnetic dipole moment and electric dipole moment operators.

Experimental efforts to detect EDMs of atoms, nucleons and nuclei have constrained new CP violating physics to lie at, or above the TeV scale. Utilizing these constraints to improve our understanding of quarks and gluons requires knowledge of their nonperturbative dynamics in bound state nucleons. These nonperturbative effects can be understood on the lattice.

The goal of lattice calculations is to compute the electric dipole form factor (EDFF) F_3,

$$\langle N_{p'} | \overline{q} \gamma^\mu q | N_p \rangle_{CPV} = \overline{u}_{p'} \left[F_1(Q^2)\gamma^\mu + (F_2(Q^2) + iF_3(Q^2)\gamma_5) \frac{\sigma^{\mu\nu} q_\nu}{2m_N} \right] u_p, \tag{3.2}$$

which exists in the presence of the EDM and CEDM terms in equation (3.1). The path integral for this correlator on the lattice is

$$\langle N_{p'} | \overline{q} \gamma^\mu q | N_p \rangle_{CPV} = \frac{1}{Z} \int \mathcal{D}U \mathcal{D}\overline{q} \mathcal{D}q e^{-S_{QCD} - S_{dim\geq 5}} N \overline{q} \gamma^\mu q \overline{N}. \tag{3.3}$$

At the energy scales of interest, $S_{dim\geq 5}$ is small, and the exponential can be expanded to give

$$\left\langle N \overline{q} \gamma^\mu q \overline{N} \right\rangle_{CPV} \approx \left\langle N \overline{q} \gamma^\mu q \overline{N} \right\rangle - \left\langle N \overline{q} \gamma^\mu q \overline{N} S_{dim\geq 5} \right\rangle, \tag{3.4}$$

where the correlator on left in equation (3.4) is weighted by the entire lagrangian, equation (3.1), and the correlators on the right are weighted by the QCD action. To extract F_3, one must also compute

$$\left\langle N \overline{N} \right\rangle_{CPV} = \left\langle N \overline{N} \right\rangle - \left\langle N \overline{N} S_{dim\geq 5} \right\rangle \tag{3.5}$$

Several analyses and lattice EDM and CEDM computations have been conducted [50, 51, 52], however, they have been carried out using bare lattice operators, and cannot be compared to measurements made and expressed in $\overline{MS}$. In what follows, preliminary results of the analytical portion of the renormalization of dimension 5 operators will be reviewed.

Non-Perturbative Renormalization

To obtain physically meaningful results for the nucleon electric dipole form factors, the operators used in equations (3.5) and (3.4) must be renormalized. Renormalization is the process of removing unphysical contributions to amplitudes. This process however, is not unique, and different methods for subtracting unphysical contributions are outlined in different renormalization schemes. The standard scheme for reporting physical quantities is $\overline{MS}$. However, $\overline{MS}$ is defined by subtractions to be made at each perturbative order in the theory's coupling constant, in a dimensionally regulated (dim-reg) theory. It is therefore, not suited for non-perturbative computations, made using any other regulator. Non-perturbative renormalization is an active area of research, where schemes better suited for non-perturbative compuation are defined. The next two subsections will be dedicated to briefly reviewing two schemes that can be imposed non-perturbatively.

RI-Mom

Developed by Martinelli et al in their seminal paper [53], the regularization independent momentum subtraction scheme (RI-Mom) is a renormalization condition imposed on green functions with operator insertions. Following the example given in [53], the process of lattice renormalization, and perturbative renormalization is illustrated using quark bilinear operators $\overline{\psi}\Gamma\psi$, where Γ is an arbitrary tensor that could have either spin or color indices.

For arbitrary composite operator, O_Γ, the RI-Mom renormalization condition is

$$Z_\Gamma \left\langle p|O_\Gamma|p\right\rangle\big|_{p^2=-\mu^2} = \left\langle p|O_\Gamma|p\right\rangle_{\text{tree order}}. \tag{3.6}$$

This renormalization condition states that the renormalization constant Z_Γ is fixed to ensure that, at $p^2 = -\mu^2$, the full correlator is equal to the tree order

correlator. In order to avoid both non-perturbative effects and discretization effects, μ should fall within the "window" $\Lambda_{QCD} << \mu << 1/a$.

When $O_\Gamma(x) = \overline{\psi}(x)\Gamma\psi(x)$, the green function to be used in condition 3.6 is

$$\begin{aligned} G_0(x,y) =& \left\langle \psi(x) O_\Gamma(0) \overline{\psi}(y) \right\rangle \\ =& \frac{1}{N} \sum_{i=1}^{N} S_i(x|0)\Gamma S_i(0|y), \end{aligned} \tag{3.7}$$

where $S_i(x|0)$ is the quark propagator in the ith gauge field configuration. In order to use G_0 and the quark propagators in condition 3.6, they must be fourier transformed, and expressed in momentum space. The quark propagators become

$$S(pa) = \left\langle \int d^4x e^{-ip\cdot x} S(x|0) \right\rangle = \frac{1}{N} \sum_{i=1}^{N} S_i(p|0). \tag{3.8}$$

The green function becomes

$$G_0(pa) = \int d^4x d^4y e^{-ip\cdot(x-y)} G_0(x,y) = \frac{1}{N} \sum_{i=1}^{N} S_i(p|0)\Gamma(\gamma_5 S_i^\dagger(p|0)\gamma_5). \tag{3.9}$$

Using these in condition 3.6 gives

$$Z_\Gamma Z_\psi^{-1}\ S^{-1}(pa) G_0(pa) S^{-1}(pa)\big|_{p^2=-\mu^2} = \Gamma \tag{3.10}$$

Using an appropriate projector $\hat{P}$, such that $\hat{P}\Gamma = \mathbf{1}$,

$$Z_\Gamma = 12 Z_\psi Tr\left[\left(\hat{P} S^{-1}(pa) G_0(pa) S^{-1}(pa)\Big|_{p^2=-\mu^2} \right)^{-1} \right]. \tag{3.11}$$

Therefore, to compute non-perturbative renormalization constant, Z_Γ, one needs lattice computations of the quark propagators $S(pa)$, the green function $G_0(pa)$ and the quark field renormalization constant Z_ψ. The non-perturbative quark field renormalization can be computed using the conserved vector current, and the knowledge that vector current renormalization is equal to 1.

Perturbatively, the renormalization constants are expanded, such that at $p^2 = -\mu^2$, loop corrections vanish. Below, the perturbative renormalization is computed to 1-loop for the quark mass and field in RI-MOM using naive dim-reg theory, where the number of dimensions d is $4 - 2\epsilon$. Explicit calculation for the 1-loop diagram has been carried out in appendix .8.1. Those results will be used here. Given the structure of the bare quark propagator, (see equation (241)) the RI-MOM condition is

$$S_R|_{p^2=-\mu^2} = \left.\frac{Z_\psi^{-1}}{\not{p} - m_0 - \Sigma_0(p)}\right|_{\substack{p^2=-\mu^2 \\ m_0=Z_m m}} = \frac{1}{\not{p} - m}, \tag{3.12}$$

where S_R is the renormalized quark propagator, Z_ψ and Z_m are the quark field and mass renormalization constants, and Σ_0 are the bare loop corrections to the propagator. By expressing Σ_0 in terms of its Dirac structure, convenient RI-MOM renormalization conditions can be derived.

$$S_R^{-1}(p) = Z_\psi \left(\not{p}(1 - \Sigma_V(p)) - Z_m m(1 + \Sigma_s(p))\right). \tag{3.13}$$

The condition for the quark field renormalization is

$$\begin{aligned} &\lim_{m\to 0} \frac{1}{12d} Z_\psi Tr\left[\gamma_\mu \frac{\partial}{\partial p_\mu} S_0^{-1}(p, Z_m m)\right]\Big|_{p^2=-\mu^2} \\ &= \lim_{m\to 0} \frac{1}{12d} Z_\psi Tr\left[\gamma_\mu \frac{\partial}{\partial p_\mu} (\not{p}(1 - \Sigma_V))\right]\Big|_{p^2=-\mu^2} = 1, \end{aligned} \tag{3.14}$$

and for the quark mass, it is

$$\begin{aligned} &\lim_{m\to 0} \frac{1}{12m} Z_\psi Z_m Tr\left[S_0^{-1}\right]\Big|_{p^2=-\mu^2} \\ &= -\lim_{m\to 0} \frac{1}{12} Z_\psi Z_m Tr\left[1 + \Sigma_s\right]\Big|_{p^2=-\mu^2} = -1. \end{aligned} \tag{3.15}$$

Σ_v and Σ_s have been computed, and can be found in equations (245) and (247). Plugging these into the renormalization conditions gives

$$Z_\psi = 1 - \xi \frac{\alpha}{4\pi}\left(\frac{C(R)}{2} + \frac{C(R)}{\epsilon}\right) + \cdots \tag{3.16}$$

$$Z_m = 1 - \frac{\alpha}{4\pi}\left(\frac{C(R)}{2}(8 + 3\xi) + 3\frac{C(R)}{\epsilon}\right) + \cdots \tag{3.17}$$

One clear difference between renormalization in MS and RI-MOM is that MS only has 1 as a finite contribution, whereas RI-MOM requires a different finite part to meet the renormalization condition.

Having demonstrated both non-perturbative, and perturbative implementation of RI-MOM, we now discuss the X-space scheme.

X-Space Scheme

Similarly to RI-MOM, the X-space scheme is a renormalization scheme whose condition is imposed on green functions. The green functions, however, are two point functions of composite operators in coordinate space. The X-space scheme condition, again imposed in the chiral limit is

$$\lim_{a\to 0} \left\langle O_\Gamma^X(x) O_\Gamma^X(0)\right\rangle\Big|_{x^2=x_0^2} = \langle O_\Gamma(x_0) O_\Gamma(0)\rangle|_{\substack{\text{free}\\ \text{cont}}}, \tag{3.18}$$

where $O_\Gamma^X = Z_\Gamma^X O_\Gamma$ is the renormalized operator in the X-scheme, and x_0 is the renormalization point. One big advantage to the X-scheme, over RI-MOM is that the correlators are gauage invariant. This results in less mixing for higher dimensional operators. It does however have a window, necessary for matching to a perturbative scheme like $\overline{MS}$. To avoid discretization effects, $x_0 >> a$ where a is the lattice discretization. To avoid nonperturbative contamination, $x_0 << \Lambda_{QCD}$.The process of non-perturbative renormalization will be illustrated using the quark vector current to vector current correlator ($O_\gamma^\mu(x) = \overline{\psi}(x)\gamma^\mu\psi(x)$), and the plots generated by Gimenez et al [1] in the original X-space scheme paper.

The first step in renormalizing the vector current in the X-scheme is finding the bare correlator, with interactions

$$C_{vv}(x) = \left\langle \overline{\psi}(x)\gamma^\mu\psi(x)\overline{\psi}(0)\gamma^\nu\psi(0)\right\rangle. \tag{3.19}$$

In [1], $C_{vv}(x)$ was computed on the lattice using wilson fermions, and plotted. This plot is displayed as figure 3.1.

Figure 3.1 shows a large spread of points. This effect was investigated, and after finding a very similar spread in the free lattice theory 3.2, it was concluded that these are discretizaton effects.

Gimenez et al removed these discretization effects by taking the ratio of the free lattice theory, to the free continuum theory.

$$\Delta_{vv}(x) = \frac{\langle O_v(x) O_v(0)\rangle|_{\substack{\text{free}\\ \text{lat}}}}{\langle O_v(x) O_v(0)\rangle|_{\substack{\text{free}\\ \text{cont}}}}. \tag{3.20}$$

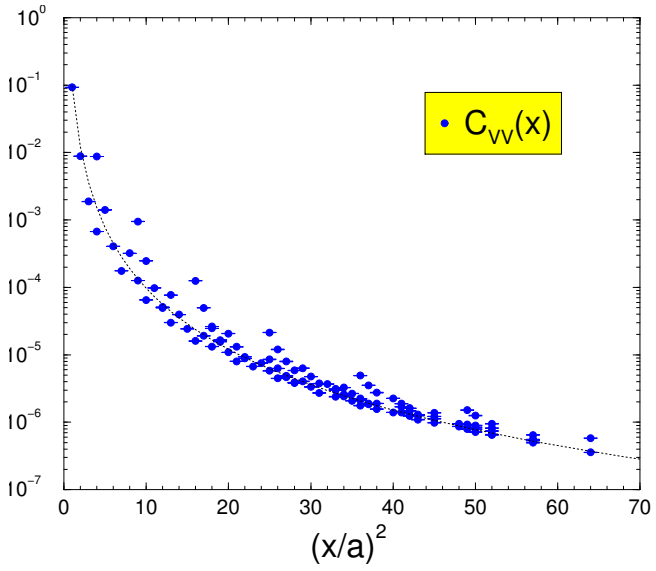

Figure 3.1: *Vector-vector correlator $C_{vv}(x)$ in the interacting theory [1].*

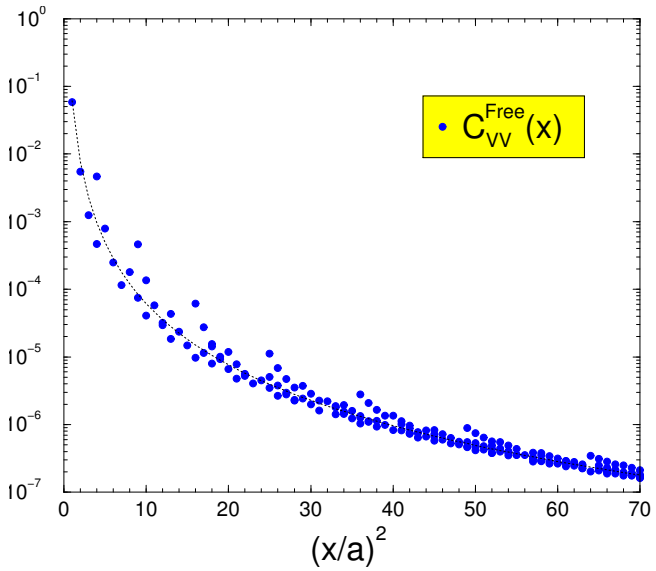

Figure 3.2: *Vector-vector correlator $C_{vv}(x)$ in the free theory [1].*

Δ_{vv} is equal to unity everywhere, except for where there discretization errors. Therefore, dividing $C_{vv}(x)$ by $\Delta_{vv}(x)$ will eliminate the discretization errors.

The corrected correlator,

$$C'_{vv}(x) = \frac{C_{vv}(x)}{\Delta_{vv}(x)}, \tag{3.21}$$

was plotted in figure 3.3.

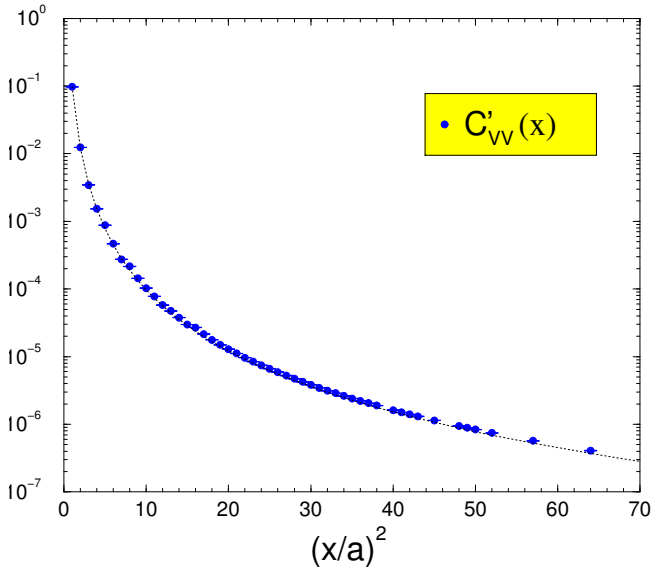

Figure 3.3: *Corrected vector-vector correlator $C'_{vv}(x)$ [1].*

Using the curve corrected for discretization errors, C'_{vv}, in equation (3.18), one finds the renormalization constant $Z_v(x_0)$ is

$$\begin{aligned} 1 =& Z_v(x_0)^2 \frac{C'_{vv}(x)}{\langle O_v(x) O_v(0) \rangle|_{\substack{\text{free} \\ \text{cont}}}} \\ Z_v(x_0) =& \left[\frac{C'_{vv}(x)}{\langle O_v(x) O_v(0) \rangle|_{\substack{\text{free} \\ \text{cont}}}} \right]^{-\frac{1}{2}}. \end{aligned} \tag{3.22}$$

In what follows, the analytic work required in renormalizing the CP violating dimension 5 operators in the X-space scheme will be explained, and compared with work previously done for these operators in RI-MOM [54].

Momentum Space Correlators

To properly express lattice correlators in $\overline{MS}$, the two point correlators must first be dimensionally regulated, computed in the continuum, and renormalized using $\overline{MS}$. Correlators in coordinate space will be computed by fourier transforming the renormalized mometum space correlators (for details on fourier transform, see appendix .2). In this section, operator mixing, and an outline of the chromoelectric and chromomagnetic dipole moment renormalization will be given.

The chromoelectric dipole moment operator is

$$C_e = \frac{1}{2} g \overline{\psi}^{(i)} G^a_{\mu\nu} T^a \sigma^{\mu\nu} \gamma_5 \psi^{(j)}, \tag{3.23}$$

where the i and j label the quark flavor, and are different to emphasize that only off diagonal flavor operators are studied. The chromoelectric dipole moment operator mixes with the pseudoscalar current operator upon renormalization. The pseudo scalar operator is

$$P = \overline{\psi}^{(i)} \gamma_5 \psi^{(j)}. \tag{3.24}$$

The Feynman rules for these operators can be found in appendix .1. The three correlators that must be computed in the continuum for renormalization of the CEDM operator are

$$\Pi_0^P(Q^2, m_0^2) = \int d^d x e^{iQ\cdot x} \langle P_0(x) P_0(0) \rangle \tag{3.25}$$

$$\Pi_0^{C_e P}(Q^2, m_0^2) = \int d^d x e^{iQ\cdot x} \langle C_{e0}(x) P_0(x) \rangle \tag{3.26}$$

$$\Pi_0^{C_e}(Q^2, m_0^2) = \int d^d x e^{iQ\cdot x} \langle C_{e0}(x) C_{e0}(0) \rangle . \tag{3.27}$$

These correlators are computed using bare quark fields ψ_0, bare gluon fields A_0, bare ghost fields c_0 and bare coupling and mass parameters g_0 and m_0. This choice allows us to ignore counter terms, and decreases the number of diagrams. In the dimensionally regulated theory, we work in $d = 4 - 2\epsilon$ dimensions. In d dimensions, the dimensionality of g_0 is

$$[g_0] = 2 - \frac{d}{2} = \epsilon. \tag{3.28}$$

For convenience, in calculations, the dimensionless constant

$$\frac{\alpha_0}{4\pi} = \mu^{-2\epsilon} \frac{g_0^2}{(4\pi)^{d/2}} \tag{3.29}$$

is used. The renormalization constants Z_α and Z_m to renormalize the coupling and mass are computed in appendix .8.

The dimensions of the pseudoscalar operator, and CEDM operator in d dimensions are

$$[P] = d - 1 \tag{3.30}$$

$$[C] = d + 1 \tag{3.31}$$

Their renormalization matrix has the form

$$\begin{pmatrix} C_e \\ Q^2 P \\ m^2 P \end{pmatrix} = \begin{pmatrix} Z_{ce} & Z_{cep} & Z_{cem} \\ 0 & Z_p & 0 \\ 0 & 0 & Z_p \end{pmatrix} \begin{pmatrix} C_{e0} \\ Q^2 P_0 \\ m^2 P_0 \end{pmatrix} \tag{3.32}$$

Where Q is momentum, C_{e0} is the bare CEDM, P_0 is the bare pseudoscalar current. From this matrix, it is clear that the renormalized CEDM operator is

$$C_e = Z_{ce} C_{e0} + Q^2 Z_{cep} P_0 + Z_{cem} m^2 P_0 \tag{3.33}$$

The renormalized pseudoscalar current is

$$P = Z_p P_0 \tag{3.34}$$

In momentum space, the renormalized pseudoscalar current density $\langle PP \rangle$ is

$$\Pi^P(Q^2, m^2, \mu^2) = (Z_p(\alpha))^2 \, \Pi_0^P(Q^2, Z_m m^2) + Q^2 (\mu^2)^{-\epsilon} Z_{qP}(\alpha) + m^2 (\mu^2)^{-\epsilon} Z_{mP}, \tag{3.35}$$

where Z^{qSS} and Z^{mSS} are subtractive renormalization constants.

The renormalized cedm to pseudoscalar density correlator is

$$\begin{aligned} \Pi^{C_e P}(Q^2, m^2, \mu^2) =& Z_{ce} Z_p \langle C_0 P_0 \rangle + \left(Q^2 Z_{cep} + m^2 Z_{cem}\right) Z_p \langle P_0 P_0 \rangle \\ &+ (Q^2)^2 (\mu^2)^{-\epsilon} Z_{qCeP} + Q^2 m^2 (\mu^2)^{-\epsilon} Z_{qmCeP} + (m^2)^2 (\mu^2)^{-\epsilon} Z_{mCeP} \end{aligned} \tag{3.36}$$

$$\begin{aligned} =& Z_c Z_p \Pi_0^{C_e P}(Q^2, Z_m m^2) + \left(Q^2 Z_{cep} + m^2 Z_{cem}\right) Z_p \Pi_0^P(Q^2, Z_m m^2) \\ &+ (Q^2)^2 (\mu^2)^{-\epsilon} Z_{qCeP} + Q^2 m^2 (\mu^2)^{-\epsilon} Z_{qmCeP} + (m^2)^2 (\mu^2)^{-\epsilon} Z_{mCeP} \end{aligned} \tag{3.37}$$

It's clear from equation (3.32) that Z_{ce} and Z_p both have the structure $1 + \mathcal{O}(\alpha) + \cdots$. However, Π^{CeP} is of $\mathcal{O}(\alpha)$, and Π^S is of $\mathcal{O}(1)$. Therefore, Z_{cep} must start at $\mathcal{O}(\alpha)$.

The renormalized cedm to cedm correlator is

$$\begin{aligned}\Pi^{C_e}(Q^2, m^2, \mu^2) =&(Z_{ce})^2\langle C_{e0}C_{e0}\rangle + 2\left(Q^2 Z_{cep} + m^2 Z_{cem}\right) Z_{ce}\langle C_{e0}P_0\rangle + \left(Q^2 Z_{cep} + m^2 Z_{cem}\right)^2 \langle P_0 P_0\rangle \\ &+ (Q^2)^3(\mu^2)^{-\epsilon} Z_{qCe} + (Q^2)^2 m^2(\mu^2)^{-\epsilon} Z_{q2mCe} + Q^2(m^2)^2(\mu^2)^{-\epsilon} Z_{qm2Ce} \\ &+ (m^2)^2(\mu^2)^{-\epsilon} Z_{mCe}\end{aligned} \tag{3.38}$$

$$\begin{aligned}=&(Z_{ce})^2\Pi_0^{C_e}(Q^2, Z_m m^2) + 2\left(Q^2 Z_{cep} + m^2 Z_{cem}\right) Z_{ce}\Pi_0^{CeP}(Q^2, Z_m m^2) \\ &+ \left(Q^2 Z_{cep} + m^2 Z_{cem}\right)^2 \Pi_0^P(Q^2, Z_m m^2) + \\ &(Q^2)^3(\mu^2)^{-\epsilon} Z_{qCe} + (Q^2)^2 m^2(\mu^2)^{-\epsilon} Z_{q2mCe} + Q^2(m^2)^2(\mu^2)^{-\epsilon} Z_{qm2Ce} + \\ &(m^2)^2(\mu^2)^{-\epsilon} Z_{mCe}\end{aligned} \tag{3.39}$$

All terms in the above renormalized correlators that are not proportional to a bare correlator are subtractive divergences, and describe divergences arizing when $x = 0$. These constants are explicitly calculated below, however, vanish upon fourier transforming to coordinate space.

In the calculations that follow, only the up and down quark masses are used, and are assumed to be equal ($m_u = m_d = m$), and very small compared to the energy scales of interest. Therefore, only terms of order m^2 are kept, and $\mathcal{O}(m^3)$ and smaller are neglected.

The scalar and chromomagnetic moment operator correlators have the same structure, only C_e and P are replaced by C_M and S, respectively.

The results for calculations for the bare correlators are described and shown in appendices .4, .6 and .7. The renormalized correlators described above, and the renormalization constants are:

$$\begin{aligned}\Pi^P(Q^2, m^2, \mu^2) =&\frac{D(R)}{128\pi^3}\left[16m^2\left(3\alpha C(R)\log^2\left(\frac{Q^2}{\mu^2}\right)\right.\right. \\ &\left.-2(\alpha C(R) + \pi)\log\left(\frac{Q^2}{\mu^2}\right) + 3\alpha C(R)(1 - 2\zeta(3))\right) \\ &+Q^2\left(131\alpha C(R) + 4\log\left(\frac{Q^2}{\mu^2}\right)\left(-17\alpha C(R) + 3\alpha C(R)\log\left(\frac{Q^2}{\mu^2}\right) - 4\pi\right)\right. \\ &\left.-48\alpha C(R)\zeta(3) + 32\pi)\right].\end{aligned} \tag{3.40}$$

The renormalization constants are

$$Z_p = 1 - \frac{3\alpha C(R)}{(4\pi)\epsilon} \tag{3.41}$$

$$Z_m = 1 - \frac{3\alpha C(R)}{(4\pi)\epsilon} \tag{3.42}$$

$$Z_{ccm} = \frac{3\alpha C(R)D(R)}{8\pi^3\epsilon^2} - \frac{\alpha C(R)D(R)}{8\pi^3\epsilon} - \frac{D(R)}{4\pi^2\epsilon} \tag{3.43}$$

$$Z_{ccp} = \frac{3\alpha C(R)D(R)}{32\pi^3\epsilon^2} - \frac{5\alpha C(R)D(R)}{64\pi^3\epsilon} - \frac{D(R)}{8\pi^2\epsilon} \tag{3.44}$$

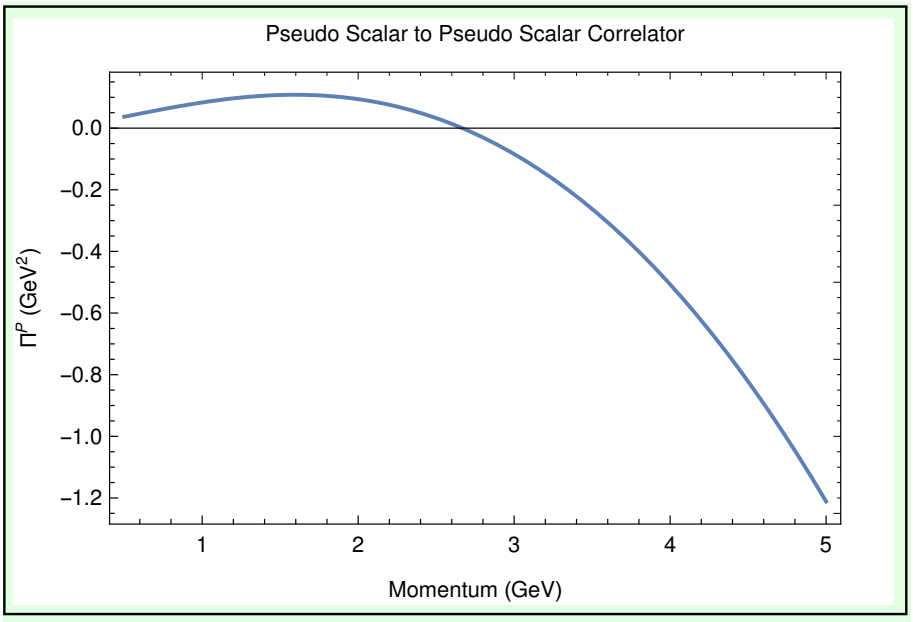

Figure 3.4: Pseudo Scalar to Pseudo Scalar correaltor as a function of momentum

Figure 3.4 is a plot of the pseudo scalar to pseudo scalar correlator. The renormalization point is set to $1GeV$, and the quark mass is set to $1.5MeV$. The correlator increases up until about $1.7GeV$ and then because to decline. Shifting the renormalization point changes both the height and position of the maximum. Increasing the renormalization point increases the maximum, and causes it to occur at higher momenta. Decreasing the renormalization point

has the opposite effect. As the momentum scale increases, the maximum decreases, until eventually the correlator becomes a decreasing function.

The result for the renormalized Scalar to Scalar correlator is

$$\begin{aligned}\Pi^S(Q^2,m^2,\mu^2) =&\frac{D(R)}{128\pi^3}\left[16m^2\left(-9\alpha C(R)\log^2\left(\frac{Q^2}{\mu^2}\right)+6(5\alpha C(R)+\pi)\log\left(\frac{Q^2}{\mu^2}\right)\right.\right.\\ &+\alpha C(R)(18\zeta(3)-47)-8\pi)+Q.Q\left(-131\alpha C(R)+4\log\left(\frac{Q^2}{\mu^2}\right)(17\alpha C(R)\right.\\ &\left.\left.-3\alpha C(R)\log\left(\frac{Q^2}{\mu^2}\right)+4\pi\right)+48\alpha C(R)\zeta(3)-32\pi\right)\Bigg]\end{aligned} \tag{3.45}$$

with renormalization constants

$$Z_s = 1-\frac{3\alpha C(R)}{(4\pi)\epsilon} \tag{3.46}$$

$$Z_m = 1-\frac{3\alpha C(R)}{(4\pi)\epsilon} \tag{3.47}$$

$$Z_{ssq} = \frac{3\left(-80\pi^3\alpha C(R)D(R)\right)}{2560\pi^6\epsilon^2}+\frac{-100\pi^3\alpha C(R)D(R)-160\pi^4D(R)}{1280\pi^6\epsilon} \tag{3.48}$$

$$Z_{ssm} = \frac{3\left(-960\pi^3\alpha C(R)D(R)\right)}{2560\pi^6\epsilon^2}+\frac{-480\pi^3\alpha C(R)D(R)-960\pi^4D(R)}{1280\pi^6\epsilon} \tag{3.49}$$

Figure 3.5 is as a plot of the scalar to scalar correlator. Its behavior appears to be the opposite of the pseudo scalar to pseudo scalar correlator. It begins decreasing, and at momenta of about $1.7GeV$, the correlator starts to increase. This opposite behavior is caused by the absense of the γ_5 matrix. Several terms in the pseudo scalar to pseudo scalar correlator will have a minus sign, relative to the scalar correlator. As the momentum scale increases, the minimum begins to disappear, and the correlator becomes an increasing function.

The renormalized CEDM to Pseudo Scalar correlator is

$$\begin{aligned}\Pi^{C_eP}(Q^2,m^2,\mu^2) =&\frac{C(R)D(R)}{384\pi^3}\alpha\left[(Q^2)^2\left(35-12\log\left(\frac{Q^2}{\mu^2}\right)\right)\right.\\ &\left.-3Q^2m^2\left(4\log\left(\frac{Q^2}{\mu^2}\right)\left(3\log\left(\frac{Q^2}{\mu^2}\right)-5\right)+11\right)\right],\end{aligned} \tag{3.50}$$

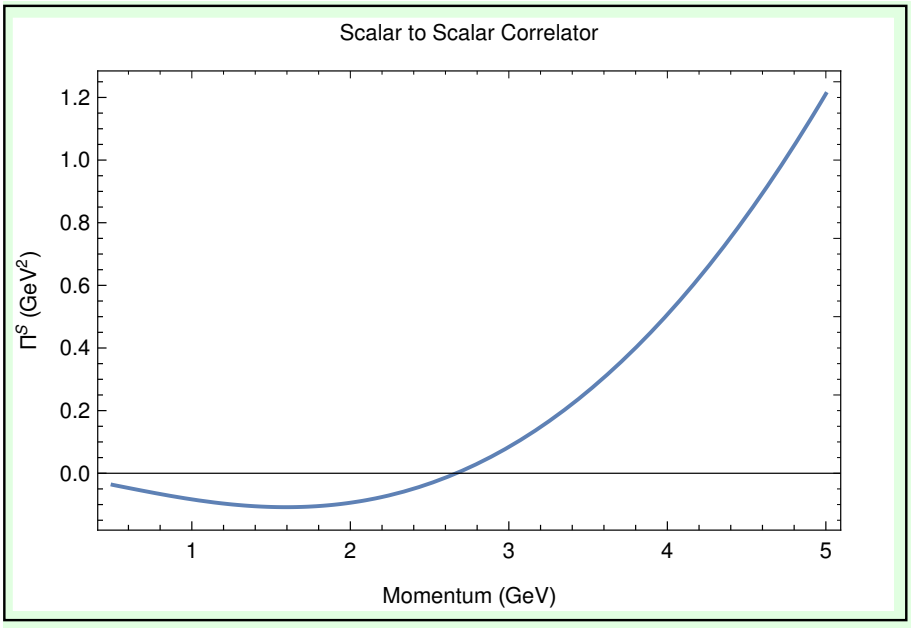

Figure 3.5: Scalar to Scalar correaltor as a function of momentum

with renormalization constants

$$Z_{cep} = 0 \tag{3.51}$$

$$Z_{cem} = \frac{6\alpha C(R)}{(4\pi)\epsilon} \tag{3.52}$$

$$Z_{qCeP} = -\frac{\alpha C(R) D(R)}{64\pi^3 \epsilon} \tag{3.53}$$

$$Z_{qmCeP} = \frac{\alpha C(R) D(R)(7\epsilon + 6)}{64\pi^3 \epsilon^2} \tag{3.54}$$

Figure 3.6 is a plot of the CEDM to pseudo scalar correlator. Again, the renormalization point was set to $1GeV$, and the quark mass was set to $1.5MeV$. The correlator appears to increase until it reaches a max at around $3.5GeV$, and then decreases. It's peak is smaller than the pseudo scalar to pseudo scalar correlator, and does not decrease as fast.

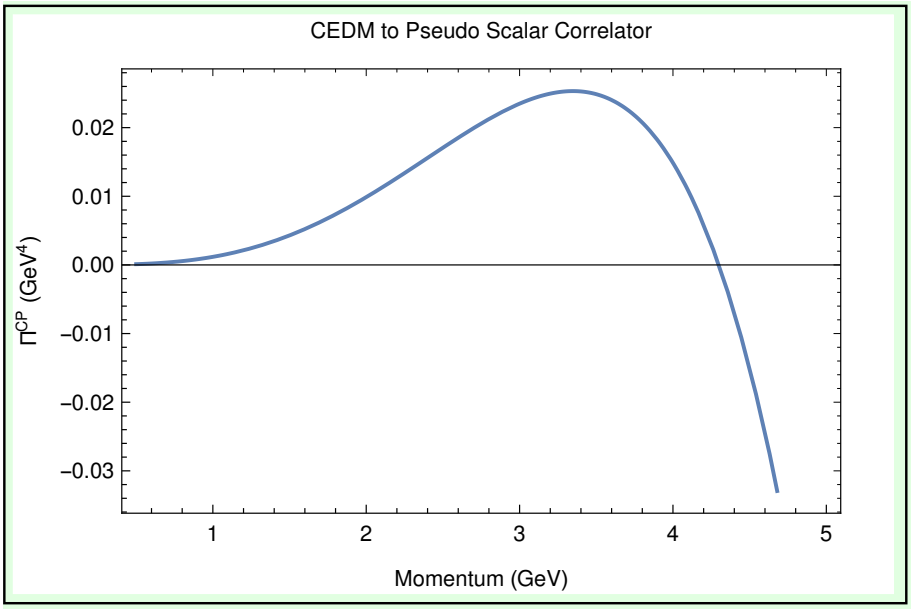

Figure 3.6: CEDM to Pseudo Scalar correaltor as a function of momentum

The renormalized CMDM to Scalar correlator is

$$\Pi^{C_m S}(Q^2, m^2, \mu^2) = \alpha \frac{C(R)D(R)}{384\pi^3} \left[3Q^2 m_r^2 \left(4 \log\left(\frac{Q^2}{\mu^2}\right) \left(3 \log\left(\frac{Q^2}{\mu^2}\right) - 5 \right) + 11 \right) + (Q^2)^2 \left(12 \log\left(\frac{Q^2}{\mu^2}\right) - 35 \right) \right], \tag{3.55}$$

with renormalization constants

$$Z_{cmp} = 0 \tag{3.56}$$

$$Z_{cmm} = \frac{\alpha(6C(R))}{(4\pi)\epsilon} \tag{3.57}$$

$$Z_{qmCmS} = \frac{3\alpha C(R)D(R)}{32\pi^3\epsilon^2} + \frac{2240\pi^4 \alpha C(R)D(R)}{20480\pi^7\epsilon} \tag{3.58}$$

$$Z_{qCmS} = -\frac{320\pi^4 \alpha C(R)D(R)}{20480\pi^7\epsilon}. \tag{3.59}$$

Figure 3.7 is a plot of the CMDM to scalar correlator. Its parameter settings are the same as the previous plot. This plot displays behavior very similar to that of figure 3.6, only flipped over the momentum axis. This is

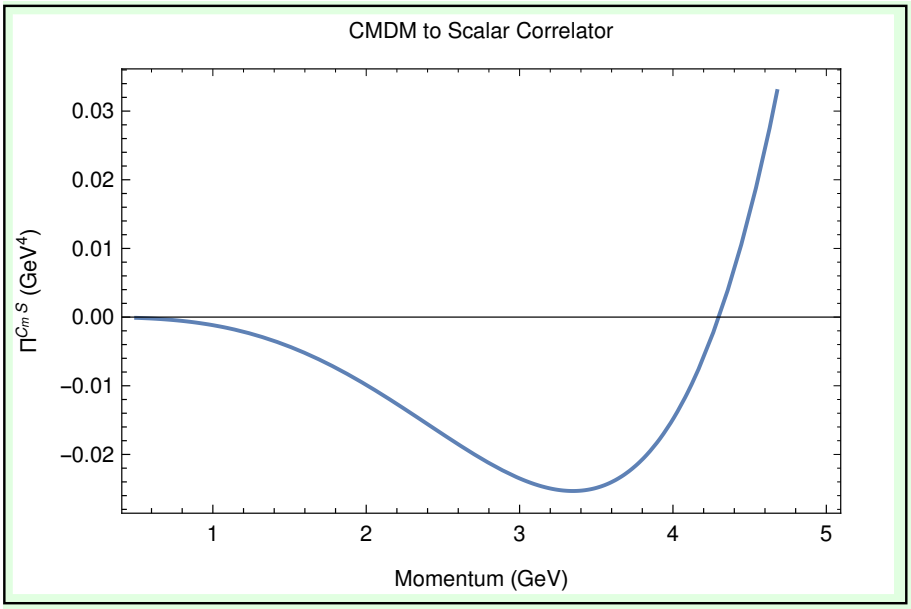

Figure 3.7: CMDM to Scalar correaltor as a function of momentum

caused by the absence of the γ_5 matrix. The correlator starts off decreasing, reaching a min at around $3.5GeV$, and begins to increase.

The renormalized CEDM to CEDM correlator is

$$\begin{aligned}\Pi^{C_e}(Q^2, m^2, \mu^2) = &- \frac{\alpha C(R) D(R)}{3981312\pi^4} \Bigg[96m^2(Q^2)^2 \left(108 \log\left(\frac{Q^2}{\mu^2}\right)(-661\alpha C(R)\right.\\ &+\alpha \log\left(\frac{Q^2}{\mu^2}\right)(126C(R) + 4n_f T(R) - 47T(A)) - 38\alpha n_f T(R) + 295\alpha T(A)\\ &+24\pi) + \alpha(132420C(R) + 8432n_f T(R) - 64399T(A)) + 5184\alpha T(A)\zeta(3)\\ &-6264\pi) + (Q^2)^3 \left(72 \log\left(\frac{Q^2}{\mu^2}\right)\left(-2724\alpha C(R) + 6\alpha \log\left(\frac{Q^2}{\mu^2}\right)(90C(R)\right.\right.\\ &+4n_f T(R) - 47T(A)) - 196\alpha n_f T(R) + 1853\alpha T(A) + 144\pi)\\ &+5\alpha(65040C(R) + 6316n_f T(R) - 54305T(A))\\ &+10368\alpha\zeta(3)(2C(R) + T(A)) - 27216\pi)\Bigg] \qquad (3.60)\end{aligned}$$

with renormalization constants

$$Z_{Ce} = 1 + \frac{\alpha(5C(R) - 2T(A))}{(4\pi)\epsilon} \tag{3.61}$$

$$Z_{qCe} = -\frac{\alpha C(R)D(R)(6\alpha C(R)(37\epsilon + 60) + 4\alpha n_f T(R)(12 - 35\epsilon) + \alpha T(A)(745\epsilon - 276) + 432\pi\epsilon)}{331776\pi^4\epsilon^2} \tag{3.62}$$

$$Z_{q2mCe} = -\frac{\alpha C(R)D(R)(12\alpha C(R)(\epsilon + 15) + 8\alpha n_f T(R)(3 - 14\epsilon) + \alpha T(A)(407\epsilon - 138) + 216\pi\epsilon)}{6912\pi^4\epsilon^2} \tag{3.63}$$

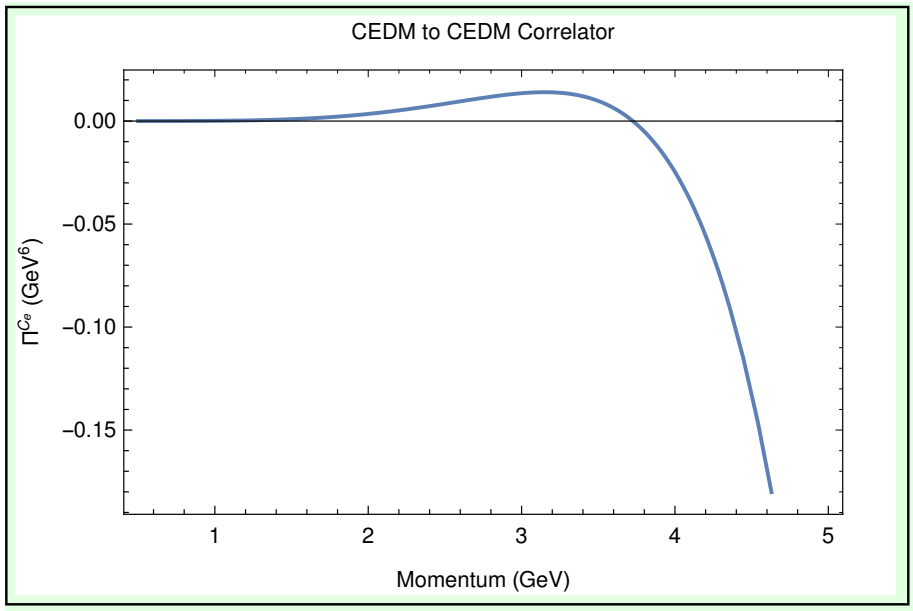

Figure 3.8: CEDM to CEDM correaltor as a function of momentum

Figure 3.8 is a plot of the CEDM to CEDM correlator. Its renormalization point μ is set to $1GeV$ and quark mass is set to $1.5MeV$. Just like the figures 3.4 and 3.6, the CEDM to CEDM correlator begins increasing, and reaches a global max of about 0.02 at roughly $3.4GeV$, and then decreases. This correlator falls off faster than the CEDM to pseudo scalar but slower than the pseudo scalar to pseudo scalar.

The renormalized CMDM to CMDM correlator is

$$\begin{aligned}\Pi^{Cm}(Q^2,m^2,\mu^2) =&\frac{C(R)D(R)\alpha}{3981312\pi^4}\Bigg[96m^2(Q^2)^2\left(108\log\left(\frac{Q^2}{\mu^2}\right)(-179\alpha C(R)\right.\\ &+\alpha\log\left(\frac{Q^2}{\mu^2}\right)(30C(R)+4n_fT(R)-23T(A))-42\alpha n_fT(R)\\ &+193\alpha T(A)+24\pi)+\alpha(30252C(R)+9992n_fT(R)-44983T(A))\\ &+5184\alpha T(A)\zeta(3)-6264\pi)\\ &+(Q^2)^3\left(72\log\left(\frac{Q^2}{\mu^2}\right)(-834\alpha C(R)\right.\\ &+6\alpha\log\left(\frac{Q^2}{\mu^2}\right)(30C(R)+4n_fT(R)-23T(A))\\ &-196\alpha n_fT(R)+1097\alpha T(A)+144\pi)+\alpha(57090C(R)\\ &+31580n_fT(R)-164281T(A))+10368\alpha\zeta(3)(2C(R)+T(A))-27216\pi)\Bigg]\end{aligned} \tag{3.64}$$

with renormalization constants

$$Z_{Cm} =1+\frac{\alpha(5C(R)-2T(A))}{(4\pi)\epsilon} \tag{3.65}$$

$$Z_{qCm} =\frac{\alpha C(R)D(R)(6\alpha C(R)(37\epsilon+60)+4\alpha n_fT(R)(12-35\epsilon)+\alpha T(A)(745\epsilon-276)+432\pi\epsilon)}{331776\pi^4\epsilon^2} \tag{3.66}$$

$$Z_{q2mCm} =-\frac{\alpha C(R)D(R)(12\alpha C(R)(8\epsilon-15)+8\alpha n_fT(R)(17\epsilon-3)+\alpha T(A)(138-491\epsilon)-216\pi\epsilon)}{6912\pi^4\epsilon^2} \tag{3.67}$$

Figure 3.9 is a plot of the CMDM to CMDM correlator in momentum space, and appears to have similar behavior to the CEDM to CEDM correlator, only flipped about the momentum axis. One noticeable difference is that the CMDM to CMDM correlator reaches its minimum at $3.4GeV$, it does not seem to increase as fast the CEDM to CEDM decreases.

The renormalization constants for the CEDM operator were computed in preparation for an RI-MOM calculation in [54], and for the CMDM in [55]. There appears to be a discrepancy in between Z_{ce} computed in this work, and in [54]. The nature of this difference is currently being investigated. However, the remaining renormalization constants for CEDM mixing, and for the CMDM are consistent.

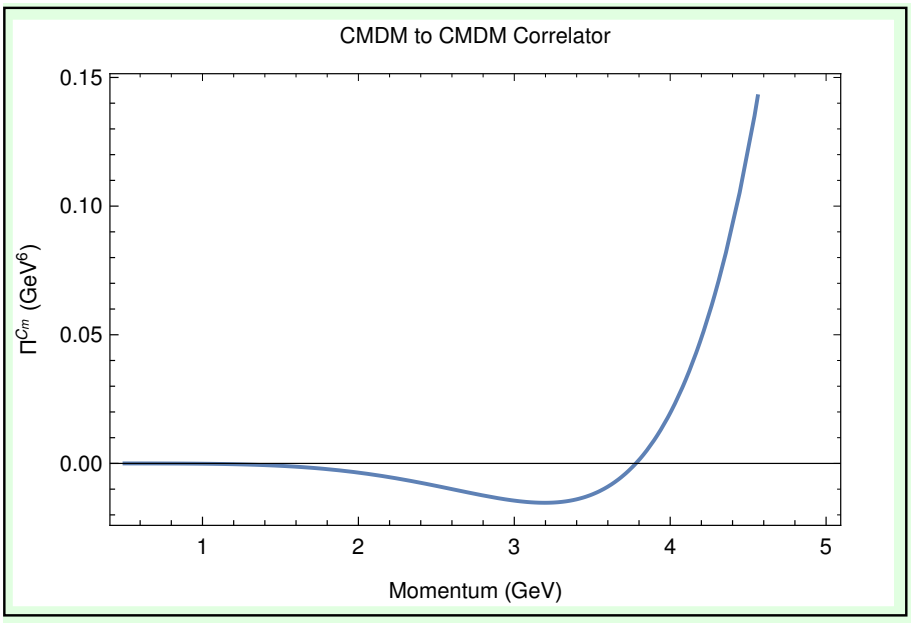

Figure 3.9: CMDM to CMDM correlator as a function of momentum

Matching Coefficient

Results obtained when computing the same physical processes in two different renormalization schemes may appear different, however, they are the same. It should therefore be possible to convert green functions expressed in one renormalization scheme, into a different scheme. Since schemes do not impact the physics, results computed on the lattice in the X-space scheme can be expressed in $\overline{MS}$. In this section, the process for computing the conversion, or matching coefficient, from the X-space scheme to $\overline{MS}$ is reviewed.

$$\langle O_i^X(x, x_0, a) O_i^X(0, x_0, a)\rangle = Z_{ij}^X(x_0, a) Z_{ik}^X(x_0, a) \langle O_j^0(x, a) O_k^0(0, a)\rangle \quad (3.68)$$

Where O_i^X is the i^{th} component of the renormalized operator vector in the $X - space$ scheme, O_i^0 is the corresponding bare operator, and Z_{ij}^X is the renormalization constant in the X-space scheme.

$$\langle O_i^{\overline{MS}}(x, \mu) O_i^{\overline{MS}}(0, \mu)\rangle = Z_{ij}^{\overline{MS}}(\mu) Z_{ik}^{\overline{MS}}(\mu) \langle O_j^0(x) O_k^0(0)\rangle \quad (3.69)$$

In the continuum ($a \to 0$), a relationship between the two schemes can be made using the bare correlators.

$$\langle O_i^{\overline{MS}}(x,\mu) O_i^{\overline{MS}}(0,\mu)\rangle = Z_{ij}^{\overline{MS}}(\mu) Z_{ik}^{\overline{MS}}(\mu) \left(Z_{lj}^X(x_0) Z_{lk}^X(x_0)\right)^{-1} \langle O_l^X(x,x_0) O_l^X(0,x_0)\rangle \tag{3.70}$$

$$= Tr\left\{\left[\left(Z^{\overline{MS}}(\mu)\right)^T Z^{\overline{MS}}(\mu)\right]\left[\left(Z^X(x_0)\right)^T Z^X(x_0)\right]^{-1}\right\}\langle O_l^X(x,x_0) O_l^X(0,x_0)\rangle \tag{3.71}$$

The matching factor relating the $X-space$ scheme to $\overline{MS}$ is

$$Tr\left\{\left[\left(Z^{\overline{MS}}(\mu)\right)^T Z^{\overline{MS}}(\mu)\right]\left[\left(Z^X(x_0)\right)^T Z^X(x_0)\right]^{-1}\right\}$$

. This can be simplified at the renormalization point x_0. Using the definition of the $X-space$ scheme, line 3.71 becomes

$$\langle O_i^{\overline{MS}}(x_0,\mu) O_i^{\overline{MS}}(0,\mu)\rangle = Tr\left\{\left[\left(Z^{\overline{MS}}(\mu)\right)^T Z^{\overline{MS}}(\mu)\right]\left[\left(Z^X(x_0)\right)^T Z^X(x_0)\right]^{-1}\right\} \langle O_l(x_0) O_l(0)\rangle|_{\substack{\text{Free}\\\text{Cont}}} \tag{3.72}$$

$$Tr\left\{\left[\left(Z^{\overline{MS}}(\mu)\right)^T Z^{\overline{MS}}(\mu)\right]\left[\left(Z^X(x_0)\right)^T Z^X(x_0)\right]^{-1}\right\} = \frac{\langle O_i^{\overline{MS}}(x_0,\mu) O_i^{\overline{MS}}(0,\mu)\rangle}{\langle O_l(x_0) O_l(0)\rangle_{\substack{\text{Free}\\\text{Cont}}}} \tag{3.73}$$

The matching factor for correlators with just one operator in the X-space scheme is given by taking the square root of equation 3.73

Therefore, to obtain the matching factor, the amplitude must be computed to the desired order in $\overline{MS}$.

In what follows, the matching factors for the CP violating dimension 5 operators will be computed.

Coordinate Space Correlators

Using the fourier transform identities in appendix .2, in this section the renormalized CEDM and CMDM correlators are fourier transformed, and shown in coordinate space. These are then used to find the matching coefficients.

The coordinate space pseudo scalar to pseudo scalar correlator is

$$\Pi^P(x^2,\mu^2,m) = \int \frac{d^dq}{(2\pi)^d} e^{iq\cdot x}\Pi^P(Q^2,\mu^2,m) \tag{3.74}$$

$$\begin{aligned}=&\frac{D(R)}{4\pi^5x^6}\left[6\alpha C(R)\left(m^2x^2-2\right)\log\left(\frac{\mu^2x^2}{4}\right)+\alpha C(R)\left(m^2\left(x^2-6\right)x^2\right.\right.\\&+12\gamma_E\left(m^2x^2-2\right)+1\Big)+\pi\left(m^2x^4-4\right)6\alpha C(R)\left(m^2x^2-2\right)\log\left(\frac{\mu^2x^2}{4}\right)\\&\left.+\alpha C(R)\left(m^2\left(x^2-6\right)x^2+12\gamma_E\left(m^2x^2-2\right)+1\right)+\pi\left(m^2x^4-4\right)\right]\end{aligned} \tag{3.75}$$

The pseudo scalar to pseudo scalar matching factor is

$$\begin{aligned}=&\frac{1}{\pi(m^2x^2-4)}\left[(1-24\gamma_E)\alpha C(R)+6\alpha C(R)\left(m^2x^2-2\right)\log\left(\frac{\mu^2x^2}{4}\right)\right.\\&\left.+\alpha C(R)m^2\left(x^2+12\gamma-6\right)x^2+\pi\left(m^2x^4-4\right)\right]\end{aligned} \tag{3.76}$$

Figure 3.10 is a plot of the pseudo scalar to pseudo scalar matching factor as a function of distance. The renormalization point μ is set to $1GeV$, the coupling α is set to 0.1 and quark mass is set to $1.5MeV$. For small distances, the matching is small, and increases with distance.

The coordinate space scalar to scalar correlator is

$$\Pi^S(x^2,\mu^2,m) = \int \frac{d^dQ}{(2\pi)^d} e^{iQ\cdot x}\Pi^S(Q^2,\mu^2,m) \tag{3.77}$$

$$\begin{aligned}=&\frac{D(R)}{4\pi^5x^6}\left[2(1+6\gamma_E)\alpha C(R)-3m^2x^2\left(2(1+3\gamma_E)\alpha C(R)+3\alpha C(R)\log\left(\frac{\mu^2x^2}{4}\right)\right.\right.\\&\left.\left.+\pi\right)+6\alpha C(R)\log\left(\frac{\mu^2x^2}{4}\right)+4\pi\right]\end{aligned} \tag{3.78}$$

The matching factor for the scalar to scalar correlator is

$$\begin{aligned}=&\frac{1}{\pi(4-3m^2x^2)}\left[3\alpha C(R)\left(2-3m^2x^2\right)\log\left(\frac{\mu^2x^2}{4}\right)\right.\\&\left.+2\alpha C(R)\left(-3(1+3\gamma_E)m^2x^2+6\gamma_E+1\right)+\pi\left(4-3m^2x^2\right)\right]\end{aligned} \tag{3.79}$$

Figure 3.11 is a plot of the scalar to scalar matching factor. Similarly to the psuedo scalar matching factor, it increases with distance, however, it does not increase as fast.

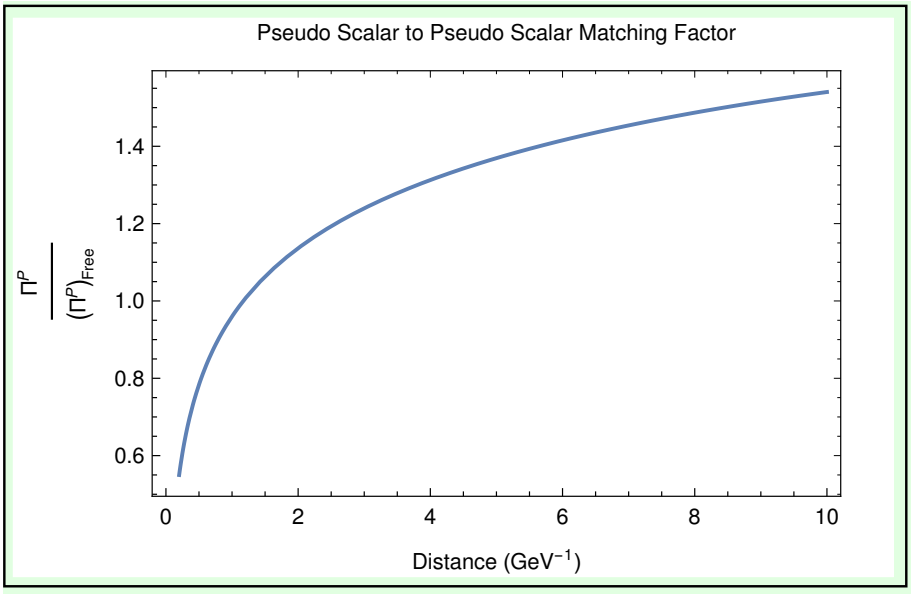

Figure 3.10: Pseudo Scalar to Pseudo Scalar matching factor as a function of distance

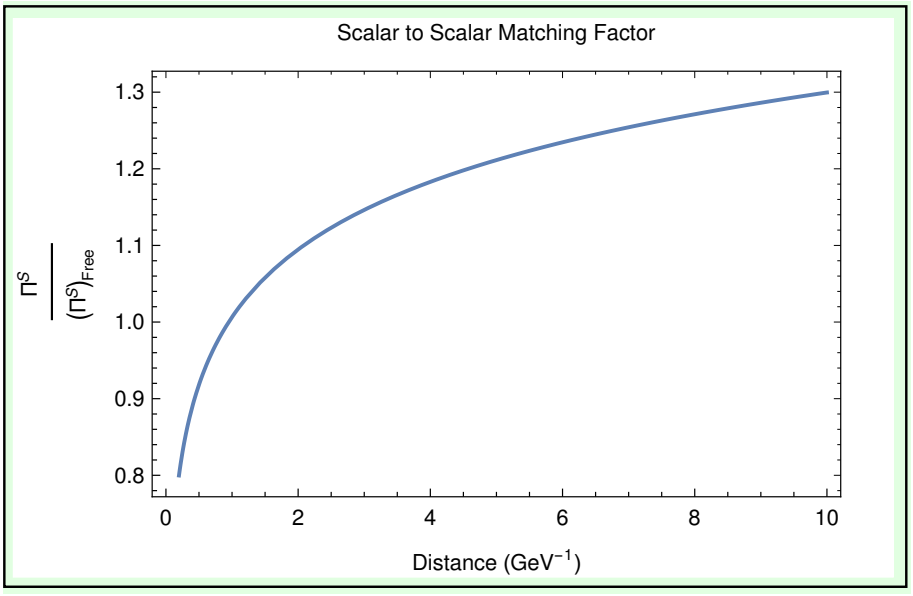

Figure 3.11: Scalar to Scalar matching factor as a function of distance

In coordinate space, the CEDM to pseudo scalar correlator is

$$\Pi^{C_e P}(x^2,\mu^2,m) = \int \frac{d^dQ}{(2\pi)^d} e^{iQ\cdot x}\Pi^{C_e P}(Q^2,\mu^2,m) \tag{3.80}$$

$$= \frac{\alpha C(R) D(R)}{2\pi^5 x^8}\left[m^2x^2\left(3\log\left(\frac{\mu^2x^2}{4}\right)+6\gamma_E-5\right)+12\right] \tag{3.81}$$

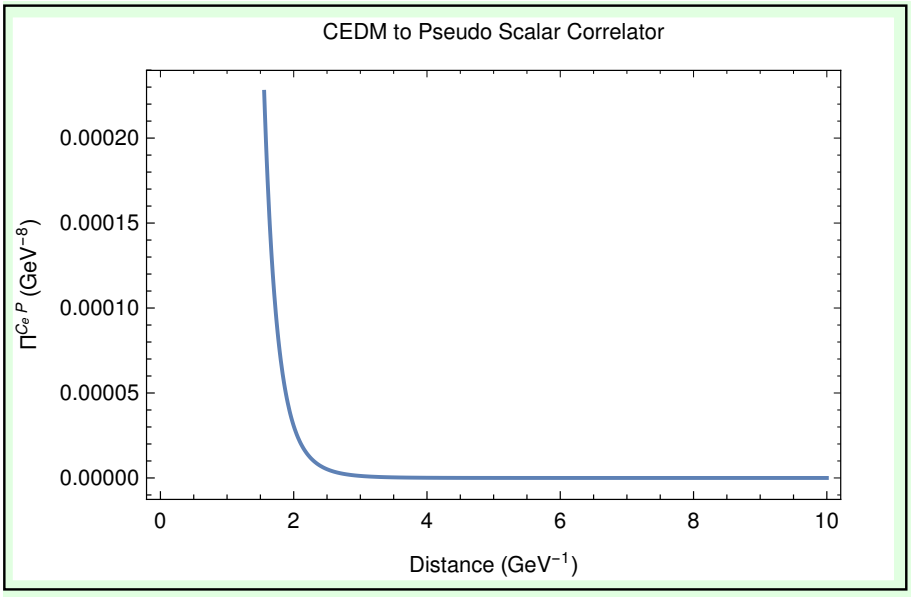

Figure 3.12: CEDM to Pseudo Scalar correlator as a function of distance

Figure 3.12 is a plot of the CEDM to pseudo scalar correlator with distance. At small distances, the correlator is dominated by the $\frac{1}{x^8}$ term in the correlator. As the distance increases, the correlator decreases, assymptoting the distance axis.

The coordinate space CMDM to scalar correlator is

$$\Pi^{C_m S}(x^2,\mu^2,m) = \int \frac{d^dQ}{(2\pi)^d} e^{iQ\cdot x}\Pi^{C_m S}(Q^2,\mu^2,m) \tag{3.82}$$

$$= -\frac{\alpha C(R) D(R)}{2\pi^5 x^8}\left[m^2x^2\left(3\log\left(\frac{\mu^2x^2}{4}\right)+6\gamma_E-5\right)+12\right] \tag{3.83}$$

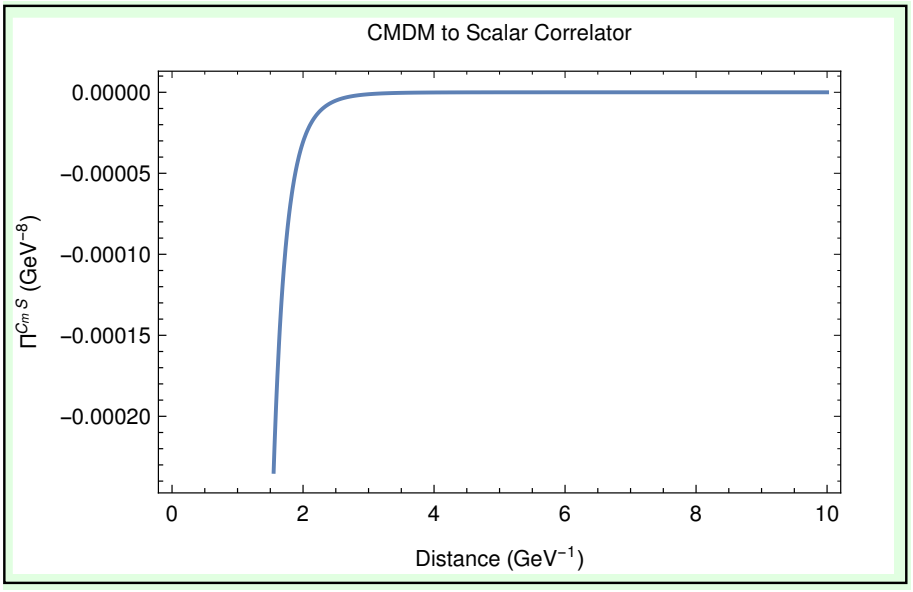

Figure 3.13: CMDM to Scalar correlator as a function of distance

Figure 3.13 is a plot of the CMDM to scalar correlator as a function of distance. At small distances, the $-\frac{1}{x^8}$ term dominates the correlator. Correlator is a constantly increasing function, and assymptotes the distance axis.

In coordinate space, the CEDM to CEDM correlator is

$$\begin{aligned}\Pi^{Ce}(x^2,\mu^2,m) &= \int \frac{d^dQ}{(2\pi)^d} e^{iQ\cdot x}\Pi^{Ce}(Q^2,\mu^2,m)\\ &= \frac{C(R)D(R)\alpha}{6\pi^6 x^{10}}\left[-12\alpha\log\left(\mu^2x^2\right)\left(^2x^2(126C(R)+4n_fT(R)\right.\right.\\ &\quad -47T(A))-180C(R)-8n_fT(R)+94T(A))\\ &\quad +\alpha m^2x^2((3057-3024\gamma_E)C(R)-96\gamma_En_fT(R)+46n_fT(R)\\ &\quad +1128\gamma_ET(A)-995T(A))+24\alpha\log(2)\left(m^2x^2(126C(R)+4n_fT(R)\right.\\ &\quad -47T(A))-180C(R)-8n_fT(R)+94T(A))+3\alpha(8(180\gamma_E-239)C(R)\\ &\quad \left.\left.+64\gamma_En_fT(R)-60n_fT(R)-752\gamma_ET(A)+855T(A))+72\pi\left(m^2x^2-2\right)\right]\end{aligned} \tag{3.84}$$

The CEDM to CEDM matching factor is

$$
\begin{aligned}
=&\frac{1}{72\pi D(A)T(R)\left(m^2x^2-2\right)}\Big[C(R)D(R)\left(-12\alpha\log\left(\mu^2x^2\right)\left(m^2x^2(126C(R)+4n_fT(R)\right.\right.\\
&-47T(A))-180C(R)-8n_fT(R)+94T(A))+\alpha m^2x^2((3057-3024\gamma_E)C(R)\\
&+2(23-48\gamma_E)n_fT(R)+(1128\gamma_E-995)T(A))+24\alpha\log(2)\left(m^2x^2(126C(R)\right.\\
&+4n_fT(R)-47T(A))-180C(R)-8n_fT(R)+94T(A))\\
&+3\alpha(8(180\gamma_E-239)C(R)+4(16\gamma_E-15)n_fT(R)+(855-752\gamma_E)T(A))+72\pi\left(m^2x^2-2\right)\Big)\Big]
\end{aligned}
\tag{3.85}
$$

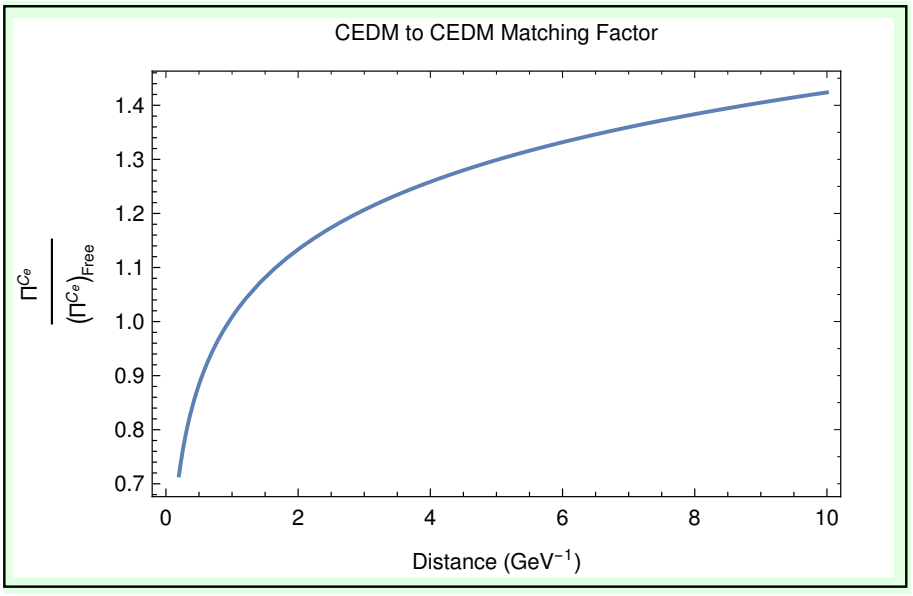

Figure 3.14: CEDM to CEDM matching factor as a function of distance

Figure 3.14 is a plot of the CEDM to CEDM matching factor as a function of distance. It increases with distance, and behaves similarly to the pseudo scalar to pseudo scalar, and scalar to scalar matching factors.

The coordinate space CMDM to CMDM correlator is

$$\begin{aligned}\Pi^{Cm}(x^2,\mu^2,m) =& \int \frac{d^dQ}{(2\pi)^d} e^{iQ\cdot x}\Pi^{Ce}(Q^2,\mu^2,m)\\ =&\frac{C(R)D(R)\alpha}{6\pi^6x^{10}}\left[12\alpha\left(m^2x^2-2\right)\log\left(\mu^2x^2\right)(30C(R)+4n_fT(R)\right.\\ &-23T(A))+\alpha m^2x^2((720\gamma_E-663)C(R)+96\gamma_En_fT(R)\\ &-34n_fT(R)-552\gamma_ET(A)+341T(A))-24\alpha\log(2)\left(m^2x^2-2\right)(30C(R)\\ &+4n_fT(R)-23T(A))-3\alpha((480\gamma_E-662)C(R)\\ &\left.+64\gamma_En_fT(R)-60n_fT(R)-368\gamma_ET(A)+355T(A))-72\pi\left(m^2x^2-2\right)\right],\end{aligned} \tag{3.86}$$

and the CMDM to CMDM matching factor is

$$\begin{aligned}=&\frac{1}{72}\left[-\frac{\alpha m^2x^2((720\gamma_E-663)C(R)+2(48\gamma_E-17)n_fT(R)+(341-552\gamma_E)T(A))}{\pi\left(m^2x^2-2\right)}\right.\\ &+\frac{3\alpha((480\gamma_E-662)C(R)+4(16\gamma_E-15)n_fT(R)+(355-368\gamma_E)T(A))}{\pi\left(m^2x^2-2\right)}\\ &+\frac{24\alpha\log(2)(30C(R)+4n_fT(R)-23T(A))}{\pi}\\ &\left.-\frac{12\alpha\log\left(\mu^2x^2\right)(30C(R)+4n_fT(R)-23T(A))}{\pi}+72\right]\end{aligned} \tag{3.87}$$

Figure 3.15 is a plot of the CMDM to CMDM matching factor and is an increasing function of distance.

Due to assymptotic freedom, the small distance behavior of figures 3.10, 3.11, 3.14, and 3.15 is expected to approach 1 (i.e. α should approach 0). The fact that they do not shows that, at these energy scales, either more terms in the perturbative series are needed, or the renormalization point must be run to higher energies for a physical result at small distances.

RG Flow

In order to express correlators computed at renormalization point μ as correlators at μ', one must add up results from infinitesimal changes in μ. This is done using the renormalization group equation

$$\frac{d}{d\ln\mu^2}\Pi=\left(\frac{\partial}{\partial\ln\mu^2}-\beta\alpha\frac{\partial}{\partial\alpha}-m^2\gamma_m\frac{\partial}{\partial m^2}\right)\Pi, \tag{3.88}$$

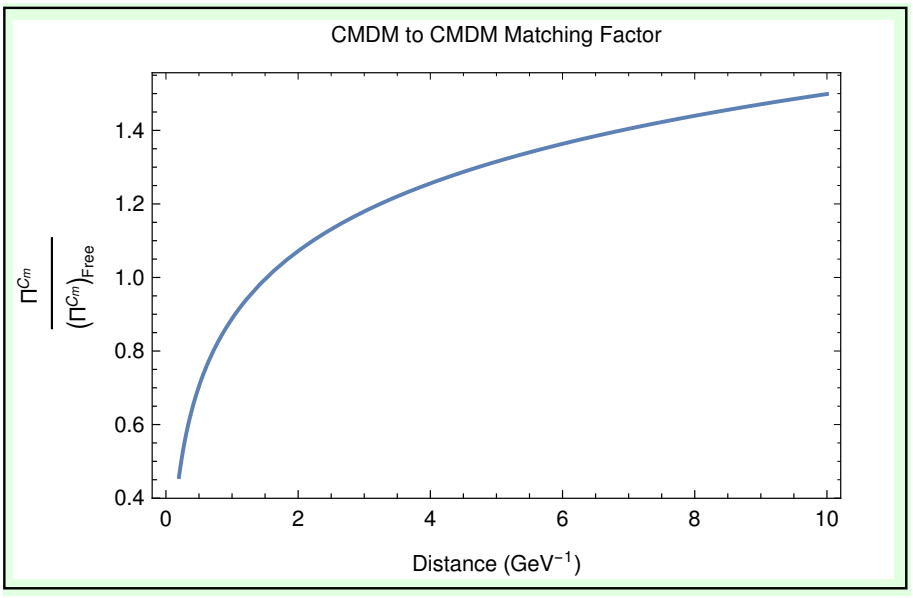

Figure 3.15: CMDM to CMDM matching factor as a function of distance

and integrating over μ. Rearranging equation (3.88) to solve for the partial derivative with respect to μ simplifies the integration

$$\frac{\partial}{\partial \ln \mu^2}\Pi = \frac{d}{d \ln \mu^2}\Pi + \beta\alpha\frac{\partial}{\partial \alpha}\Pi + m^2\gamma_m\frac{\partial}{\partial m^2}\Pi \tag{3.89}$$

Equation (3.89) is a polynomial in logarithms of μ

Anomalous Dimension

In this section, the analysis of Collins [56] is followed to find the multiplicative anomalous dimension for the renormalized dimension 5 operators. The renormalized cedm operator in equation (3.32) can be written

$$[C_e] = M[C_e]_0, \tag{3.90}$$

where M is the mixing matrix, $[C_e]$ is the renormalized CEDM vector and $[C_e]_0$ is the bare CEDM vector. All of the μ dependence on the right hand side of equation (3.90) is contained in the mixing matrix M. Therefore, the

anomalous dimension can be found by differentiating C_e with respect to $\ln \mu^2$.

$$\begin{aligned}\frac{d}{d\ln\mu^2}[C_e] =& \frac{d}{d\ln\mu^2} M[C_e]_0 \\ =& \frac{dM}{d\ln\mu^2} M^{-1}[C_e] = \gamma_c[C_e].\end{aligned} \tag{3.91}$$

The derivative in equation 3.91 is initially taken in d dimensions. Using the renormalization group equations and coefficients in appendix .8, the matrix γ_c can be found. In $d = 4$ dimensions, to order α, it is

$$\begin{aligned}\gamma_c =& \begin{pmatrix} \gamma_{ce} & \gamma_{cep} & \gamma_{cem} \\ 0 & \gamma_{Pq} & 0 \\ 0 & 0 & \gamma_{Pm} \end{pmatrix} \\ =& \frac{\alpha}{4\pi} \begin{pmatrix} -(2T(A) - 5C(R)) & 0 & -\left(\frac{11}{3}T(A) - \frac{4}{3}n_f T(R)\right) \\ 0 & 3C(R) & 0 \\ 0 & 0 & 6C(R) \end{pmatrix}\end{aligned} \tag{3.92}$$

The anomalous dimension for the chromomagnetic moment operator, γ_{cm} is

$$\gamma_{cm} = \begin{pmatrix} \gamma_M & \gamma_{Mes} & \gamma_{Mem} \\ 0 & \gamma_{Sq} & 0 \\ 0 & 0 & \gamma_{Sm} \end{pmatrix}, \tag{3.93}$$

and is numerically the same as the chromoelectric dipole moment anomalous dimension.

In momentum space, the anomalous dimension is more complicated because it includes the contact terms. These terms however, do not appear in the coordinate space correlators, and are also specific to this particular correlator. The anomalous dimension matrix computed in this section accounts for the evolution of the the correlator in coordinate space, and will be used to evolve the CEDM or CMDM any time they appear in a correlator (such as equations 3.4 and 3.5).

Correlator Running

Using the RGE equation (3.89), the renormalization group coefficients computed in appendix .8 and the α as a function of μ,

$$\alpha(\mu) = \frac{12\pi}{12\pi + (4n_f T(R) - 11T(A)) \log\left(\frac{\mu^2}{\Lambda^2}\right)}, \tag{3.94}$$

the renormalization group flow of the correlators was computed. When matching the lattice correlators to the continuum correlators, the spatial dependence should be the same. Differences should come from the $\overline{MS}$ renormalization scale μ, and lattice spacing a. By computing the running of these correlators, the renormalization point μ can be tuned for a better match. Here, we present results still in preparation.

The running of the pseudo scalar to pseudo scalar correlator is

$$\begin{aligned}\Pi^P(Q^2,\mu_2) =&\frac{D(R)}{768\pi^4}\Big[Q^2\left(2C(R)(11T(A)-4n_fT(R))\alpha(\mu_1)^2\log^3\left(\mu_1^2\right)\right.\\
&+C(R)\alpha(\mu_1)(187T(A)\alpha(\mu_1)-68n_fT(R)\alpha(\mu_1)+(24n_fT(R)\alpha(\mu_1)\\
&-66T(A)\alpha(\mu_1))\log(Q^2)+72\pi)\log^2\left(\mu_1^2\right)+2\Bigg(3C(R)(11T(A)-4n_fT(R))\log^2(Q^2)\alpha\\
&-4n_fT(R))\log\left(\frac{Q^2}{\mu_1^2}\right)\alpha(\mu_1)^2+C(R)(-187T(A)\alpha(\mu_1)+68n_fT(R)\alpha(\mu_1)\\
&-72\pi)\log(Q^2)\alpha(\mu_1)+12\pi(17C(R)\alpha(\mu_1)+4\pi)\Big)\log\left(\mu_1^2\right)\\
&-\log\left(\mu_2^2\right)\left(2C(R)(11T(A)-4n_fT(R))\log^2\left(\mu_2^2\right)\alpha(\mu_2)^2+6C(R)(11T(A)\right.\\
&-4n_fT(R))\log^2(Q^2)\alpha(\mu_2)^2+6C(R)(4n_fT(R)-11T(A))\log^2\left(\frac{Q^2}{\mu_2^2}\right)\alpha(\mu_2)^2\\
&+34C(R)(11T(A)-4n_fT(R))\log\left(\frac{Q^2}{\mu_2^2}\right)\alpha(\mu_2)^2-2C(R)(187T(A)\alpha(\mu_2)\\
&-68n_fT(R)\alpha(\mu_2)+72\pi)\log(Q^2)\alpha(\mu_2)+C(R)\log\left(\mu_2^2\right)(187T(A)\alpha(\mu_2)\\
&-68n_fT(R)\alpha(\mu_2)+(24n_fT(R)\alpha(\mu_2)-66T(A)\alpha(\mu_2))\log(Q^2)+72\pi)\alpha(\mu_2)\\
&+24\pi(17C(R)\alpha(\mu_2)+4\pi)))+8\left(C(R)m(\mu_1)^2(-36C(R)\right.\\
&+11T(A)-4n_fT(R))\alpha(\mu_1)^2\log^3\left(\mu_1^2\right)+C(R)m(\mu_1)^2(36C(R)\\
&-11T(A)+4n_fT(R))\alpha(\mu_1)^2(3\log(Q^2)-1)\log^2\left(\mu_1^2\right)+m(\mu_1)^2\left(-3C(R)(36C(R)\right.\\
&-11T(A)+4n_fT(R))\log^2(Q^2)\alpha(\mu_1)^2-3C(R)(36C(R)m(\mu_1)+11T(A)\\
&-4n_fT(R))\log^2\left(\frac{Q^2}{\mu_1^2}\right)\alpha(\mu_1)^2+2C(R)(36C(R)-11T(A)\\
&+4n_fT(R))\log(Q^2)\alpha(\mu_1)^2+2C(R)((11T(A)-4n_fT(R))\alpha(\mu_1)\\
&+36m(\mu_1)(C(R)\alpha(\mu_1)+\pi))\log\left(\frac{Q^2}{\mu_1^2}\right)\alpha(\mu_1)+12\left(9C(R)^2(m(\mu_1)+1)(-1\right.\\
&\left.+2\zeta(3))\alpha(\mu_1)^2+2C(R)\pi\alpha(\mu_1)+2\pi^2\right)\Big)\log\left(\mu_1^2\right)\\
&-m(\mu_2)^2\log\left(\mu_2^2\right)\left(-108C(R)^2\alpha(\mu_2)^2+C(R)(-36C(R)+11T(A)\right.\\
&-4n_fT(R))\log^2\left(\mu_2^2\right)\alpha(\mu_2)^2-3C(R)(36C(R)-11T(A)\\
&+4n_fT(R))\log^2(Q^2)\alpha(\mu_2)^2-108C(R)^2m(\mu_2)\log^2\left(\frac{Q^2}{\mu_2^2}\right)\alpha(\mu_2)^2\\
&-33C(R)T(A)\log^2\left(\frac{Q^2}{\mu_2^2}\right)\alpha(\mu_2)^2+12C(R)n_fT(R)\log^2\left(\frac{Q^2}{\mu_2^2}\right)\alpha(\mu_2)^2\\
&-108C(R)^2m(\mu_2)\alpha(\mu_2)^2+2C(R)(36C(R)-11T(A)+4n_fT(R))\log(Q^2)\alpha(\mu_2)^2\\
&+C(R)(36C(R)-11T(A)+4n_fT(R))\log\left(\mu_2^2\right)(3\log(Q^2)-1)\alpha(\mu_2)^2\\
&+72C(R)^2m(\mu_2)\log\left(\frac{Q^2}{\mu_2^2}\right)\alpha(\mu_2)^2+22C(R)T(A)\log\left(\frac{Q^2}{\mu_2^2}\right)\alpha(\mu_2)^2\\
&-8C(R)n_fT(R)\log\left(\frac{Q^2}{\mu_2^2}\right)\alpha(\mu_2)^2\\
&+216C(R)^2\zeta(3)\alpha(\mu_2)^2+216C(R)^2m(\mu_2)\zeta(3)\alpha(\mu_2)^2\\
&\left.\left.+72C(R)m(\mu_2)\pi\log\left(\frac{Q^2}{\mu_2^2}\right)\alpha(\mu_2)+24C(R)\pi\alpha(\mu_2)+24\pi^2\right)\right)\Big]\end{aligned}\tag{3.95}$$

The running of the scalar to scalar correlator is

$$\begin{aligned}
\Pi^S(Q^2,\mu_2) =& \frac{D(R)}{768\pi^4}\Big[\log\left(\mu_2^2\right)\Big(24m(\mu_2)^2\Big(-564\alpha(\mu_2)^2C(R)^2(m(\mu_2)+1)\\
&+24\pi\alpha(\mu_2)C(R)(1-4m(\mu_2))+\alpha(\mu_2)C(R)\left(\alpha(\mu_2)\left(-\log\left(\frac{Q^2}{\mu_2^2}\right)\left(3\log\left(\frac{Q^2}{\mu_2^2}\right)\right.\right.\right.\\
&-10\Big)\left(36C(R)m(\mu_2)-4n_fT(R)+11T(A)\right)+216C(R)(m(\mu_2)+1)\zeta(3)\\
&+\log\left(\mu_2^2\right)\left(3\log(Q^2)-5\right)\left(36C(R)+4n_fT(R)-11T(A)\right)-3\log^2(Q^2)\left(36C(R)\right.\\
&\left.+4n_fT(R)-11T(A)\right)+10\log(Q^2)\left(36C(R)+4n_fT(R)-11T(A)\right)\\
&\left.+\log^2\left(\mu_2^2\right)\left(-36C(R)-4n_fT(R)+11T(A)\right)\right)+72\pi m(\mu_2)\log\left(\frac{Q^2}{\mu_2^2}\right)\Big)+24\pi^2\Big)\\
&+Q^2\Big(24\pi(17\alpha(\mu_2)C(R)+4\pi)+\alpha(\mu_2)C(R)\Big(\log\left(\mu_2^2\right)\left(6\alpha(\mu_2)\log(Q^2)(4n_fT(R)\right.\\
&-11T(A))-68\alpha(\mu_2)n_fT(R)+187\alpha(\mu_2)T(A)+72\pi\Big)+2\alpha(\mu_2)(11T(A)\\
&-4n_fT(R))\left(17-3\log\left(\frac{Q^2}{\mu_2^2}\right)\right)\log\left(\frac{Q^2}{\mu_2^2}\right)+6\alpha(\mu_2)\log^2(Q^2)(11T(A)\\
&-4n_fT(R))-2\log(Q^2)(-68\alpha(\mu_2)n_fT(R)+187\alpha(\mu_2)T(A)+72\pi)\\
&\left.+\log^2\left(\mu_2^2\right)\left(22\alpha(\mu_2)T(A)-8\alpha(\mu_2)n_fT(R)\right)\right)\Big)\Big)\\
&-\log\left(\mu_1^2\right)\Big(24m(\mu_1)^2\Big(-564\alpha(\mu_1)^2C(R)^2(m(\mu_1)+1)+24\pi\alpha(\mu_1)C(R)(1\\
&-4m(\mu_1))+\alpha(\mu_1)C(R)\left(\alpha(\mu_1)\left(-\log\left(\frac{Q^2}{\mu_1^2}\right)\left(3\log\left(\frac{Q^2}{\mu_1^2}\right)\right.\right.\right.\\
&-10\Big)\left(36C(R)m(\mu_1)-4n_fT(R)+11T(A)\right)+216C(R)(m(\mu_1)+1)\zeta(3)\\
&+\log\left(\mu_1^2\right)\left(3\log(Q^2)-5\right)\left(36C(R)+4n_fT(R)-11T(A)\right)-3\log^2(Q^2)\left(36C(R)\right.\\
&\left.+4n_fT(R)-11T(A)\right)+10\log(Q^2)\left(36C(R)+4n_fT(R)-11T(A)\right)\\
&\left.+\log^2\left(\mu_1^2\right)\left(-36C(R)-4n_fT(R)+11T(A)\right)\right)+72\pi m(\mu_1)\log\left(\frac{Q^2}{\mu_1^2}\right)\Big)+24\pi^2\Big)\\
&+Q^2\Big(24\pi(17\alpha(\mu_1)C(R)+4\pi)+\alpha(\mu_1)C(R)\Big(\log\left(\mu_1^2\right)\left(6\alpha(\mu_1)\log(Q^2)(4n_fT(R)\right.\\
&-11T(A))-68\alpha(\mu_1)n_fT(R)+187\alpha(\mu_1)T(A)+72\pi\Big)+2\alpha(\mu_1)(11T(A)\\
&-4n_fT(R))\left(17-3\log\left(\frac{Q^2}{\mu_1^2}\right)\right)\log\left(\frac{Q^2}{\mu_1^2}\right)+6\alpha(\mu_1)\log^2(Q^2)(11T(A)\\
&-4n_fT(R))-2\log(Q^2)(-68\alpha(\mu_1)n_fT(R)+187\alpha(\mu_1)T(A)+72\pi)\\
&\left.+\log^2\left(\mu_1^2\right)\left(22\alpha(\mu_1)T(A)-8\alpha(\mu_1)n_fT(R)\right)\right)\Big)\Big)\Big] \qquad (3.96)
\end{aligned}$$

The pseudo scalar to CEDM correlator running is

$$\begin{aligned}\Pi^{C_eP}(Q^2,\mu_2) =&\frac{C(R)D(R)}{768\pi^4}\left[\alpha(\mu_1)\log\left(\mu_1^2\right)\left(m(\mu_1)^2Q^2\left(2\left(99\alpha(\mu_1)C(R)(m(\mu_1)+1)\right.\right.\right.\right.\\
&+\alpha(\mu_1)\log\left(\frac{Q^2}{\mu_1^2}\right)\left(3\log\left(\frac{Q^2}{\mu_1^2}\right)-5\right)(36C(R)m(\mu_1)-4n_fT(R)+11T(A))\\
&+3\alpha(\mu_1)\log^2(Q^2)(36C(R)+4n_fT(R)-11T(A))+\log(Q^2)(72\pi\\
&-5\alpha(\mu_1)(36C(R)+4n_fT(R)-11T(A)))-60\pi)\\
&+\log\left(\mu_1^2\right)(-6\alpha(\mu_1)\log(Q^2)(36C(R)+4n_fT(R)-11T(A))+5\alpha(\mu_1)(36C(R)\\
&+4n_fT(R)-11T(A))-72\pi)+2\alpha(\mu_1)\log^2\left(\mu_1^2\right)(36C(R)+4n_fT(R)\\
&-11T(A)))+(Q^2)^2\left(\alpha(\mu_1)(11T(A)-4n_fT(R))\left(\log\left(\mu_1^2\right)+2\log\left(\frac{Q^2}{\mu_1^2}\right)\right.\right.\\
&\left.\left.-2\log(Q^2)\right)+24\pi\right))-\alpha(\mu_2)\log\left(\mu_2^2\right)\left(m(\mu_2)^2Q^2\left(2\left(99\alpha(\mu_2)C(R)(m(\mu_2)+1)\right.\right.\right.\\
&+\alpha(\mu_2)\log\left(\frac{Q^2}{\mu_2^2}\right)\left(3\log\left(\frac{Q^2}{\mu_2^2}\right)-5\right)(36C(R)m(\mu_2)-4n_fT(R)+11T(A))\\
&+3\alpha(\mu_2)\log^2(Q^2)(36C(R)+4n_fT(R)-11T(A))+\log(Q^2)(72\pi\\
&-5\alpha(\mu_2)(36C(R)+4n_fT(R)-11T(A)))-60\pi)\\
&+\log\left(\mu_2^2\right)(-6\alpha(\mu_2)\log(Q^2)(36C(R)+4n_fT(R)-11T(A))+5\alpha(\mu_2)(36C(R)\\
&+4n_fT(R)-11T(A))-72\pi)+2\alpha(\mu_2)\log^2\left(\mu_2^2\right)(36C(R)+4n_fT(R)\\
&-11T(A)))+(Q^2)^2\left(\alpha(\mu_2)(11T(A)-4n_fT(R))\left(\log\left(\mu_2^2\right)+2\log\left(\frac{Q^2}{\mu_2^2}\right)\right.\right.\\
&\left.\left.\left.-2\log(Q^2)\right)+24\pi\right)\right)\Big] \qquad (3.97)\end{aligned}$$

The scalar to CMDM correlator running is

$$\begin{aligned}\Pi^{C_m S}(Q^2,\mu_2) =& \frac{C(R)D(R)}{768\pi^4}\left[\alpha(\mu_2)\log\left(\mu_2^2\right)\left(m(\mu_2)^2Q^2\left(2\left(99\alpha(\mu_2)C(R)(m(\mu_2)+1)\right.\right.\right.\right.\\
&+\alpha(\mu_2)\log\left(\frac{Q^2}{\mu_2^2}\right)\left(3\log\left(\frac{Q^2}{\mu_2^2}\right)-5\right)(36C(R)m(\mu_2)-4n_fT(R)+11T(A))\\
&+3\alpha(\mu_2)\log^2(Q^2)(36C(R)+4n_fT(R)-11T(A))+\log(Q^2)(72\pi\\
&-5\alpha(\mu_2)(36C(R)+4n_fT(R)-11T(A)))-60\pi)\\
&+\log\left(\mu_2^2\right)(-6\alpha(\mu_2)\log(Q^2)(36C(R)+4n_fT(R)-11T(A))+5\alpha(\mu_2)(36C(R)\\
&+4n_fT(R)-11T(A))-72\pi)+2\alpha(\mu_2)\log^2\left(\mu_2^2\right)(36C(R)+4n_fT(R)-11T(A))\Big)\\
&+(Q^2)^2\left(\alpha(\mu_2)(11T(A)-4n_fT(R))\left(\log\left(\mu_2^2\right)+2\log\left(\frac{Q^2}{\mu_2^2}\right)-2\log(Q^2)\right)+24\pi\right)\\
&-\alpha(\mu_1)\log\left(\mu_1^2\right)\left(m(\mu_1)^2Q^2\left(2\left(99\alpha(\mu_1)C(R)(m(\mu_1)+1)\right.\right.\right.\right.\\
&+\alpha(\mu_1)\log\left(\frac{Q^2}{\mu_1^2}\right)\left(3\log\left(\frac{Q^2}{\mu_1^2}\right)-5\right)(36C(R)m(\mu_1)-4n_fT(R)+11T(A))\\
&+3\alpha(\mu_1)\log^2(Q^2)(36C(R)+4n_fT(R)-11T(A))+\log(Q^2)(72\pi\\
&-5\alpha(\mu_1)(36C(R)+4n_fT(R)-11T(A)))-60\pi)\\
&+\log\left(\mu_1^2\right)(-6\alpha(\mu_1)\log(Q^2)(36C(R)+4n_fT(R)-11T(A))+5\alpha(\mu_1)(36C(R)\\
&+4n_fT(R)-11T(A))-72\pi)+2\alpha(\mu_1)\log^2\left(\mu_1^2\right)(36C(R)+4n_fT(R)-11T(A))\Big)\\
&+(Q^2)^2\left(\alpha(\mu_1)(11T(A)-4n_fT(R))\left(\log\left(\mu_1^2\right)+2\log\left(\frac{Q^2}{\mu_1^2}\right)-2\log(Q^2)\right)\right.\\
&\left.+24\pi)\right)] \qquad (3.98)\end{aligned}$$

The CEDM to CEDM correlator running is

$$\Pi^{C_e}(Q^2,\mu_2) = \frac{C(R)D(R)}{663552\pi^5}$$
$$\Bigg[\alpha(\mu_1)\log\left(\mu_1^2\right)\left(48m(\mu_1)^2(Q^2)^2\left(\alpha(\mu_1)\left(6\left(\alpha(\mu_1)\log^2\left(\frac{Q^2}{\mu_1^2}\right)(126C(R)\right.\right.\right.$$
$$+4n_fT(R)-47T(A))(18C(R)m(\mu_1)-4n_fT(R)+11T(A))$$
$$+\log\left(\frac{Q^2}{\mu_1^2}\right)(12\pi(36C(R)m(\mu_1)-4n_fT(R)+11T(A))-\alpha(\mu_1)(661C(R)$$
$$+38n_fT(R)-295T(A))(18C(R)m(\mu_1)-4n_fT(R)+11T(A)))$$
$$+864\alpha(\mu_1)C(R)(m(\mu_1)+1)T(A)\zeta(3)+\alpha(\mu_1)\log^2(Q^2)(126C(R)+4n_fT(R)$$
$$-47T(A))(18C(R)+4n_fT(R)-11T(A))+\log(Q^2)(24\pi(81C(R)+4n_fT(R)$$
$$-29T(A))-\alpha(\mu_1)(18C(R)+4n_fT(R)-11T(A))(661C(R)+38n_fT(R)$$
$$-295T(A))))+3\log\left(\mu_1^2\right)(-2\alpha(\mu_1)\log(Q^2)(126C(R)$$
$$+4n_fT(R)-47T(A))(18C(R)+4n_fT(R)-11T(A))+\alpha(\mu_1)(18C(R)$$
$$+4n_fT(R)-11T(A))(661C(R)+38n_fT(R)-295T(A))-24\pi(81C(R)$$
$$+4n_fT(R)-29T(A)))+2\alpha(\mu_1)\log^2\left(\mu_1^2\right)(126C(R)+4n_fT(R)$$
$$-47T(A))(18C(R)+4n_fT(R)-11T(A)))+\alpha(\mu_1)^2C(R)(m(\mu_1)$$
$$+1)(132420C(R)+8432n_fT(R)-64399T(A))-36\pi\alpha(\mu_1)(C(R)(174m(\mu_1)+835)$$
$$+38n_fT(R)-295T(A))+864\pi^2)+(Q^2)^3(\alpha(\mu_1)(2((11T(A)$$
$$-4n_fT(R))\log\left(\frac{Q^2}{\mu_1^2}\right)\left(-2724\alpha(\mu_1)C(R)+6\alpha(\mu_1)\log\left(\frac{Q^2}{\mu_1^2}\right)(90C(R)\right.$$
$$+4n_fT(R)-47T(A))-196\alpha(\mu_1)n_fT(R)+1853\alpha(\mu_1)T(A)+72\pi)$$
$$+6\alpha(\mu_1)\log^2(Q^2)(11T(A)-4n_fT(R))(-90C(R)-4n_fT(R)+47T(A))$$
$$+\log(Q^2)(\alpha(\mu_1)(11T(A)-4n_fT(R))(2724C(R)+196n_fT(R)-1853T(A))$$
$$+144\pi(45C(R)+4n_fT(R)-29T(A))))+\log\left(\mu_1^2\right)(-12\alpha(\mu_1)\log(Q^2)(11T(A)$$
$$-4n_fT(R))(-90C(R)-4n_fT(R)+47T(A))+\alpha(\mu_1)(11T(A)$$
$$-4n_fT(R))(-2724C(R)-196n_fT(R)+1853T(A))-144\pi(45C(R)+4n_fT(R)$$
$$-29T(A)))+4\alpha(\mu_1)\log^2\left(\mu_1^2\right)(11T(A)-4n_fT(R))(-90C(R)-4n_fT(R)$$
$$+47T(A)))+12\pi(\alpha(\mu_1)(-2724C(R)-196n_fT(R)+1853T(A))+144\pi)))$$
$$-\alpha(\mu_2)\log\left(\mu_2^2\right)\left(48m(\mu_2)^2(Q^2)^2\left(\alpha(\mu_2)\left(6\left(\alpha(\mu_2)\log^2\left(\frac{Q^2}{\mu_2^2}\right)(126C(R)\right.\right.\right.$$
$$+4n_fT(R)-47T(A))(18C(R)m(\mu_2)-4n_fT(R)+11T(A))$$
$$+\log\left(\frac{Q^2}{\mu_2^2}\right)(12\pi(36C(R)m(\mu_2)-4n_fT(R)+11T(A))-\alpha(\mu_2)(661C(R)$$

$$
\begin{aligned}
&+38n_fT(R)-295T(A))(18C(R)m(\mu_2)-4n_fT(R)+11T(A)))\\
&+864\alpha(\mu_2)C(R)(m(\mu_2)+1)T(A)\zeta(3)+\alpha(\mu_2)\log^2(Q^2)(126C(R)+4n_fT(R)\\
&-47T(A))(18C(R)+4n_fT(R)-11T(A))+\log(Q^2)(24\pi(81C(R)+4n_fT(R)\\
&-29T(A))-\alpha(\mu_2)(18C(R)+4n_fT(R)-11T(A))(661C(R)+38n_fT(R)\\
&-295T(A))))+3\log\left(\mu_2^2\right)(-2\alpha(\mu_2)\log(Q^2)(126C(R)+4n_fT(R)\\
&-47T(A))(18C(R)+4n_fT(R)-11T(A))+\alpha(\mu_2)(18C(R)+4n_fT(R)\\
&-11T(A))(661C(R)+38n_fT(R)-295T(A))-24\pi(81C(R)+4n_fT(R)\\
&-29T(A)))+2\alpha(\mu_2)\log^2\left(\mu_2^2\right)(126C(R)+4n_fT(R)-47T(A))(18C(R)\\
&+4n_fT(R)-11T(A)))+\alpha(\mu_2)^2C(R)(m(\mu_2)+1)(132420C(R)+8432n_fT(R)\\
&-64399T(A))-36\pi\alpha(\mu_2)(C(R)(174m(\mu_2)+835)+38n_fT(R)-295T(A))+864\pi^2\Big)\\
&+(Q^2)^3\left(\alpha(\mu_2)\left(2\left((11T(A)-4n_fT(R))\log\left(\frac{Q^2}{\mu_2^2}\right)(-2724\alpha(\mu_2)C(R)\right.\right.\right.\\
&\left.\left.\left.+6\alpha(\mu_2)\log\left(\frac{Q^2}{\mu_2^2}\right)(90C(R)+4n_fT(R)-47T(A))-196\alpha(\mu_2)n_fT(R)+1853\alpha(\mu_2)T(A)+72\pi\right)\right.\right.\\
&+6\alpha(\mu_2)\log^2(Q^2)(11T(A)-4n_fT(R))(-90C(R)-4n_fT(R)+47T(A))\\
&+\log(Q^2)(\alpha(\mu_2)(11T(A)-4n_fT(R))(2724C(R)+196n_fT(R)-1853T(A))+144\pi(45C(R)\\
&+4n_fT(R)-29T(A))))+\log\left(\mu_2^2\right)(-12\alpha(\mu_2)\log(Q^2)(11T(A)-4n_fT(R))(-90C(R)\\
&-4n_fT(R)+47T(A))+\alpha(\mu_2)(11T(A)-4n_fT(R))(-2724C(R)-196n_fT(R)+1853T(A))\\
&-144\pi(45C(R)+4n_fT(R)-29T(A)))+4\alpha(\mu_2)\log^2\left(\mu_2^2\right)(11T(A)-4n_fT(R))(-90C(R)\\
&-4n_fT(R)+47T(A)))+12\pi(\alpha(\mu_2)(-2724C(R)-196n_fT(R)+1853T(A))+144\pi)))]
\end{aligned}
\tag{3.99}
$$

The CMDM to CMDM running is

$$\Pi^{C_m}(Q^2,\mu_2) = \frac{C(R)D(R)}{663552\pi^5}$$
$$\Bigg[-\alpha(\mu_1)\log\left(\mu_1^2\right)\left(48m(\mu_1)^2(Q^2)^2\left(\alpha(\mu_1)\left(6\left(\alpha(\mu_1)\log^2\left(\frac{Q^2}{\mu_1^2}\right)(30C(R)\right.\right.\right.$$
$$+4n_fT(R)-23T(A))(18C(R)m(\mu_1)-4n_fT(R)+11T(A))$$
$$+\log\left(\frac{Q^2}{\mu_1^2}\right)(12\pi(36C(R)m(\mu_1)-4n_fT(R)+11T(A))-\alpha(\mu_1)(179C(R)$$
$$+42n_fT(R)-193T(A))(18C(R)m(\mu_1)-4n_fT(R)+11T(A)))$$
$$+864\alpha(\mu_1)C(R)(m(\mu_1)+1)T(A)\zeta(3)+\alpha(\mu_1)\log^2((Q^2))(30C(R)+4n_fT(R)$$
$$-23T(A))(18C(R)+4n_fT(R)-11T(A))+\log(Q^2)(24\pi(33C(R)+4n_fT(R)$$
$$-17T(A))-\alpha(\mu_1)(18C(R)+4n_fT(R)-11T(A))(179C(R)+42n_fT(R)$$
$$-193T(A))))+3\log\left(\mu_1^2\right)(-2\alpha(\mu_1)\log(Q^2)(30C(R)+4n_fT(R)$$
$$-23T(A))(18C(R)+4n_fT(R)-11T(A))+\alpha(\mu_1)(18C(R)+4n_fT(R)$$
$$-11T(A))(179C(R)+42n_fT(R)-193T(A))-24\pi(33C(R)+4n_fT(R)$$
$$-17T(A)))+2\alpha(\mu_1)\log^2\left(\mu_1^2\right)(30C(R)+4n_fT(R)-23T(A))(18C(R)$$
$$+4n_fT(R)-11T(A)))+\alpha(\mu_1)^2C(R)(m(\mu_1)+1)(30252C(R)+9992n_fT(R)$$
$$-44983T(A))-36\pi\alpha(\mu_1)(C(R)(174m(\mu_1)+353)+42n_fT(R)-193T(A))$$
$$\left.+864\pi^2\right)+(Q^2)^3\left(\alpha(\mu_1)\left(2\left((11T(A)-4n_fT(R))\log\left(\frac{Q^2}{\mu_1^2}\right)(-834\alpha(\mu_1)C(R)\right.\right.\right.$$
$$+6\alpha(\mu_1)\log\left(\frac{Q^2}{\mu_1^2}\right)(30C(R)+4n_fT(R)-23T(A))-196\alpha(\mu_1)n_fT(R)$$
$$+1097\alpha(\mu_1)T(A)+72\pi)+6\alpha(\mu_1)\log^2(Q^2)(11T(A)-4n_fT(R))(-30C(R)$$
$$-4n_fT(R)+23T(A))+\log(Q^2)(\alpha(\mu_1)(11T(A)-4n_fT(R))(834C(R)$$
$$+196n_fT(R)-1097T(A))+144\pi(15C(R)+4n_fT(R)-17T(A))))$$
$$+\log\left(\mu_1^2\right)(-12\alpha(\mu_1)\log(Q^2)(11T(A)-4n_fT(R))(-30C(R)-4n_fT(R)$$
$$+23T(A))+\alpha(\mu_1)(11T(A)-4n_fT(R))(-834C(R)-196n_fT(R)$$
$$+1097T(A))-144\pi(15C(R)+4n_fT(R)-17T(A)))$$
$$\left.+4\alpha(\mu_1)\log^2\left(\mu_1^2\right)(11T(A)-4n_fT(R))(-30C(R)-4n_fT(R)+23T(A))\right)$$
$$+12\pi(\alpha(\mu_1)(-834C(R)-196n_fT(R)+1097T(A))+144\pi)))$$

$$\alpha(\mu_2)\log\left(\mu_2^2\right)\left(48m(\mu_2)^2(Q^2)^2\left(\alpha(\mu_2)\left(6\left(\alpha(\mu_2)\log^2\left(\frac{Q^2}{\mu_2^2}\right)(30C(R)+4n_fT(R)\right.\right.\right.\right.$$
$$-23T(A))(18C(R)m(\mu_2)-4n_fT(R)+11T(A))+\log\left(\frac{Q^2}{\mu_2^2}\right)(12\pi(36C(R)m(\mu_2)-4n_fT(R)$$
$$+11T(A))-\alpha(\mu_2)(179C(R)+42n_fT(R)-193T(A))(18C(R)m(\mu_2)-4n_fT(R)+11T(A)))$$
$$+864\alpha(\mu_2)C(R)(m(\mu_2)+1)T(A)\zeta(3)+\alpha(\mu_2)\log^2(Q^2)(30C(R)+4n_fT(R)-23T(A))(18C(R)$$
$$+4n_fT(R)-11T(A))+\log(Q^2)(24\pi(33C(R)+4n_fT(R)-17T(A))-\alpha(\mu_2)(18C(R)$$
$$+4n_fT(R)-11T(A))(179C(R)+42n_fT(R)-193T(A))))$$
$$+3\log\left(\mu_2^2\right)(-2\alpha(\mu_2)\log(Q^2)(30C(R)+4n_fT(R)-23T(A))(18C(R)+4n_fT(R)-11T(A))$$
$$+\alpha(\mu_2)(18C(R)+4n_fT(R)-11T(A))(179C(R)+42n_fT(R)-193T(A))-24\pi(33C(R)$$
$$+4n_fT(R)-17T(A)))+2\alpha(\mu_2)\log^2\left(\mu_2^2\right)(30C(R)+4n_fT(R)-23T(A))(18C(R)+4n_fT(R)$$
$$-11T(A)))+\alpha(\mu_2)^2C(R)(m(\mu_2)+1)(30252C(R)+9992n_fT(R)-44983T(A))$$
$$-36\pi\alpha(\mu_2)(C(R)(174m(\mu_2)+353)+42n_fT(R)-193T(A))+864\pi^2\Big)$$
$$+(Q^2)^3\left(\alpha(\mu_2)\left(2\left((11T(A)-4n_fT(R))\log\left(\frac{Q^2}{\mu_2^2}\right)(-834\alpha(\mu_2)C(R)\right.\right.\right.$$
$$\left.\left.+6\alpha(\mu_2)\log\left(\frac{Q^2}{\mu_2^2}\right)(30C(R)+4n_fT(R)-23T(A))-196\alpha(\mu_2)n_fT(R)+1097\alpha(\mu_2)T(A)+72\pi\right)\right.$$
$$+6\alpha(\mu_2)\log^2(Q^2)(11T(A)-4n_fT(R))(-30C(R)-4n_fT(R)+23T(A))$$
$$+\log(Q^2)(\alpha(\mu_2)(11T(A)-4n_fT(R))(834C(R)+196n_fT(R)-1097T(A))+144\pi(15C(R)$$
$$+4n_fT(R)-17T(A))))+\log\left(\mu_2^2\right)(-12\alpha(\mu_2)\log(Q^2)(11T(A)-4n_fT(R))(-30C(R)-4n_fT(R)$$
$$+23T(A))+\alpha(\mu_2)(11T(A)-4n_fT(R))(-834C(R)-196n_fT(R)+1097T(A))-144\pi(15C(R)$$
$$+4n_fT(R)-17T(A)))+4\alpha(\mu_2)\log^2\left(\mu_2^2\right)(11T(A)-4n_fT(R))(-30C(R)-4n_fT(R)+23T(A)))\Big)$$
$$+12\pi(\alpha(\mu_2)(-834C(R)-196n_fT(R)+1097T(A))+144\pi)))] \qquad (3.100)$$

Conclusions

The lattice can serve as an excellent tool for improved bounds on CP violating physics. Before it can be used properly, however, the lattice operators must be renormalized. $\overline{MS}$ is the standard renormalization scheme for continuum calculations, but is not a suitable scheme for lattice measurements. In this work, preliminary results of the analytic computations required for nonperturbative renormalization of the CEDM and CMDM operators were

presented. We have computed the matching factors to convert coordinate space CEDM to CEDM and CMDM to CMDM correlators from the X-space scheme into $\overline{MS}$. We have also computed the running of these correlators, providing all of the analytic factors for proper use of the CEDM and CMDM operators on the lattice.

Appendices

Conventions

The euclidean path integral is

$$Z = \int \mathcal{D}\overline{\psi}\mathcal{D}\psi\mathcal{D}A\mathcal{D}c\mathcal{D}\overline{c}\; e^{-S_F - S_{YM} - S_{GF} - S_{ghost}} \tag{101}$$

S_F, the fermion action is

$$S_F = \int d^d x \overline{\psi}(x) \left[\gamma_\mu \left(\partial_\mu + igA_\mu(x)\right) + M\right] \psi(x), \tag{102}$$

where μ runs from 1 to 4. The fermion propagator, $S(p)$ is

$$S(p) = \frac{-i\not{p} + M}{p^2 + M^2}, \tag{103}$$

and the fermion-fermion-gluon vertex factor, V_μ^a, is

$$V_\mu^a = -ig\gamma_\mu T^a. \tag{104}$$

The covariant derivative, D_μ, is

$$D_\mu(x) = \partial_\mu + igA_\mu^a(x)T^a \tag{105}$$

The field strength tensor $G_{\mu\nu}$ is

$$G_{\mu\nu} = -\frac{i}{g}\left[D_\mu, D_\nu\right] \tag{106}$$

$$= \partial_\mu A_\nu^a(x)T^a - \partial_\nu A_\mu^a(x)T^a - gf^{abc}T^a A_\mu^b(x)A_\nu^c(x) \tag{107}$$

The yang-mills action, S_{YM} is

$$S_{YM} = \frac{1}{4}\int d^d x G_{\mu\nu}^a G^{a\,\mu\nu} \tag{108}$$

$$= \int d^d x \left(\frac{1}{2}\partial_\mu A_\nu^a(x)\partial^\mu A^{a\,\nu}(x) - \frac{1}{2}\partial^\mu A^{a\,\nu}(x)\partial_\nu A_\mu^a(x) - gf^{bca}A^{b\,\mu}(x)A^{c\,\nu}(x)\partial_\mu A_\nu^a(x) + \frac{1}{4}g^2 f^{bca}f^{dea}A^{b\,\mu}(x)A^{c\,\nu}(x)A_\mu^d(x)A_\nu^e(x)\right) \tag{109}$$

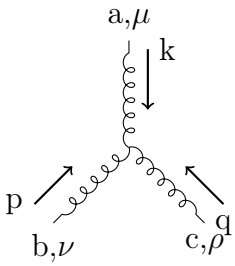

The three gluon vertex factor is

$$V^{abc}_{\mu\nu\rho}(q,p,k) = igf^{abc}\left(g_{\nu\rho}(q_\mu - p_\mu) + g_{\mu\rho}(k_\nu - q_\nu) + g_{\mu\nu}(p_\rho - k_\rho)\right) \tag{110}$$

The field $A_\mu(x)$ is equal to

$$A_\mu(x) = \int \frac{d^dk}{(2\pi)^d} e^{ik\cdot x}\tilde{A}_\mu(k) \tag{111}$$

For momentum k flowing into the vertex x.

The gauge fixing action, S_{GF}, and the ghost action, S_{ghost}, are used to remove the gauge redundancy from the yang mills action. Using the Lorentz gauge condition, one finds

$$\mathcal{L}_{GF} = \frac{1}{2\xi}(\partial^\mu A^a_\mu)^2 \tag{112}$$

$$\mathcal{L}_{ghost} = \overline{c}^a\left(\partial^2\delta^{ac} + gf^{abc}\partial^\mu A^b_\mu\right)c^c \tag{113}$$

The ghost propagator is

$$\Delta_{ghost}(k) = -\frac{1}{k^2}\delta^{ac} \tag{114}$$

The ghost-gluon vertex factor is

$$= -igf^{abc}k^\mu \tag{115}$$

The chromoelectric dipole moment is

$$\begin{aligned} C_e(x) =& \frac{1}{2}g\overline{\psi}(x)\sigma^{\mu\nu}\gamma_5 G^a_{\mu\nu}(x)T^a\psi(x) \\ =& g\overline{\psi}(x)\sigma^{\mu\nu}\gamma_5 T^a\left(\partial_\mu A^a_\nu(x) - \frac{1}{2}gf^{abc}A^b_\mu(x)A^c_\nu(x)\right)\psi(x) \end{aligned} \tag{116}$$

The chromomagnetic dipole moment is

$$\begin{aligned} C_m(x) =& \frac{1}{2} g \overline{\psi}(x) \sigma^{\mu\nu} \gamma_5 G^a_{\mu\nu}(x) T^a \psi(x) \\ =& g \overline{\psi}(x) \sigma^{\mu\nu} T^a \left(\partial_\mu A^a_\nu(x) - \frac{1}{2} g f^{abc} A^b_\mu(x) A^c_\nu(x) \right) \psi(x) \end{aligned} \tag{117}$$

where $\sigma^{\mu\nu} = \frac{i}{2} [\gamma^\mu, \gamma^\nu]$

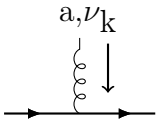

Figure 16: $\mathcal{O}(g)$ CEDM/CMDM vertex diagram

the vertex in figure 16 is produced by the first term of the chromoelectric dipole moment, and is equal to

$$i k_\mu g \sigma^{\mu\nu} \gamma_5 T^a \tag{118}$$

and the first term of the chromomagnetic dipole moment is

$$i k_\mu g \sigma^{\mu\nu} T^a \tag{119}$$

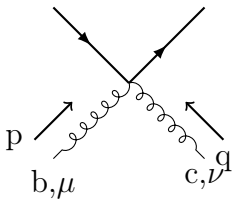

Figure 17: $\mathcal{O}(g^2)$ CEDM/CMDM vertex diagram

The vertex in figure 17 comes from the second term of the chromoelectric (chromomagnetic) dipole moment, and for the chromoelectric dipole moment is equal to

$$-g^2 f^{abc} T^a \sigma^{\mu\nu} \gamma_5. \tag{120}$$

For the chromomagnetic dipole moment, figure 17 gives

$$-g^2 f^{abc} T^a \sigma^{\mu\nu}. \tag{121}$$

Fourier Transform

The X-space scheme is defined in coordinate space. Perturbative calculations, however, are significantly easier in momentum space. Therefore, all perturbative calculations were done in momentum space, and fourier transformed coordinate space. In this section, general details of the fourier transform are explained.

This paper deals with massless propagators. The fourier transform of a massless propagator is

$$\int \frac{d^d q}{(2\pi)^d} \frac{e^{iq\cdot x}}{(q^2)^a} = \frac{1}{\Gamma(a)} \int \frac{d^d q}{(2\pi)^d} \int_0^\infty d\alpha \alpha^{a-1} e^{-\alpha q^2 + iq\cdot x}, \tag{122}$$

where the integral definition of the Gamma Function (also referred to as α parameterization) was used to express the denomenator of the propagator $(q^2)^{-a}$ as a gaussian.

$$= \frac{1}{(4\pi)^{d/2}\Gamma(a)} \int_0^\infty d\alpha \alpha^{a-1-d/2} \exp\left[-\frac{x^2}{4\alpha}\right]. \tag{123}$$

Changing variables from α to $s = \alpha^{-1}$ yields

$$= \frac{1}{(4\pi)^{d/2}\Gamma(a)} \int_0^\infty ds s^{d/2-a-1} \exp\left[-s\frac{x^2}{4}\right] \tag{124}$$

$$= \frac{\Gamma\left(\frac{d}{2}-a\right)}{(4\pi)^{d/2}\Gamma(a)} \left(\frac{x^2}{4}\right)^{a-d/2} \tag{125}$$

where the α parameterization was used to go from line 124 to line 125.

When fourier transforming objects with lorentz structure, the lorentz structure can be factored out of the integral as a derivative

$$\int \frac{d^d q}{(2\pi)^d} e^{iq\cdot x} \frac{\prod_i q_{\alpha_i}}{(q^2)^a} = \prod_i (-i\partial_{\alpha_i}) \int \frac{d^d q}{(2\pi)^d} \frac{e^{iq\cdot x}}{(q^2)^a} \tag{126}$$

$$= \frac{\Gamma\left(\frac{d}{2}-a\right)}{(4\pi)^{d/2}\Gamma(a)} \left[\prod_i (-i\partial_{\alpha_i})\right] \left(\frac{x^2}{4}\right)^{a-d/2} \tag{127}$$

Using the identity

$$\left(\log q^2\right)^r = r! \lim_{\delta\to 0} \left(\frac{\partial}{\partial\delta}\right)^r (q^2)^\delta, \tag{128}$$

the fourier transform of a logarithm can be found.

$$\int \frac{d^d q}{(2\pi)^d} e^{iq\cdot x} \frac{(\log q^2)^r}{(q^2)^a} = r! \lim_{\delta\to 0} \left(\frac{\partial}{\partial \delta}\right)^r \int \frac{d^d q}{(2\pi)^d} \frac{e^{iq\cdot x}}{(q^2)^{a-\delta}} \tag{129}$$

$$= r! \lim_{\delta\to 0} \left(\frac{\partial}{\partial \delta}\right)^r \left[\frac{\Gamma\left(\frac{d}{2} - a + \delta\right)}{(4\pi)^{d/2}\Gamma(a-\delta)} \left(\frac{x^2}{4}\right)^{a-\delta-d/2}\right] \tag{130}$$

A list of fourier transform identities can be found in reference [57]. Here, we add to that list.

Momentum Space	Coordinate Space
$\log\left(\frac{Q^2}{\mu^2}\right)$	$-\frac{1}{\pi^2 x^4}$
$Q^2 \log\left(\frac{Q^2}{\mu^2}\right)$	$\frac{8}{\pi^2 x^6}$
$\log^2\left(\frac{Q^2}{\mu^2}\right)$	$\frac{2}{\pi^2 x^4}\left(-1 + 2\gamma_E + \log\left(\frac{x^2\mu^2}{4}\right)\right)$
$Q^2 \log^2\left(\frac{Q^2}{\mu^2}\right)$	$\frac{8}{\pi^2 x^6}\left(5 - 4\gamma_E - 2\log\left(\frac{x^2\mu^2}{4}\right)\right)$
$(Q^2)^2 \log\left(\frac{Q^2}{\mu^2}\right)$	$-\frac{192}{\pi^2 x^8}$
$(Q^2)^2 \log^2\left(\frac{Q^2}{\mu^2}\right)$	$\frac{128\left(6\gamma_E 3\log\left(\frac{\mu^2 x^2}{4}\right) - 10\right)}{\pi^2 x^8}$
$(Q^2)^3 \log\left(\frac{Q^2}{\mu^2}\right)$	$\frac{9216}{\pi^2 x^{10}}$
$(Q^2)^3 \log^2\left(\frac{Q^2}{\mu^2}\right)$	$-\frac{1536\left(12\log\left(\frac{\mu^2 x^2}{4}\right) + 24\gamma_E - 47\right)}{\pi^2 x^{10}}$

One Loop Calculation

Converting from $\overline{MS}$ to the X-scheme involves computing the finite part of the correlator of interest in $\overline{MS}$. In this appendix, we obtain a closed form expression for a massless, one loop, dimensionally regulated feynman integral. For more detailed reviews of multiloop theory, see [58, 59]. The feynman integral is

$$\int \frac{d^d p}{(2\pi)^d} \frac{1}{[p^2]^{n_1}[(p+q)^2]^{n_2}} \tag{131}$$

Using the α parameterization, we convert the denominators of this integral into a product of Gaussians

$$=\frac{1}{\Gamma(n_1)\Gamma(n_2)}\int\frac{d^dp}{(2\pi)^d}\int_0^\infty d\alpha_1 d\alpha_2 \alpha_1^{n_1-1}\alpha_2^{n_2-1}\exp\left[-\alpha_1 p^2-\alpha_2(p+q)^2\right] \tag{132}$$

$$=\frac{1}{(4\pi)^{d/2}\Gamma(n_1)\Gamma(n_2)}\int_0^\infty d\alpha_1 d\alpha_2 \frac{\alpha_1^{n_1-1}\alpha_2^{n_2-1}}{(\alpha_1+\alpha_2)^{d/2}}\exp\left[-\frac{\alpha_1\alpha_2}{\alpha_1+\alpha_2}q^2\right] \tag{133}$$

Making the change of variables $\alpha_1 = \eta x$ and $\alpha_2 = \eta(1-x)$, the integral becomes

$$=\frac{1}{(4\pi)^{d/2}\Gamma(n_1)\Gamma(n_2)}\int_0^\infty d\eta\int_0^1 dx \eta^{n_1+n_2-1-d/2}x^{n_1-1}(1-x)^{n_2-1}\exp\left[-\eta x(1-x)q^2\right] \tag{134}$$

$$=\frac{\Gamma\left(n_1+n_2-\frac{d}{2}\right)\Gamma\left(\frac{d}{2}-n_1\right)\Gamma\left(\frac{d}{2}-n_2\right)}{(4\pi)^{d/2}\Gamma(n_1)\Gamma(n_2)\Gamma(d-n_1-n_2)}(q^2)^{d/2-n_1-n_2} \tag{135}$$

Massless Pseudo Scalar to Pseudo Scalar Correlator

Throughout this document, amplitudes are computed using the method of integration by parts. In this section, the massless pseudo scalar to pseudo scalar amplitude is computed analytically to illustrate integration by parts.

The propagators being used in this section are the euclidean, massless, momentum space Dirac propagator $\frac{-i\not{p}}{p^2}$. In R_ξ gauge, the gluon propagators used are $\Delta^{ab}_{\mu\nu}(k) = \frac{\delta^{ab}}{k^2}\left(g_{\mu\nu}+(\xi-1)\frac{k_\mu k_\nu}{k^2}\right)$. In the calculations below, the feynman gauge is used ($\xi = 1$). The integrals are regulated using naive dimreg (ndr). It is the convention of ndr that γ_5 anticommutes with γ_μ, and $Tr_D(\mathbf{1}) = 4$.

Evaluating the lowest order contribution to the two point pseudo scalar correlator, figure 18, gives

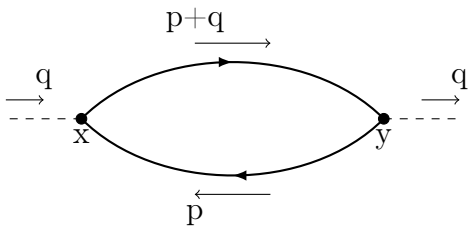

Figure 18: lowest order pseudoscalar density two point function from y to x

$$\begin{aligned}
\langle P(x)P(y)\rangle =& \langle\overline{\psi}(x)\gamma_5\psi(x)\overline{\psi}(y)\gamma_5\psi(y)\rangle && (136)\\
=& - S(y-x)^{ji}_{\sigma\alpha}\left(\gamma_5\right)_{\alpha\beta} S(x-y)^{ij}_{\beta\rho}\left(\gamma_5\right)_{\rho\sigma} && (137)\\
& x-y\to x && (138)\\
=& - D(R)\int \frac{d^dq}{(2\pi)^d}e^{iq.x}\int\frac{d^dp}{(2\pi)^d}Tr_D\left\{\frac{-i(\not{p}+\not{q})}{(p+q)^2}\gamma_5\frac{-i\not{p}}{p^2}\gamma_5\right\} && (139)\\
r \equiv& p+q && (140)\\
=& - D(R)Tr_D\left\{\left[-i\partial_\mu\gamma^\mu\int\frac{d^dr}{(2\pi)^d}\frac{e^{ir.x}}{r^2}\right]\left[i\partial_\nu\gamma^\nu\int\frac{d^dp}{(2\pi)^d}\frac{e^{-ip.x}}{p^2}\right]\right\} && (141)\\
=& - \frac{4D(R)}{(4\pi)^d}\Gamma\left(\frac{d}{2}\right)^2\left(\frac{x^2}{4}\right)^{1-d}\equiv G(d,x) && (142)
\end{aligned}$$

Where the fourier transforms in line 141 were computed using the identity in appendix .2

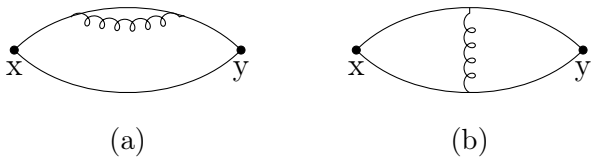

(a) (b)

Figure 19: order g^2 diagrams

In momentum space, diagram 19a is

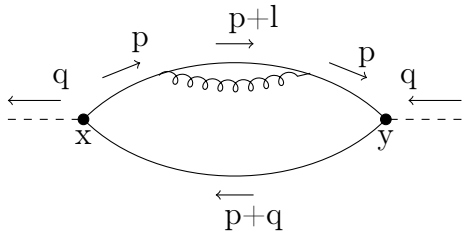

Figure 20: diagram 19a in momentum space

$$=g^2(\mu^2)^{2-d/2}\int d^dmd^dnT^a_{cd}(\gamma^\mu)_{\eta\epsilon}S(m-x)^{di}_{\epsilon\alpha}(\gamma_5)_{\alpha\beta}S(x-y)^{ij}_{\beta\sigma}(\gamma_5)_{\sigma\rho}S(y-n)^{jh}_{\rho\omega}T^b_{hs}(\gamma^\nu)_{\omega\tau}$$
$$S(n-m)^{sc}_{\tau\eta}\Delta^{ab}_{\mu\nu}(m-n) \tag{143}$$
$$=g^2(\mu^2)^{2-d/2}C(R)D(R)\int\frac{d^dq}{(2\pi)^d}e^{iq\cdot x}$$
$$\int\frac{d^dp}{(2\pi)^d}Tr_D\left\{\frac{-i\not p}{p^2}\frac{i(\not p+\not q)}{(p+q)^2}\frac{-i\not p}{p^2}\left[\gamma^\nu\int\frac{d^dl}{(2\pi)^d}\frac{-i(\not p+\not l)}{(p+l)^2}\frac{g_{\mu\nu}}{l^2}\gamma^\mu\right]\right\} \tag{144}$$

In the above line, the subloop diagram (with loop momentum l) has been put in square brackets. This feynman integral is just the gluon correction to the fermion propagator. The massless quark propagator has a structure $-i\not p\Sigma(p^2)$ where $\Sigma(p^2)$ is a scalar function.

$$-i\not p\Sigma(p^2)=\gamma^\nu\int\frac{d^dl}{(2\pi)^d}\frac{-i(\not p+\not l)}{(p+l)^2}\frac{g_{\mu\nu}}{l^2}\gamma^\mu \tag{145}$$

$\Sigma(p^2)$ can be evaluated by multiplying both sides by $\frac{\not p}{4}$ and then taking the trace over Dirac space. One finds $-i\not p\Sigma(p^2)=-i\gamma_\mu\frac{\not p}{(p^2)^{2-d/2}}\gamma^\mu$.

$$=-g^2(\mu^2)^{2-d/2}\frac{C(R)D(R)}{(4\pi)^{d/2}}\frac{\Gamma\left(2-\frac{d}{2}\right)}{\Gamma(d-1)}\Gamma\left(\frac{d}{2}-1\right)\Gamma\left(\frac{d}{2}\right)\int\frac{d^dq}{(2\pi)^d}e^{iq\cdot x}$$
$$\int\frac{d^dp}{(2\pi)^d}Tr_D\left\{\frac{\not p}{p^2}\frac{\not p+\not q}{(p+q)^2}\frac{\not p}{p^2}\gamma_\mu\frac{\not p}{(p^2)^{2-d/2}}\gamma^\mu\right\} \tag{146}$$

Making the change of variables $p+q=r$ puts the integral into a form where both the top, and bottom fermion lines can be seperately Fourier

transformed.

$$
\begin{aligned}
&= -\, g^2(\mu^2)^{2-d/2}\frac{C(R)D(R)}{(4\pi)^{d/2}}\frac{\Gamma\left(2-\frac{d}{2}\right)}{\Gamma(d-1)}\Gamma\left(\frac{d}{2}-1\right)\Gamma\left(\frac{d}{2}\right) \\
&\quad Tr_D\left\{\int\frac{d^dr}{(2\pi)^d}e^{ir\cdot x}\frac{\not{r}}{r^2}\int\frac{d^dp}{(2\pi)^d}e^{-ip\cdot x}\frac{\not{p}\gamma_\mu\not{p}\gamma^\mu\not{p}}{(p^2)^{4-d/2}}\right\} \qquad (147)\\
&= G(d,x)\left[g^2(\mu^2)^{2-d/2}\frac{(d-2)\pi\csc\left(d\frac{\pi}{2}\right)}{(4\pi)^{d/2}\Gamma\left(4-\frac{d}{2}\right)}\left(\frac{x^2}{4}\right)^{2-d/2}\right] \qquad (148)\\
&\approx G(d,x)\left(\frac{\alpha C(R)}{(4\pi)\epsilon}-\frac{(\alpha C(R))\left(-\log\left(\mu^2\right)-\log\left(x^2\right)+2+2\log(2)\right)}{4\pi}+O\left(\epsilon^1\right)\right) \qquad (149)
\end{aligned}
$$

In momentum space, diagram 19b is

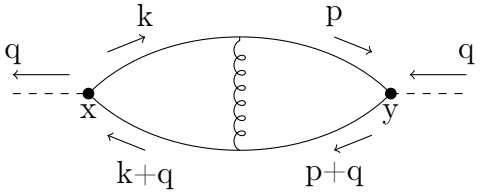

Figure 21: diagram 19b in momentum space

$$
\begin{aligned}
&= g^2(\mu^2)^{2-d/2}C(R)D(R)\int\frac{d^dq}{(2\pi)^d}e^{iq\cdot x} \\
&\quad \int\frac{d^dkd^dp}{(2\pi)^{2d}}Tr_D\left\{\gamma^\mu\frac{-i\not{k}}{k^2}\gamma_5\frac{-i(\not{k}+\not{q})}{(k+q)^2}\gamma^\nu\frac{-i(\not{p}+\not{q})}{(p+q)^2}\gamma_5\frac{-i\not{p}}{p^2}\frac{g_{\mu\nu}}{(p-k)^2}\right\} \qquad (150)\\
& \qquad (151)
\end{aligned}
$$

Taking the trace over the numerator yields

$$
\begin{aligned}
&= -\, g^2(\mu^2)^{2-d/2}C(R)D(R)\int\frac{d^dq}{(2\pi)^d}e^{iq\cdot x} \\
&\quad \int\frac{d^dkd^dp}{(2\pi)^{2d}}\left[\frac{dk^2(p^2+(p\cdot q))+(k\cdot q)(dp^2+4(p\cdot q))+(d-4)(k\cdot p)q^2}{k^2(k+q)^2(p+q)^2p^2(p-k)^2}\right] \qquad (152)
\end{aligned}
$$

The integrand can be simplified by making the substitutions

$$(p \cdot q) = \frac{1}{2}\left[(p+q)^2 - p^2 - q^2\right] \tag{153}$$

$$(k \cdot q) = \frac{1}{2}\left[(k+q)^2 - k^2 - q^2\right] \tag{154}$$

$$(k \cdot p) = \frac{1}{2}\left[p^2 + k^2 - (p-k)^2\right] \tag{155}$$

These substitutions express the numerators in terms of inverse propagators. Upon simplification, factors from the denominator cancel inverse propagators in the numerator, ultimately expressing the diagram as a sum of scalar one- and two-loop integrals.

$$\begin{aligned} = &-2g^2(\mu^2)^{2-d/2}C(R)D(R)\int \frac{d^dq}{(2\pi)^d}e^{iq\cdot x} \\ &\int \frac{d^dkd^dp}{(2\pi)^{2d}}\left[-\frac{8q^2}{(k+q)^2(p+q)^2p^2(p-k)^2} + \frac{(8-2d)q^2}{k^2(k+q)^2(p+q)^2p^2} + \right. \\ &\left. \frac{4q^4}{k^2(k+q)^2(p+q)^2p^2(p-k)^2} - \frac{8q^2}{k^2(p+q)^2p^2(p-k)^2} + \frac{(4d-8)}{(k+q)^2p^2(p-k)^2}\right] \end{aligned} \tag{156}$$

With the exception of the third term, each integral can be solved by recursively applying the one-loop integral, solved in appendix .3. The third term can be solved using the multiloop method of Integration By Parts. Integration By Parts exploits the fundamental theorem of calculus for the purpose of expressing multiloop integrals as sums of one-loop integrals.

The third term is

$$\int \frac{d^dkd^dp}{(2\pi)^{2d}} \frac{1}{k^2(k+q)^2(p+q)^2p^2(p-k)^2} \tag{157}$$

Taking the derivative of the product of $(k^\mu + q^\mu)$ and the integrand with respect to k_μ gives

$$\int \frac{d^dkd^dp}{(2\pi)^{2d}} \frac{\partial}{\partial k_\mu} \frac{k^\mu + q^\mu}{k^2(k+q)^2(p+q)^2p^2(p-k)^2} = 0. \tag{158}$$

Explicitly taking the derivative gives

$$\int \frac{d^dk d^dp}{(2\pi)^{2d}} \left[\frac{d-2}{k^2(k+q)^2(p+q)^2p^2(p-k)^2} - \frac{2k\cdot(k+q)}{(k^2)^2(k+q)^2(p+q)^2p^2(p-k)^2} - \frac{2(k+q)\cdot(k-p)}{k^2\left[(k+q)^2\right]^2(p+q)^2p^2(p-k)^2} \right] = 0 \tag{159}$$

By performing similar substitutions to those done in line 152, the above expression will contain the two-loop integral, and a sum of recursive one-loop integrals. Moving the recursive one-loop integrals to the right hand side gives a solvable expression for the two-loop integral.

Solving all of the integrals gives

$$\approx G(d,x)\left(\frac{2\alpha C(R)}{\pi\epsilon} - \frac{(\alpha C(R))\left(-4\log\left(\mu^2x^2\right)-1+8\log(2)\right)}{2\pi} + O\left(\epsilon^1\right) \right) \tag{160}$$

For fermions in the fundamental representation, $R = F$ and $C(F) = \frac{4}{3}$. Diagram 19a still needs to be multiplied by its symmetry factor, 2, because the gluon loop can be on either fermion line. In $\overline{MS}$, the finite part to order α is

$$= \frac{3}{\pi^4(x^2)^3}\left(1 + \frac{2}{3\pi}\alpha\left(1/\sqrt{x^2}\right) + \mathcal{O}(\alpha^2)\right) \tag{161}$$

Gauge Invariance of Pseudo Scalar to Pseudo Scalar Correlator

The pseudo scalar to pseudo scalar correlator, shown in line 136, is gauge invariant. In R_ξ gauge, gauge invariance manifests through the vanishing of all ξ dependence of the correlator, at each perturbative order. Checking for gauge invariance ensures the presence of each diagram required for the correlator, along with proper symmetry factors. Below, gauge invariance for the pseudo scalar correlator is calculated.

The ξ dependent term (GI) from figure 19b is

$$GI = -g^2C(R)D(R)(\xi-1)\int \frac{d^dq}{(2\pi)^d}e^{iq\cdot x} \int \frac{d^dpd^dk}{(2\pi)^{2d}} Tr_{CD}\left\{ \frac{\not{p}}{p^2}\gamma_5\left[\frac{\not{q}+\not{p}}{(q+p)^2}\frac{\not{p}-\not{k}}{(p-k)^2}\frac{\not{q}+\not{k}}{(q+k)^2}\right]\gamma_5\frac{\not{k}}{k^2}\frac{\not{p}-\not{k}}{(p-k)^2}\right\} \tag{162}$$

The term in square brackets can be simplified using the following trick

$$[\dots] = \frac{1}{(p-k)^2}\left(\frac{\not{q}+\not{p}}{(q+p)^2}(\not{p}-\not{k})\frac{\not{q}+\not{k}}{(q+k)^2}\right) \tag{163}$$

$$= \frac{1}{(p-k)^2}\left(\frac{\not{q}+\not{p}}{(q+p)^2}\left((\not{p}+\not{q})-(\not{k}+\not{q})\right)\frac{\not{q}+\not{k}}{(q+k)^2}\right) \tag{164}$$

Where in line 164, $\not{q}$ has been added and subtracted to $(\not{p}-\not{k})$

$$= \frac{1}{(p-k)^2}\left(\frac{\not{q}+\not{k}}{(q+k)^2} - \frac{\not{q}+\not{p}}{(q+p)^2}\right) \tag{165}$$

Putting this back in GI gives

$$GI = -g^2 C(R) D(R)(\xi-1)\int \frac{d^d q}{(2\pi)^d} e^{iq\cdot x} \int \frac{d^d p d^d k}{(2\pi)^{2d}} Tr_{CD}\left\{\frac{\not{p}}{p^2}\gamma_5\left[\frac{1}{(p-k)^2}\left(\frac{\not{q}+\not{k}}{(q+k)^2} - \frac{\not{q}+\not{p}}{(q+p)^2}\right)\right]\gamma_5\frac{\not{k}}{k^2}\frac{\not{p}-\not{k}}{(p-k)^2}\right\} \tag{166}$$

Repeating this trick with the other propagators, and anticommuting the γ_5 past the propagators results in

$$GI = g^2 C(R) D(R)(\xi-1)\int \frac{d^d q}{(2\pi)^d} e^{iq\cdot x} \int \frac{d^d p d^d k}{(2\pi)^{2d}} Tr_{CD}\left\{\frac{1}{[(p-k)^2]^2}\left(\frac{\not{q}+\not{k}}{(q+k)^2} - \frac{\not{q}+\not{p}}{(q+p)^2}\right)\left(\frac{\not{k}}{k^2} - \frac{\not{p}}{p^2}\right)\right\} \tag{167}$$

$$= -2g^2 C(R) D(R)(\xi-1)\int \frac{d^d q}{(2\pi)^d} e^{iq\cdot x} \int \frac{d^d p d^d k}{(2\pi)^{2d}} Tr_{CD}\left\{\frac{1}{[(p-k)^2]^2}\left(\frac{\not{q}+\not{k}}{(q+k)^2}\frac{\not{p}}{p^2}\right)\right\} \tag{168}$$

The ξ dependent part of figure 19a ($GI2$) is

$$GI2 = -g^2(\xi-1)C(R)D(R)\int\frac{d^dq}{(2\pi)^d}e^{iq\cdot x}$$
$$\int\frac{d^dpd^dl}{(2\pi)^{2d}}Tr_{CD}\left\{\frac{\not p+\not q}{(p+q)^2}\gamma_5\frac{\not p}{p^2}\gamma_5\left[\frac{\not p+\not q}{(p+q)^2}\frac{\not l}{l^2}\frac{\not p+\not q+\not l}{(p+q+l)^2}\right]\frac{\not l}{l^2}\right\} \tag{169}$$

$$= -g^2(\xi-1)C(R)D(R)\int\frac{d^dq}{(2\pi)^d}e^{iq\cdot x}$$
$$\int\frac{d^dpd^dl}{(2\pi)^{2d}}Tr_{CD}\left\{\frac{\not p+\not q}{(p+q)^2}\gamma_5\frac{\not p}{p^2}\gamma_5\frac{1}{(l^2)^2}\left[-\frac{\not p+\not q+\not l}{(p+q+l)^2}\right]\not l\right\} \tag{170}$$

$$=g^2(\xi-1)C(R)D(R)\int\frac{d^dq}{(2\pi)^d}e^{iq\cdot x}\int\frac{d^dpd^dl}{(2\pi)^{2d}}Tr_{CD}\left\{\frac{\not p}{p^2}\frac{1}{(l^2)^2}\left[\frac{\not p+\not q+\not l}{(p+q+l)^2}\right]\right\} \tag{171}$$

Massive Pseudo Scalar to Pseudo Scalar and Scalar to Scalar Correlators

The quarks of interest for this problem are the up and down quarks. Since their mass is much less than the energy scales of interest, the massive quark propagators (equation (103)) can be expanded about $M \approx 0$. The propagators used are

$$S(p) = \frac{-i\not p+M}{p^2}\left(1-\frac{M^2}{p^2}+\mathcal{O}(M^4)\right) \tag{172}$$

This expanded propagator now appears to be a product of massless quark propagators. Diagrams using these can be solved using integration by parts. Calculations are carried out using Mincer for form.

The bare pseudoscalar to pseudoscalar correlator computed to $\mathcal{O}(\alpha)$ is

$$\begin{aligned}\Pi_0^P(Q^2,m_0^2) =&\frac{D(R)(Q^2)^{-\epsilon}\left(2\left(2m_0^2+Q^2\left(4\epsilon^2+2\epsilon+1\right)\right)\right)}{(4\pi)^2\epsilon}\\ &+\frac{\alpha C(R)D(R)(Q^2)^{-2\epsilon}\mu^{2\epsilon}}{1280\pi^3\epsilon^2}\left[Q^2\left(\left(-2240\zeta(3)-8\pi^4+8045\right)\epsilon^3\right.\right.\\ &+(2270-480\zeta(3))\epsilon^2+580\epsilon+120\Big)\\ &\left.-16m_0^2\left(\left(200\zeta(3)+\pi^4+50\right)\epsilon^3+30(2\zeta(3)-1)\epsilon^2-10\epsilon-30\right)\right]\end{aligned} \tag{173}$$

The scalar to scalar correlator has the same diagrams as figures 18 and 25, except the heavy dots at x and y have a vertex of 1. The bare scalar to sclar correlator is

$$\Pi_0^S(Q^2,m_0^2) =\frac{D(R)\left(Q^2\right)^{-\epsilon}\left(-32m_0^2\epsilon-\frac{12m_0^2}{\epsilon}-16m_0^2-8Q^2\epsilon-\frac{2Q^2}{\epsilon}-4Q^2\right)}{16\pi^2} \tag{174}$$

Massive Pseudo Scalar to CEDM and Scalar to CMDM Correlator

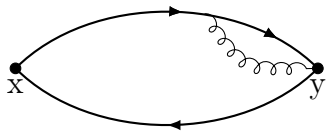

Figure 22: p-c diagram

The psuedo scalar to CEDM correlator is $\langle P(x)C_e(y)\rangle = \left\langle\overline{\psi}(x)\gamma_5\psi(x)\bar{\psi}(y)\sigma^{\mu\nu}G_{\mu\nu}(y)\gamma_5\psi(y)\right\rangle$. The lowest order diagram is depicted in figure 22, and is of $\mathcal{O}(\alpha)$. In coordinate space, this is equal to

$$\langle P(x)C_e(y)\rangle = \int d^dz\gamma_5 S(x-y)\sigma^{\mu\nu}T^a\gamma_5 S(y-z)\gamma^\rho T^b S(z-x)\frac{\partial}{\partial x^\mu}\Delta^{ab}_{\nu\rho}(y-z) \tag{175}$$

In momentum space, the bare pseudoscalar to CEDM correlator is equal to

$$\Pi_0^{C_e P}(Q^2, m_0^2) = \frac{\alpha C(R) D(R) (q^2)^{-2\epsilon} \mu^{2\epsilon}}{768\pi^3\epsilon^2} \left[3m_0^2 q^2 \left((256\zeta(3) - 657)\epsilon^3 - 214\epsilon^2 - 68\epsilon - 24\right) + (q^2)^2 \epsilon \left(293\epsilon^2 + 70\epsilon + 12\right)\right] \quad (176)$$

The bare Scalar to CMDM correlator is

$$\Pi_0^{C_m S}(Q^2, m_0^2) = -\frac{(Q^2)^{-2\epsilon}}{(4\pi)^4} \frac{C(R) D(R) \pi\alpha\mu^{2\epsilon}}{3\epsilon^2} \left[3m_0^2 Q^2 (\epsilon(\epsilon((256\zeta(3) - 657)\epsilon - 214) - 68) - 24) + (Q^2)^2 \epsilon(\epsilon(293\epsilon + 70) + 12)\right] \quad (177)$$

CEDM to CEDM and CMDM to CMDM Correlators

In the work that follows, the bare CEDM to CEDM and bare CMDM to CMDM correlators will be computed. These computations were made using the Form version of MINCER [60].

Leading Order Calculation

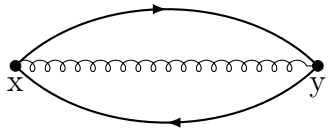

Figure 23: chromoelectric or chromomagnetic dipole moment at point y propagating to point x

Figure 23 is the leading order contribution to the correlator $\langle\bar{\psi}(x)\sigma^{\mu\nu}G_{\mu\nu}(x)\gamma_5\psi(x)\bar{\psi}(y)\sigma^{\alpha\beta}G_{\alpha\beta}(y)\gamma_5\psi(y)\rangle$, used to renormalize in the (c)edm in the x-scheme. At leading order in coordinate space, with fixed coordinates x and y, this diagram is

$$\langle C_e(x)C_e(y)\rangle = -\,Tr_{CD}\left(S(y-x)\sigma^{\mu\nu}T^a\gamma_5 S(x-y)\sigma^{\alpha\beta}T^b\gamma_5\frac{\partial}{\partial x^\mu}\frac{\partial}{\partial y^\alpha}\Delta^{ab}_{\nu\beta}(x-y)\right) \tag{178}$$

where Tr_{CD} means the trace over both color and Dirac indices. It's clear that at leading order, despite this being a 2-loop diagram, this diagram is just the trace of the product of the position space propagators.

In order to account for the vertices fixed at points x and y when evaluating the diagram in momentum space, the vertices themselves must be given an incoming momentum q at x and an outgoing momentum q at y. x and y can be fixed by fourier transforming q.

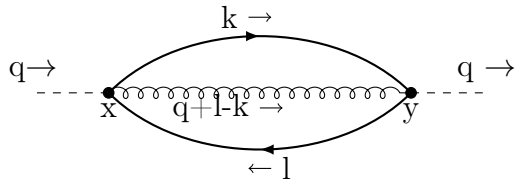

Figure 24: CEDM to CEDM or CMDM to CMDM with fixed vertices in momentum space. The dashed line represents the vertex momentum to be used in the fourier transform

At leading order in momentum space, this diagram is

$$= -\int d^dq e^{iq\cdot x}\int\frac{d^dkd^dl}{(2\pi)^{3d}}Tr_{CD}\left[S(k)\sigma^{\mu\nu}T^a\gamma_5 S(-l)\sigma^{\alpha\beta}T^b\gamma_5(q+l-k)_\mu(q+l-k)_\alpha\Delta^{ab}_{\nu\beta}(q+l-k)\right] \tag{179}$$

$$= -\,C(R)D(R)\int\frac{d^dq}{(2\pi)^d}e^{iq\cdot x}\int\frac{d^dpd^dl}{(2\pi)^{2d}}Tr_D\left\{\frac{\not{p}}{p^2}\sigma^{\mu\nu}\frac{\not{l}}{l^2}\sigma^\alpha{}_\nu\frac{(p+q-l)_\mu(p+q-l)_\alpha}{(p+q-l)^2}\right\} \tag{180}$$

Fourier transforming the gluon line gives

$$r \equiv p+q-l \tag{181}$$

$$q = r+l-p \tag{182}$$

the integral becomes

$$= - C(R)D(R)Tr_D \left\{ \int \frac{d^dp}{(2\pi)^d} e^{-ip\cdot x} \frac{\not{p}}{p^2} \sigma^{\mu\nu} \int \frac{d^dl}{(2\pi)^d} e^{il\cdot x} \frac{\not{l}}{l^2} \sigma^{\alpha}{}_{\nu} \int \frac{d^dr}{(2\pi)^d} e^{ir\cdot x} \frac{r_\mu r_\alpha}{r^2} \right\} \tag{183}$$

Replacing the numerators in each of the integrals by derivatives acting on the exponential puts each integral in a form that can be fourier transformed using the techniques discussed above

$$\begin{aligned} = - C(R)D(R)Tr_D \left\{ \gamma^\eta \sigma^{\mu\nu} \gamma^\lambda \sigma^{\alpha}{}_{\nu} \right\} \left[i \frac{\partial}{\partial x^\eta} \int \frac{d^dp}{(2\pi)^d} e^{-ip\cdot x} \frac{1}{p^2} \right] \\ \left[-i \frac{\partial}{\partial x^\lambda} \int \frac{d^dl}{(2\pi)^d} e^{il\cdot x} \frac{1}{l^2} \right] \left[-\frac{\partial}{\partial x^\mu} \frac{\partial}{\partial x^\alpha} \int \frac{d^dr}{(2\pi)^d} e^{ir\cdot x} \frac{1}{r^2} \right] \end{aligned} \tag{184}$$

Solving the fourier transforms of each propagator, and taking the derivatives gives,

$$= \frac{4}{(4\pi)^{\frac{3}{2}d}} C(R)D(R)\Gamma \left(\frac{d}{2} - 1 \right)^3 \left(1 - \frac{d}{2} \right)^3 (d-1)(d-2) \left(\frac{x^2}{4} \right)^{1-\frac{3}{2}d}. \tag{185}$$

This was computed with massive propagators using Form. In momentum space, the CEDM-CEDM lowest order is

$$\begin{aligned} \langle C_e(x) C_e(y) \rangle_{LO} = - \frac{\alpha D(A) T(R) (q^2)^{-2\epsilon} \mu^{2\epsilon}}{64\pi^3} \left(-\frac{223}{6} m_0^2 (q^2)^2 \epsilon - \frac{2m_0^2 (q^2)^2}{\epsilon} \right. \\ \left. + \frac{1}{3}(-29) m_0^2 (q^2)^2 - \frac{331}{192} (q^2)^3 \epsilon - \frac{(q^2)^3}{12\epsilon} - \frac{7(q^2)^3}{16} \right) \end{aligned} \tag{186}$$

The CMDM-CMDM lowest order is

$$\begin{aligned} \langle C_m(x) C_m(y) \rangle_{LO} = - \frac{\alpha C(R) D(R) (q^2)^{-2\epsilon}}{12288\pi^3 \epsilon} \mu^{2\epsilon} \left[32 m_0^2 (q^2)^2 (\epsilon(223\epsilon + 58) + 12) \right. \\ \left. + (q^2)^3 (\epsilon(331\epsilon + 84) + 16) \right] \end{aligned} \tag{187}$$

The next to leading order CEDM to CEDM amplitude diagrams are displayed in figure 25, and calculated in this section.

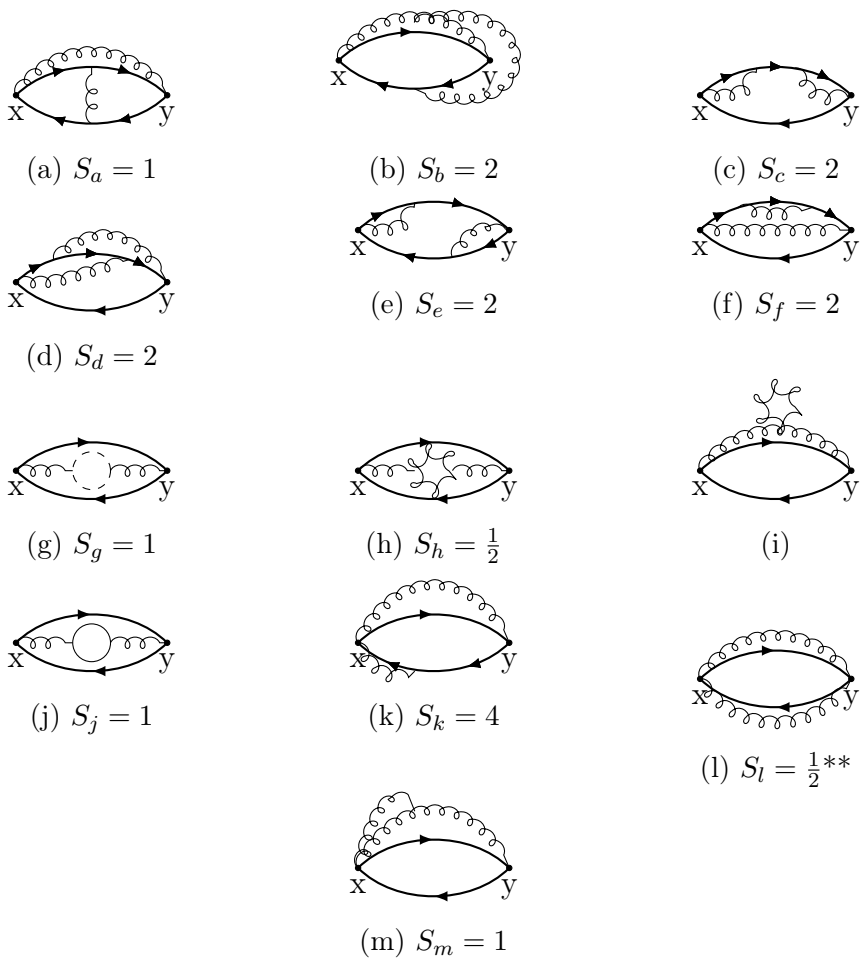

(a) $S_a = 1$ (b) $S_b = 2$ (c) $S_c = 2$

(d) $S_d = 2$ (e) $S_e = 2$ (f) $S_f = 2$

(g) $S_g = 1$ (h) $S_h = \frac{1}{2}$ (i)

(j) $S_j = 1$ (k) $S_k = 4$ (l) $S_l = \frac{1}{2}$**

(m) $S_m = 1$

Figure 25: NLO CEDM and CMDM diagrams

Symmetry Factors

The symmetry factor for diagrams 25a, 25g and 25j is 1.

The symmetry factor for diagrams 25b,25c,25d, 25e, 25f and 25k is 2. This is because the same diagram is produced when the quark-quark-gluon vertex is attached to the top fermion line, or the bottom.

The symmetry factors for diagrams 25h, 25l and 25m is $\frac{1}{2}$. This is because the diagrams are symmetric under the exchange of the gluons in the gluon loop.

Diagrams 25m and25k appear twice in the amplitude with their vertices interchanged. Therefore, they are multiplied by a factor of 2. The total symmetry factor for diagram 25k is 4, and for diagram 25m is 1.

Color Factors

T_R^a, are $D(R)\times D(R)$ matrix representations of the $SU(n)$ generators, obeying the group Lie algebra,

$$\left[T_R^a, T_R^b\right] = if^{abc}T_R^c, \tag{188}$$

Where f^{abc} are the structure constants.

Two numbers, characteristic of a representation are the Casimir invariant $C(R)$, and the index $T(R)$. The Casimir invariant is

$$T_R^a T_R^a = C(R)\mathbf{1}_R, \tag{189}$$

where $\mathbf{1}_R$ is the $D(R) \times D(R)$ identity matrix, and the index is defined by

$$Tr\left[T_R^a T_R^b\right] = T(R)\delta^{ab}. \tag{190}$$

The anticommutator of $SU(n)$ matrices in the fundamental representation is

$$\left\{T^a, T^b\right\} = \frac{1}{n}\delta^{ab}\mathbf{1}_n + d^{abc}T^c, \tag{191}$$

where d^{abc} is a tensor, symmetric in its indices. The tensor d^{abc} obeys the relation

$$d^{ace}d^{bce} = \frac{n^2-4}{n}\delta^{ab}. \tag{192}$$

Each of the correlators involves computing the trace over both color, and Dirac structure of the feynman diagrams. In this section, the traces over the color structure are computed.

The leading order diagram has color structure

$$Tr[T^a T^b]\delta^{ab} = T(R)D(A) = C(R)D(R), \tag{193}$$

Where $C(R)$ is the casimir invariant for representation R, $T(R)$ is the dinkin index for representation R, $D(R)$ is the dimension of representation R, and $D(A)$ is the dimension of the adjoint representation of $su(n)$.

Diagrams 25a and 25d have color structure

$$Tr[T^aT^bT^aT^b] = \frac{1}{4}Tr\left[\left([T^a,T^b]+\left\{T^a,T^b\right\}\right)\left([T^a,T^b]+\left\{T^a,T^b\right\}\right)\right] \tag{194}$$

$$= \frac{1}{4}Tr\left[[T^a,T^b]^2+\left\{T^a,T^b\right\}^2\right] \tag{195}$$

$$= \frac{1}{4}Tr\left[-f^{abc}f^{abd}T^cT^d+\left(\frac{1}{n}\delta^{ab}+d^{abc}T^c\right)^2\right] \tag{196}$$

$$= \frac{1}{4}Tr\left[-f^{abc}f^{abd}T^cT^d+\frac{1}{n^2}D(A)+d^{abc}d^{abd}T^cT^d\right] \tag{197}$$

$$= \frac{1}{4}\left(-T(A)T(R)D(A)+\frac{1}{n^2}D(A)D(R)+T(R)d^{abc}d^{abd}\delta^{cd}\right) \tag{198}$$

$$= \frac{1}{4}\left(-T(A)T(R)D(A)+\frac{1}{n^2}D(A)D(R)+T(R)D(A)\frac{n^2-4}{n}\right) \tag{199}$$

$$\tag{200}$$

Diagrams 25a and 25d also can be expressed with the color factors

$$Tr[T^aT^bT^aT^b] = Tr\left[if^{abc}T^cT^aT^b+T^aT^aT^bT^b\right] \tag{201}$$

$$= \frac{i}{2}f^{abc}Tr\left[T^c([T^a,T^b]+\left\{T^a,T^b\right\}\right]+C^2(R)D(R) \tag{202}$$

$$= -\frac{1}{2}f^{abc}f^{abd}Tr[T^cT^d]+C^2(R)D(R) \tag{203}$$

$$= C^2(R)D(R)-\frac{1}{2}T(R)C(A)D(A) \tag{204}$$

Diagrams 25b and 25k have color structure

$$f^{abc}Tr\left[T^aT^bT^c\right] = \frac{i}{2}f^{abc}f^{abd}Tr\left[T^dT^c\right] \tag{205}$$

$$= \frac{i}{2}T(R)f^{abc}f^{abc} \tag{206}$$

$$= \frac{i}{2}T(R)C(A)D(A) \tag{207}$$

Diagrams 25c, 25e and 25f have color structure

$$Tr\left[T^aT^aT^bT^b\right] = C(R)^2D(R) \tag{208}$$

Diagrams 25h, 25l, and 25m have color structure

$$f^{abc}f^{dbc}Tr\left[T^aT^d\right] = T(R)f^{abc}f^{abc} \tag{209}$$
$$= T(R)C(A)D(A) \tag{210}$$

and diagram 25j has color structure

$$Tr\left[T^aT^b\right]^2 = T(R)C(R)D(R) \tag{211}$$

Bare Diagrams

In the remainder of this section, momentum space results for the NLO diagrams in figure 25 will be briefly explained, and presented. All diagrams were computed in Form. Each diagram is calculated in R_ξ gauge.

Figure 25a

The CEDM contribution from diagram 25a is

$$CEDM_a = \int \frac{d^dp}{(2\pi)^d}\frac{d^dk}{(2\pi)^d}\frac{d^dl}{(2\pi)^d}\mathrm{Tr}_{CD}\left[(-ik_\alpha\sigma^{\alpha\beta}g\gamma_5T^a)S(p+k)(-ig\gamma^\rho T^c)\right.$$
$$\left.S(l+k)(ik_\beta\sigma^{\beta\nu}g\gamma_5T^b)S(Q+l)(-i\gamma^\eta T^j)S(Q+p)\Delta^{jc}_{\eta\rho}(p-l)\Delta^{ab}_{\mu\nu}(k)\right]. \tag{212}$$

Where Q is the fourier momentum injected into the diagram at x. The form output is

$$CEDM_a = -\frac{g_0^4}{19440\epsilon^2}\frac{D(A)T(R)(2C(R)-T(A))}{(4\pi)^6}\frac{(Q^2)^{-6\epsilon}}{}$$
$$\left(24m_0^2(Q^2)^2\left(\epsilon\left(-8820\xi+\epsilon\left(-51990\xi+360\zeta(3)((87\xi+7)\epsilon+12)\right.\right.\right.\right.$$
$$\left.\left.\left.\left.-265025\xi\epsilon+72\pi^4\epsilon+298985\epsilon+58830\right)+9900\right)-1080(\xi-1)\right)$$
$$+(Q^2)^3\left(\epsilon\left(-9900\xi+\epsilon\left(-61890\xi+1080\zeta(3)((29\xi+83)\epsilon+12)\right.\right.\right.$$
$$\left.\left.\left.-326915\xi\epsilon+216\pi^4\epsilon+3005\epsilon+20310\right)+6660\right)-1080(\xi-1)\right)\Big) \tag{213}$$

The contribution of diagram 25a to the chromomagnetic dipole moment

correlator is

$$
\begin{aligned}
CMDM_a =& g_0^4 \frac{C(R)D(R)(2C(R)-T(A))}{19440\epsilon^2} \frac{(Q^2)^{-6\epsilon}}{(4\pi)^6} \\
& \Big(24m_0^2(Q^2)^2 \left(\epsilon \left(-8820\xi + \epsilon \left(-51990\xi + 360\zeta(3)((87\xi+19)\epsilon+12)\right.\right.\right. \\
& \left.\left.\left. -265025\xi\epsilon + 72\pi^4\epsilon + 285485\epsilon + 57750\right) + 9900\right) - 1080(\xi-1)\right) \\
& + (Q^2)^3 \left(\epsilon \left(-9900\xi + \epsilon \left(-61890\xi + 1080\zeta(3)((29\xi+83)\epsilon+12)\right.\right.\right. \\
& \left.\left.\left. -326915\xi\epsilon + 216\pi^4\epsilon + 3005\epsilon + 20310\right) + 6660\right) - 1080(\xi-1)\right)\Big)
\end{aligned} \tag{214}
$$

Figure 25b

$$
\begin{aligned}
CEDM_b =& g_0^4 \frac{1}{38880\epsilon^2} \frac{(Q^2)^{-6\epsilon}}{(4\pi)^6} D(A)T(A)T(R) \\
& \Big(24m_0^2(Q^2)^2 \left(2160(2\xi+7) + \epsilon \left(360(89\xi+355)\right.\right. \\
& \left. + \epsilon \left(177180\xi - 2160\zeta(3)((58\xi+325)\epsilon+24) + 863450\xi\epsilon\right.\right. \\
& \left.\left. -864\pi^4\epsilon + 3878035\epsilon + 760170\right)\right) + (Q^2)^3 \left(2160(2\xi+7)\right. \\
& \left. + \epsilon \left(180(208\xi+791) + \epsilon \left(225600\xi - 4320\zeta(3)((29\xi+176)\epsilon+12)\right.\right.\right. \\
& \left.\left.\left. + 1161920\xi\epsilon - 864\pi^4\epsilon + 4742575\epsilon + 896250\right)\right)\right)\Big)
\end{aligned} \tag{215}
$$

$$
\begin{aligned}
CMDM_b =& g_0^4 \frac{C(R)D(R)T(A)}{38880\epsilon^2} \frac{(Q^2)^{-6\epsilon}}{(4\pi)^6} \\
& 48m_0^2(Q^2)^2 \left(\epsilon \left(\epsilon \left(-99570\xi + 1080\zeta(3)((58\xi+363)\epsilon+24)\right.\right.\right. \\
& \left.\left.\left. -504595\xi\epsilon + 432\pi^4\epsilon - 2490445\epsilon - 474330\right) - 90(190\xi+853)\right)\right. \\
& \left. -2160(\xi+4)\right) + (Q^2)^3 \left(\epsilon \left(\epsilon \left(-225600\xi + 4320\zeta(3)((29\xi+176)\epsilon+12)\right.\right.\right. \\
& \left.\left.\left. -1161920\xi\epsilon + 864\pi^4\epsilon - 4742575\epsilon - 896250\right) - 180(208\xi+791)\right)\right. \\
& \left. -2160(2\xi+7)\right)
\end{aligned} \tag{216}
$$

Figure 25c

$$
\begin{aligned}
CEDM_c =& g_0^4 \frac{C(R)^2D(R)}{54\epsilon^2} \frac{(Q^2)^{-6\epsilon}}{(4\pi)^6} 4m_0^2(Q^2)^2 \left(\epsilon \left(8(621\zeta(3)-5413)\epsilon^2 - 9060\epsilon - 1647\right) - 216\right) \\
& + (Q^2)^3 \left(621\zeta(3)\epsilon^3 - 8(2\epsilon(358\epsilon+75)+27)\epsilon - 27\right)
\end{aligned} \tag{217}
$$

$$CMDM_c = g_0^4 \frac{C(R)^2 D(R)}{54\epsilon^2} \frac{(Q^2)^{-6\epsilon}}{(4\pi)^6} 12 m_0^2 (Q^2)^2 (\epsilon(2\epsilon((5308 - 621\zeta(3))\epsilon + 1110) + 405) + 54) + (Q^2)^3 \left(-621\zeta(3)\epsilon^3 + 8(2\epsilon(358\epsilon + 75) + 27)\epsilon + 27\right) \quad (218)$$

Figure 25d

$$CEDM_c = g_0^4 \frac{2C(R)^2 D(R) - D(A)T(A)T(R)}{19440\epsilon^2} \frac{(Q^2)^{-6\epsilon}}{(4\pi)^6} 48 m_0^2 (Q^2)^2 \left(\epsilon \left(\epsilon \left(90\zeta(3)(173\epsilon + 24) + 36\pi^4\epsilon - 18535\epsilon + 240\right) + 855\right) + 270\right) + 5(Q^2)^3 (\epsilon(\epsilon((15971 - 2484\zeta(3))\epsilon + 3210) + 612) + 108) \quad (219)$$

$$CMDM_d = -g_0^4 \frac{2C(R)^2 D(R) - C(A)D(A)T(R)}{19440\epsilon^2} \frac{(Q^2)^{-6\epsilon}}{(4\pi)^6} 24 m_0^2 (Q^2)^2 \left(\epsilon \left(\epsilon \left(720\zeta(3)(83\epsilon + 6) + 72\pi^4\epsilon - 470165\epsilon - 86370\right) - 12870\right) - 1080\right) + 5(Q^2)^3 (\epsilon(\epsilon((15971 - 2484\zeta(3))\epsilon + 3210) + 612) + 108) \quad (220)$$

Figure 25e

$$CEDM_e = g_0^4 \frac{C(R)^2 D(R)}{216\epsilon^2} \frac{(Q^2)^{-6\epsilon}}{(4\pi)^6} \left(4 m_0^2 (Q^2)^2 (\epsilon(\epsilon((6264\zeta(3) - 57131)\epsilon - 11058) - 1836) - 216) + (Q^2)^3 \epsilon(\epsilon(2563\epsilon + 378) + 36)\right) \quad (221)$$

$$CMDM_e = g_0^4 \frac{C(R)^2 D(R)}{216\epsilon^2} \frac{(Q^2)^{-6\epsilon}}{(4\pi)^6} \left(4 m_0^2 (Q^2)^2 (\epsilon(\epsilon((57131 - 6264\zeta(3))\epsilon + 11058) + 1836) + 216) - (Q^2)^3 \epsilon(\epsilon(2563\epsilon + 378) + 36)\right) \quad (222)$$

Figure 25f

$$CEDM_f = g_0^4 \frac{C(R)^2 D(R)}{216\epsilon^2} \frac{(Q^2)^{-6\epsilon}}{(4\pi)^6} (4 m_0^2 (Q^2)^2 (\epsilon(\epsilon((6264\zeta(3) - 57131)\epsilon - 11058) - 1836) - 216) + (Q^2)^3 \epsilon(\epsilon(2563\epsilon + 378) + 36)) \quad (223)$$

$$CMDM_f = g_0^4 \frac{C(R)^2 D(R)}{1944\epsilon^2} \frac{(Q^2)^{-6\epsilon}}{(4\pi)^6}$$
$$(\xi(Q^2)^3(\epsilon(\epsilon((65383 - 6264\zeta(3))\epsilon + 12378) + 1980) + 216)$$
$$- 24m_0^2(Q^2)^2 \left(\epsilon \left(-1764\xi + \epsilon^2(-53005\xi + 6264(\xi - 3)\zeta(3) + 183705)\right.\right.$$
$$\left.\left. +6(5745 - 1733\xi)\epsilon + 5508) - 216(\xi - 3)\right)) \quad (224)$$

Figure 25g

$$CEDM_g = \frac{D(A)T(A)T(R)}{11664\epsilon^2}$$
$$(3m_0^2(Q^2)^2(\epsilon(\epsilon((123679 - 12528\zeta(3))\epsilon + 23970) + 3924) + 432)$$
$$+ 2(Q^2)^3(\epsilon(\epsilon((10171 - 783\zeta(3))\epsilon + 1857) + 279) + 27)) \quad (225)$$

$$CMDM_g = g_0^4 \frac{C(A)D(A)T(R)}{11664\epsilon^2} \frac{(Q^2)^{-6\epsilon}}{(4\pi)^6}$$
$$(3m_0^2(Q^2)^2(\epsilon(\epsilon((12528\zeta(3) - 142369)\epsilon - 26526) - 4140) - 432)$$
$$+ 2(Q^2)^3(\epsilon(\epsilon((783\zeta(3) - 10171)\epsilon - 1857) - 279) - 27)) \quad (226)$$

Figure 25h

$$CEDM_h = g_0^4 \frac{D(A)T(A)T(R)}{11664\epsilon^2} \frac{(Q^2)^{-6\epsilon}}{(4\pi)^6}$$
$$(3m_0^2(Q^2)^2 \left(-432(6\xi - 25) + \epsilon^3 \left(64062\xi^2 - 261822\xi\right.\right.$$
$$\left. +12528(6\xi - 25)\zeta(3) + 2260021) + 6(6\xi(303\xi - 1741) + 76685)\epsilon^2\right.$$
$$\left. +36(6\xi(6\xi - 65) + 2281)\epsilon) + 2(Q^2)^3 \left(-162\xi + \epsilon^3 \left(5013\xi^2 - 23520\xi + 783(6\xi - 25)\zeta(3)\right.\right.\right.$$
$$\left.\left.\left. +(9\xi(87\xi - 592) + 36480)\epsilon^2 + 9(3\xi(3\xi - 40) + 664)\epsilon + 675\right)\right)$$
$$(227)$$

$$
\begin{aligned}
CMDM_h = &- g_0^4 \frac{C(A)D(A)T(R)}{11664\epsilon^2} \frac{(Q^2)^{-6\epsilon}}{(4\pi)^6} \\
&3m_0^2(Q^2)^2 \left(-432(6\xi-25) + \epsilon^3 \left(71298\xi^2 - 320322\xi + 12528(6\xi-25)\zeta(3) + 2635723\right)\right. \\
&\left. +6(6\xi(321\xi-2035)+86003)\epsilon^2 + 36(6\xi(6\xi-71)+2431)\epsilon\right) \\
&+ 2(Q^2)^3 \left(-162\xi + \epsilon^3 \left(5013\xi^2 - 23520\xi + 783(6\xi-25)\zeta(3) + 189472\right)\right. \\
&\left. +(9\xi(87\xi-592)+36480)\epsilon^2 + 9(3\xi(3\xi-40)+664)\epsilon + 675\right)
\end{aligned} \tag{228}
$$

Figure 25i

For both the CEDM and CMDM correlators, figure 25i is equal to 0. This occurs because gluons are massless, and there is a term $\Delta(0)$, which in dim-reg, is equal to 0. This can be seen by looking at the loop

$$
\text{Gluon Loop} = \int \frac{d^d l}{(2\pi)^d} \frac{1}{l^2} \left(g_{\mu\nu} + (\xi - 1) \frac{l_\mu l_\nu}{l^2} \right) \tag{229}
$$

This is an integral with dimension $d-2$. However, there are no dimensionful parameters. Therefore, the only way this can make sense is if it is equal to 0.

Figure 25j

$$
\begin{aligned}
CEDM_j = &g_0^4 \frac{D(A)T(R)^2 n_f}{729\epsilon^2} \frac{(Q^2)^{-6\epsilon}}{(4\pi)^6} \\
&3m_0^2(Q^2)^2(\epsilon(\epsilon((12528\zeta(3) - 124963)\epsilon - 24690) - 4140) - 432) \\
&+ 2(Q^2)^3 \left(783\zeta(3)\epsilon^3 - 2(\epsilon(4157\epsilon + 789) + 126)\epsilon - 27\right)
\end{aligned} \tag{230}
$$

$$
\begin{aligned}
CMDM_j = &g_0^4 \frac{C(R)D(R)T(R)n_f}{729\epsilon^2} \frac{(Q^2)^{-6\epsilon}}{(4\pi)^6} \\
&3m_0^2(Q^2)^2(\epsilon(\epsilon((141097 - 12528\zeta(3))\epsilon + 27030) + 4356) + 432) \\
&+ 2(Q^2)^3(\epsilon(\epsilon((8314 - 783\zeta(3))\epsilon + 1578) + 252) + 27)
\end{aligned} \tag{231}
$$

Figure 25k

$$CEDM_k = g_0^4 \frac{D(A)T(A)T(R)}{7776\epsilon^2} \frac{(Q^2)^{-6\epsilon}}{(4\pi)^6} (24m_0^2(Q^2)^2(\epsilon(36(18\xi+43)+\epsilon(6156\xi+\epsilon(39330\xi-6264\zeta(3)+28567)+7338))+216)+(Q^2)^3\left(\epsilon^3(29148\xi-6264\zeta(3)+79957)+6(732\xi+2429)\epsilon^2+36(12\xi+61)\epsilon+216\right)) \quad (232)$$

$$CMDM_k = -g_0^4 \frac{C(R)D(R)T(A)}{7776\epsilon^2} \frac{Q.Q^{-6\epsilon}}{(4\pi)^6} (48m_0^2(Q^2)^2(\epsilon(36(3\xi-119)+\epsilon(882\xi+\epsilon(5091\xi+12528\zeta(3)-156461)-28374))-432)+(Q^2)^3\left(\epsilon^3(29148\xi-6264\zeta(3)+79957)+6(732\xi+2429)\epsilon^2+36(12\xi+61)\epsilon+216\right)) \quad (233)$$

Figure 25l

$$CEDM_l = g_0^4 \frac{D(A)T(A)T(R)}{1296\epsilon} \frac{(Q^2)^{-6\epsilon}}{(4\pi)^6} (\xi+1) (6m_0^2(Q^2)^2(72(\xi-2)+\epsilon(606\xi+(3559\xi-9551)\epsilon-1446)) + (Q^2)^3(18(\xi-1)+\epsilon(2\xi(557\epsilon+87)-1315\epsilon-192))) \quad (234)$$

$$CMDM_l = g_0^4 \frac{C(A)D(A)T(R)}{1296\epsilon} \frac{(Q^2)^{-6\epsilon}}{(4\pi)^6} (\xi+1)\left((Q^2)^3\left(1315\epsilon^2-2\xi(\epsilon(557\epsilon+87)+9)+192\epsilon+18\right) -6m_0^2(Q^2)^2(72\xi+\epsilon(642\xi+(3961\xi+567)\epsilon+54))\right) \quad (235)$$

Figure 25m

$$
\begin{aligned}
CEDM_m =& -g_0^4 \frac{D(A)T(A)T(R)}{1944\epsilon^2} \frac{(Q^2)^{-6\epsilon}}{(4\pi)^6} \\
& (3m_0^2(Q^2)^2 \left(432(\xi+5)+\epsilon^3\left(21354\xi^2+150407\xi-12528(\xi+5)\zeta(3)+474433\right)\right. \\
& \left.+6(\xi(606\xi+4771)+15977)\epsilon^2+36(\xi(12\xi+125)+469)\epsilon\right) \\
& +2(Q^2)^3\left(27(\xi+5)+\epsilon^3\left(1671\xi^2+12275\xi-783(\xi+5)\zeta(3)+39652\right)\right. \\
& \left.+3(\xi(87\xi+731)+2524)\epsilon^2+9(\xi(3\xi+35)+136)\epsilon\right)) \qquad (236)
\end{aligned}
$$

$$
\begin{aligned}
CMDM_m =& g_0^4 \frac{C(A)D(A)T(R)}{1944\epsilon^2} \frac{Q.Q^{-6\epsilon}}{(4\pi)^6} \\
& (3m_0^2(Q^2)^2 \left(432(\xi+5)+\epsilon^3\left(23766\xi^2+172217\xi-12528(\xi+5)\zeta(3)+552127\right)\right. \\
& \left.+6(\xi(642\xi+5245)+17879)\epsilon^2+36(\xi(12\xi+131)+499)\epsilon\right) \\
& +2(Q^2)^3\left(27(\xi+5)+\epsilon^3\left(1671\xi^2+12275\xi-783(\xi+5)\zeta(3)+39652\right)\right. \\
& \left.+3(\xi(87\xi+731)+2524)\epsilon^2+9(\xi(3\xi+35)+136)\epsilon\right)) \qquad (237)
\end{aligned}
$$

Full Bare Amplitude

Summing up all of the diagrams gives the full bare amplitudes

$$
\begin{aligned}
\Pi_0^{C_e}(Q^2,m_0^2) =& g_0^4 \frac{1}{58320\epsilon^2} \frac{(Q^2)^{-6\epsilon}}{(4\pi)^6} \\
& (24m_0^2(Q^2)^2 \left(3C(R)^2D(R)\left(\epsilon\left(\epsilon\left(720\zeta(3)(631\epsilon+12)\right.\right.\right. \\
& \left.\left.\left.+144\pi^4\epsilon-3529345\epsilon-708510\right)-122940\right)-15120\right) \\
& -24C(R)D(A)T(R)\left(\epsilon\left(\epsilon\left(360\zeta(3)(67\epsilon+3)+18\pi^4\epsilon-154885\epsilon-28380\right)\right.\right. \\
& \left.\left.-4410\right)-540\right)+2D(A)T(R)\left(5n_fT(R)(\epsilon(\epsilon(12528\zeta(3)\epsilon-124963\epsilon-24690)\right. \\
& \left.-4140)-432\right)+T(A)\left(\epsilon\left(\epsilon\left(-540\zeta(3)(1069\epsilon+72)-648\pi^4\epsilon+3321355\epsilon\right.\right.\right. \\
& \left.\left.\left.+648570\right)+108360\right)+12420\right)))+(Q^2)^3\left(60C(R)^2D(R)(\epsilon(\epsilon((9936\zeta(3)\right. \\
& \left.-83585)\epsilon-18294)-3420)-432\right)-6C(R)D(A)T(R)\left(\epsilon\left(\epsilon\left(1080\zeta(3)(83\epsilon+12)\right.\right.\right. \\
& \left.\left.\left.+216\pi^4\epsilon+3005\epsilon+20310\right)+6660\right)+1080\right)+D(A)T(R)\left(160n_fT(R)\left(783\zeta(3)\right.\right. \\
& \left.\left.\epsilon^3-2(\epsilon(4157\epsilon+789)+126)\epsilon-27\right)+T(A)\left(\epsilon\left(\epsilon\left(-1080\zeta(3)(787\epsilon+36)-648\pi^4\epsilon\right.\right.\right.\right. \\
& \left.\left.\left.\left.+7041125\epsilon+1386870\right)+229140\right)+24840\right)))) \qquad (238)
\end{aligned}
$$

$$\Pi_0^{C_m}(Q^2, m_0^2) = g_0^4 \frac{1}{11664\epsilon^2} \frac{(Q^2)^{-6\epsilon}}{(4\pi)^6}$$
$$(C(R)D(R)\left(\frac{24}{5}m^2(Q^2)^2\left(15C(R)(\epsilon(\epsilon((488419 - 47088\zeta(3))\epsilon + 101802) + 18180)\right.\right.$$
$$+2160) + 10n_f T(R)(\epsilon(\epsilon(-12528\zeta(3)\epsilon + 141097\epsilon + 27030) + 4356) + 432)$$
$$+4T(A)\left(\epsilon\left(\epsilon\left(270\zeta(3)(1033\epsilon + 72) + 324\pi^4\epsilon - 1765895\epsilon - 341790\right) - 56070\right)\right.$$
$$-6210)) + (Q^2)^3\left(6C(R)\left(\epsilon\left(\left(-1944\zeta(3) + \frac{216\pi^4}{5} + 167771\right)\epsilon^2 + 6(432\zeta(3)\right.\right.\right.$$
$$+6775)\epsilon + 8172) + 1080) + 32n_f T(R)(\epsilon(\epsilon((8314 - 783\zeta(3))\epsilon + 1578) + 252) + 27)$$
$$+T(A)\left(\epsilon\left(\epsilon\left(216\zeta(3)(787\epsilon + 36) + \frac{648\pi^4\epsilon}{5} - 1408225\epsilon - 277374\right) - 45828\right)\right.$$
$$\left.\left.\left.-4968))\right)\right) \tag{239}$$

QCD Renormalization Group Coefficients

Quark Propagator

The full quark propagator is

$$\mathbf{S}(p) = \langle \psi\overline{\psi} \rangle = \frac{1}{S_0^{-1}(p) - \Sigma(p)}, \tag{240}$$

Where $S_0^{-1}(p) = i\not{p} + m_0$, is the inverse of the free quark propagator, and $\Sigma(p) = i\not{p}\Sigma_V(p^2) + m_0\Sigma_S(p^2)$, is the corrections to the full propagator due to loops. The loop corrections have been rearranged into terms proportional to $\not{p}$, and terms proportional to $m_0\mathbf{1}$.

$$\begin{aligned}\mathbf{S}(p) =& \frac{1}{1 - \Sigma_V(p^2)} \frac{1}{i\not{p} + \frac{1+\Sigma_S}{1-\Sigma_V} m_0} \\ =& Z_\psi S_r(p;\mu)\end{aligned} \tag{241}$$

Where Z_ψ is the quark wave function renormalization, and $S_r(p;\mu)$ is the renormalized propagator. For this to be finite, and for the renormalization

constants to be found in $\overline{MS}$,

$$Pole\ Part\left[Z_\psi\left(1-\Sigma_V(p^2)\right)\right]=1 \tag{242}$$

$$Pole\ Part\left[\frac{1+\Sigma_S}{1-\Sigma_V}Z_m\right]\propto Pole\ Part\left[\left(1+\Sigma_S\right)Z_\psi Z_m\right]=1 \tag{243}$$

Z_ψ and Z_m up to order α are found by computing the one loop correction to the quark propagator, shown in figure 26.

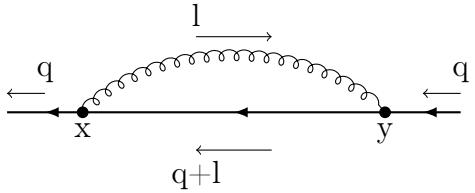

Figure 26: 1 loop correction to quark propagator

Figure 26 is

$$i\not{q}\Sigma_V(q^2)+m_0\Sigma_S(q^2)=\int\frac{d^dl}{(2\pi)^d}\left(-ig_0\gamma^\mu T^a\right)\frac{-i\left(\not{q}+\not{l}\right)+m_0}{(q+l)^2+m_0^2}\left(-ig_0\gamma^\nu T^b\right)\frac{\delta^{ab}}{l^2}\left(g_{\mu\nu}+(\xi-1)\frac{l_\mu l_\nu}{l^2}\right) \tag{244}$$

Σ_V can be found by multiplying both sides by $\not{q}$ and taking the trace over color, and Dirac indices.

$$\Sigma_V(q^2)=\frac{1}{2}\frac{g_0^2C(R)}{(4\pi)^{d/2}}\left[(2-d)\frac{\Gamma\left(2-\frac{d}{2}\right)\Gamma\left(\frac{d}{2}-1\right)^2}{\Gamma\left(d-2\right)}+\right.$$
$$\left.(\xi-1)\left(\frac{\Gamma\left(3-\frac{d}{2}\right)\Gamma\left(\frac{d}{2}-1\right)\Gamma\left(\frac{d}{2}-2\right)}{\Gamma(d-3)}-\frac{\Gamma\left(2-\frac{d}{2}\right)\Gamma\left(\frac{d}{2}-1\right)^2}{\Gamma(d-2)}\right)\right](q^2)^{d/2-2} \tag{245}$$

Plugging equation (245) into equation (242) gives

$$Z_\psi=1-\xi\frac{C(R)}{\epsilon}\frac{\alpha}{4\pi} \tag{246}$$

Σ_S can be found by taking the trace over both Dirac and color space

$$\Sigma_S(q^2) = -g_0^2 C(R)\left(d+(\xi-1)\right)\frac{\Gamma\left(2-\frac{d}{2}\right)\Gamma\left(\frac{d}{2}-1\right)^2}{(4\pi)^{d/2}\Gamma(d-2)}(q^2)^{d/2-2} \tag{247}$$

Plugging equation (247) and Z_ψ into equation (243), and solving for Z_m gives

$$Z_m = 1 - 3\frac{C(R)}{\epsilon}\frac{\alpha}{4\pi} \tag{248}$$

Using Z_m,

$$\gamma_m = 6C(R)\frac{\alpha}{4\pi} \tag{249}$$

Gluon Propagator

It can be shown that to all perturbative orders, loop corrections to the gluon propagator are transverse. Therefore, the loop corrections, $\Pi^{ab}_{\mu\nu}(q)$, will be of the form

$$\Pi^{ab}_{\mu\nu}(q) = \delta^{ab}(q^2 g_{\mu\nu} - q_\mu q_\nu)\Pi(q^2) \tag{250}$$

Therefore, there will only be loop corrections to the transverse part of the gluon propagator. The full gluon propagator is

$$\mathbf{D}^{ab}_{\mu\nu}(q) = \frac{\delta^{ab}}{q^2(1-\Pi(q^2))}\left(g_{\mu\nu} - \frac{q_\mu q_\nu}{q^2}\right) + \xi\delta^{ab}\frac{q_\mu q_\nu}{(q^2)^2} \tag{251}$$

$$= \delta^{ab} Z_A D^r_{\mu\nu}(q) \tag{252}$$

Where Z_A is the wave function renormalization to the gluon field, and $D^r_{\mu\nu}$ is the renormalized gluon propagator

$$D^r_{\mu\nu} = D^r_\perp(q^2;\mu)\left(g_{\mu\nu} - \frac{q_\mu q_\nu}{q^2}\right) + \xi(\mu)\frac{q_\mu q_\nu}{(q^2)^2} \tag{253}$$

$$D^r_\perp = \frac{Z_A^{-1}}{q^2(1-\Pi(q^2))} \tag{254}$$

Since $D^r_\perp$ is finite,

$$Pole\ Part\left[\frac{Z_A^{-1}}{q^2(1-\Pi(q^2))}\right] = 1 \tag{255}$$

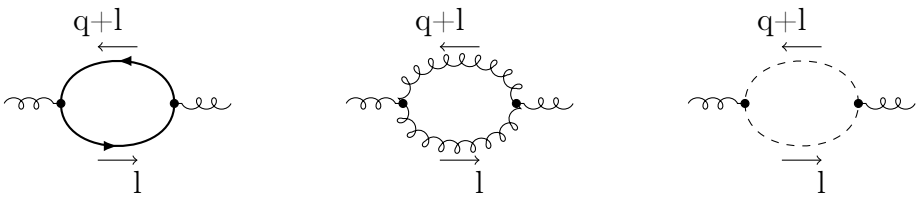

(a) (b) (c)

Figure 27: 1 loop corrections to gluon propagator

The loop corrections to the gluon propagator are shown in figure 27

Figure 27a is equal to

$$(q^2 g_{\mu\nu} - q_\mu q_\nu)\Pi_q^{ab}(q^2) = -\, n_f \int \frac{d^d l}{(2\pi)^d} Tr_{CD} \left\{ (-ig_0\gamma^\mu T^a) \frac{-i(\not{q}+\not{l}) + m_0}{(q+l)^2 + m_0^2} (-ig_0\gamma^\nu T^b) \frac{-i\not{l} + m_0}{l^2 + m_0^2} \right\} \tag{256}$$

Taking the trace over the lorentz structure and dividing both sides by $q^2(d-1)$ allows to solve for Π_1

$$\Pi_q^{ab}(q^2) = 2(2-d)\frac{g_0^2 T(R)\delta^{ab} n_f}{d-1} \frac{\Gamma\left(2-\frac{d}{2}\right)\Gamma\left(\frac{d}{2}-1\right)^2}{(4\pi)^{d/2}\Gamma(d-2)} (q^2)^{d/2-2} \tag{257}$$

This has a $\frac{1}{\epsilon}$ pole of

$$Pole\left[\Pi_q\right] = -\frac{4}{3}\frac{T(R) n_f}{\epsilon}\frac{\alpha}{4\pi} \tag{258}$$

Figure 27b is equal to

$$\begin{aligned}(q^2 g_{\mu\nu} - q_\mu q_\nu)\Pi_g^{ab}(q^2) = &-\frac{g_0^2}{2} f^{anm} f^{btr} \int \frac{d^d l}{(2\pi)^d} \left[-(2q+l)^\rho g^{\mu\eta} + (q+2l)^\mu g^{\rho\eta} + (q-l)^\eta g^{\rho\mu}\right] \\ &\left[(q-l)^\lambda g^{\nu\tau} + (2l+q)^\nu g^{\lambda\tau} - (2q+l)^\tau g^{\lambda\nu}\right] \frac{\delta^{nr}}{(q+l)^2}\left(g_{\eta\lambda} + (\xi-1)\frac{(q+l)_\eta (q\right. \\ &\left.\frac{\delta^{mt}}{l^2}\left(g_{\rho\tau} + (\xi-1)\frac{l_\rho l_\tau}{l^2}\right)\right. \\ Pole\left[\Pi_g\right] = &-T(A)\frac{\xi-4}{2\epsilon}\frac{\alpha}{4\pi}\end{aligned} \tag{259}$$

Figure 27c is equal to

$$(q^2 g_{\mu\nu} - q_\mu q_\nu)\Pi^{ab}_{ghost}(q^2) = -\frac{1}{2}\frac{d^d l}{(2\pi)^d}(-ig_0)f^{man}l_\mu \frac{\delta^{mr}}{(q+l)^2}(-ig_0)f^{sbr}(q+l)_\nu \frac{\delta^{ns}}{l^2} \tag{260}$$

$$Pole\left[\Pi_{ghost}\right] = \frac{T(A)}{12\epsilon}\frac{\alpha}{4\pi} \tag{261}$$

By plugging the poles from each of the loop corrections into equation (255), Z_A is found to be

$$Z_A = 1 - \frac{1}{\epsilon}\left[\frac{1}{2}\left(\xi - \frac{13}{3}\right)T(A) + \frac{4}{3}T(R)n_f\right]\frac{\alpha}{4\pi} \tag{262}$$

Quark Gluon Vertex

The full quark gluon vertex to all perturbative orders is

$$\Gamma^\mu = \gamma^\mu + \Lambda^\mu(q, q') \tag{263}$$

$$\Gamma^\mu = Z_\Gamma \Gamma^\mu_r \tag{264}$$

Where Γ^μ_r is finite. The diagrams corresponding to the order α contribution to Λ^μ are

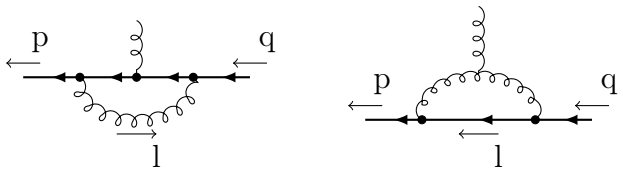

(a) (b)

Figure 28: 1 loop corrections to the quark gluon vertex

Figure 28a has the pole

$$Pole\left[\Lambda_1\right] = -ig_0\frac{\left(C(R) - \frac{1}{2}T(A)\right)\xi}{\epsilon}\frac{\alpha}{4\pi}T^a\gamma^\mu \tag{265}$$

Figure 28b has the pole

$$Pole\left[\Lambda_2\right] = -\frac{i}{2}g_0 T(A)\frac{3}{2}\frac{1+\xi}{\epsilon}\frac{\alpha}{4\pi}T^a\gamma^\mu \tag{266}$$

Demanding that the pole part of $Z_\Gamma^{-1}\Gamma^\mu = 1$, one finds

$$Z_\Gamma = 1 + \frac{1}{\epsilon}\left(\frac{3+\xi}{4}T(A) + \xi C(R)\right)\frac{\alpha}{4\pi} \tag{267}$$

Coupling and β Function

$$\begin{aligned} Z_\alpha =& (Z_\Gamma Z_q)^{-2} Z_A^{-1} \\ =& 1 - \frac{1}{\epsilon}\left(\frac{11}{3}T(A) - \frac{4}{3}n_f T(R)\right)\frac{\alpha}{4\pi} \end{aligned} \tag{268}$$

Using Z_α and the renormalization group equation for $\alpha(\mu)$

$$\frac{d\log\alpha}{d\log\mu^2} = -\epsilon - \beta, \tag{269}$$

the β function can be extracted.

$$\alpha_0 = Z_\alpha \alpha \tag{270}$$

$$\frac{d\alpha_0}{d\ln\mu^2} = 0 = \left(1 + \alpha\frac{\partial \ln Z_\alpha}{\partial\alpha}\right)\frac{d\alpha}{d\ln\mu^2} \tag{271}$$

Using equations (268) and 269 in equation (271), β can be found. In 4 dimensions ($\epsilon = 0$), at order α, it is

$$\beta(\alpha) = \frac{\alpha}{4\pi}\left(\frac{11}{3}T(A) - \frac{4}{3}n_f T(R)\right) \tag{272}$$

One can find the running of α and m in $d = 4$ using the renormalization group equations

$$\frac{d\ln\alpha}{d\ln\mu^2} = -\beta \tag{273}$$

and

$$\frac{d\ln m^2}{d\ln\mu^2} = -\gamma_m \tag{274}$$

Bibliography

[1] V. Gimenez *et al.*, Phys. Lett. **B598**, 227 (2004), hep-lat/0406019.

[2] J. Collins, Camb. Monogr. Part. Phys. Nucl. Phys. Cosmol. **32**, 1 (2011).

[3] C. Gattringer and C. B. Lang, Lect. Notes Phys. **788**, 1 (2010).

[4] C. Vafa and E. Witten, Nucl. Phys. **B234**, 173 (1984).

[5] T. Schäfer and E. V. Shuryak, Rev. Mod. Phys. **70**, 323 (1998), hep-ph/9610451.

[6] S. Scherer, Adv. Nucl. Phys. **27**, 277 (2003), hep-ph/0210398, [,277(2002)].

[7] T. Guhr, A. Muller-Groeling, and H. A. Weidenmuller, Phys. Rept. **299**, 189 (1998), cond-mat/9707301.

[8] M. L. Mehta, *Random Matrices*, 3rd ed. (, 2004).

[9] E. V. Shuryak and J. J. M. Verbaarschot, Nucl. Phys. **B341**, 1 (1990).

[10] J. J. M. Verbaarschot, Phys. Rev. Lett. **72**, 2531 (1994), hep-th/9401059.

[11] J. J. M. Verbaarschot and T. Wettig, Ann. Rev. Nucl. Part. Sci. **50**, 343 (2000), hep-ph/0003017.

[12] D. Dalmazi and J. J. M. Verbaarschot, Nucl. Phys. **B592**, 419 (2001), hep-th/0005229.

[13] J. J. M. Verbaarschot and M. R. Zirnbauer, J. Phys. **A18**, 1093 (1985).

[14] K. Splittorff and J. J. M. Verbaarschot, Nucl. Phys. **B695**, 84 (2004), hep-th/0402177.

[15] E. Kanzieper, Phys. Rev. Lett. **89**, 250201 (2002), cond-mat/0207745.

[16] P. de Forcrand, PoS **LAT2009**, 010 (2009), 1005.0539.

[17] G. Aarts, J. Phys. Conf. Ser. **706**, 022004 (2016), 1512.05145.

[18] K. Splittorff and J. J. M. Verbaarschot, Acta Phys. Polon. **B38**, 4123 (2007), 0710.0704.

[19] A. D. Jackson and J. J. M. Verbaarschot, Phys. Rev. **D53**, 7223 (1996), hep-ph/9509324.

[20] M. A. Stephanov, Phys. Rev. Lett. **76**, 4472 (1996), hep-lat/9604003.

[21] J. C. Osborn, Phys. Rev. Lett. **93**, 222001 (2004), hep-th/0403131.

[22] M. G. Alford, A. Kapustin, and F. Wilczek, Phys. Rev. **D59**, 054502 (1999), hep-lat/9807039.

[23] D. T. Son and M. A. Stephanov, Phys. Rev. Lett. **86**, 592 (2001), hep-ph/0005225.

[24] K. Splittorff and J. J. M. Verbaarschot, Nucl. Phys. **B757**, 259 (2006), hep-th/0605143.

[25] G. Akemann, J. C. Osborn, K. Splittorff, and J. J. M. Verbaarschot, Nucl. Phys. **B712**, 287 (2005), hep-th/0411030.

[26] G. Akemann, P. H. Damgaard, J. C. Osborn, and K. Splittorff, Nucl. Phys. **B766**, 34 (2007), hep-th/0609059, [Erratum: Nucl. Phys.B800,406(2008)].

[27] A. M. Halasz, A. D. Jackson, and J. J. M. Verbaarschot, Phys. Rev. **D56**, 5140 (1997), hep-lat/9703006.

[28] C. Lehner, M. Ohtani, J. J. M. Verbaarschot, and T. Wettig, Phys. Rev. **D79**, 074016 (2009), 0902.2640.

[29] R. A. Janik, M. A. Nowak, G. Papp, J. Wambach, and I. Zahed, Phys. Rev. **E55**, 4100 (1997), hep-ph/9609491.

[30] D. Toublan and J. J. M. Verbaarschot, Int. J. Mod. Phys. **B15**, 1404 (2001), hep-th/0001110, [Ser. Adv. Quant. Many Body Theor.3,114(2000)].

[31] R. A. Janik, M. A. Nowak, G. Papp, and I. Zahed, Nucl. Phys. **B501**, 603 (1997), cond-mat/9612240.

[32] K. Splittorff and J. J. M. Verbaarschot, Nucl. Phys. **B683**, 467 (2004), hep-th/0310271.

[33] K. B. Efetov, G. Schwiete, and K. Takahashi, Phys. Rev. Lett. **92**, 026807 (2004).

[34] P. Littelmann, H.-J. Sommers, and M. Zirnbauer, Communications in Mathematical Physics **283**, 343 (2008).

[35] J. E. Bunder, K. B. Efetov, V. E. Kravtsov, O. M. Yevtushenko, and M. R. Zirnbauer, Journal of Statistical Physics **129**, 809 (2007).

[36] F. Basile and G. Akemann, JHEP **12**, 043 (2007), 0710.0376.

[37] V. Kaymak, M. Kieburg, and T. Guhr, J. Phys. **A47**, 295201 (2014), 1402.3458.

[38] A. D. Jackson, M. K. Sener, and J. J. M. Verbaarschot, Nucl. Phys. **B479**, 707 (1996), hep-ph/9602225.

[39] Y. V. Fyodorov, Nucl. Phys. **B621**, 643 (2002), math-ph/0106006.

[40] A. E. Ingham, Mathematical Proceedings of the Cambridge Philosophical Society **29**, 271–276 (1933).

[41] C. L. Siegel, Annals of Mathematics , 527 (1935).

[42] M. Kellerstien, K. Splittorff, and J. Verbaarschot, PoS **LATTICE2015**, 059 (2016), 1605.03219.

[43] I. S. Gradshteyn and I. M. Ryzhik, *Table of integrals, series, and products*, Seventh ed. (Elsevier/Academic Press, Amsterdam, 2007), Translated from the Russian, Translation edited and with a preface by Alan Jeffrey and Daniel Zwillinger, With one CD-ROM (Windows, Macintosh and UNIX).

[44] G. Akemann and Y. V. Fyodorov, Nucl. Phys. **B664**, 457 (2003), hep-th/0304095.

[45] J. R. Ipsen and K. Splittorff, Phys. Rev. **D86**, 014508 (2012), 1205.3093.

[46] G. Akemann and G. Vernizzi, Nucl. Phys. **B660**, 532 (2003), hep-th/0212051.

[47] J. Verbaarschot and M. Zirnbauer, Journal of Physics A: Mathematical and General **18**, 1093 (1985).

[48] J. Engel, M. J. Ramsey-Musolf, and U. van Kolck, Prog. Part. Nucl. Phys. **71**, 21 (2013), 1303.2371.

[49] E. M. Purcell and N. F. Ramsey, Phys. Rev. **78**, 807 (1950).

[50] S. Syritsyn, T. Izubuchi, and H. Ohki, Calculation of Nucleon Electric Dipole Moments Induced by Quark Chromo-Electric Dipole Moments and the QCD θ-term, in *13th Conference on Quark Confinement and the Hadron Spectrum (Confinement XIII) Maynooth, Ireland, July 31-August 6, 2018*, 2019, 1901.05455.

[51] S. Syritsyn, T. Izubuchi, and H. Ohki, Progress in the Nucleon Electric Dipole Moment Calculations in Lattice QCD, in *13th Conference on the Intersections of Particle and Nuclear Physics (CIPANP 2018) Palm Springs, California, USA, May 29-June 3, 2018*, 2018, 1810.03721.

[52] T. Bhattacharya, B. Yoon, R. Gupta, and V. Cirigliano, Neutron Electric Dipole Moment from Beyond the Standard Model, 2018, 1812.06233.

[53] G. Martinelli, C. Pittori, C. T. Sachrajda, M. Testa, and A. Vladikas, Nucl. Phys. **B445**, 81 (1995), hep-lat/9411010.

[54] T. Bhattacharya, V. Cirigliano, R. Gupta, E. Mereghetti, and B. Yoon, Phys. Rev. **D92**, 114026 (2015), 1502.07325.

[55] M. Constantinou *et al.*, Phys. Rev. **D92**, 034505 (2015), 1506.00361.

[56] J. C. Collins, *Renormalization*, Cambridge Monographs on Mathematical Physics Vol. 26 (Cambridge University Press, Cambridge, 1986).

[57] K. G. Chetyrkin and A. Maier, Nucl. Phys. **B844**, 266 (2011), 1010.1145.

[58] A. Grozin, *Lectures on QED and QCD: Practical calculation and renormalization of one- and multi-loop Feynman diagrams* (, 2007).

[59] V. A. Smirnov, Springer Tracts Mod. Phys. **211**, 1 (2004).

[60] S. A. Larin, F. V. Tkachov, and J. A. M. Vermaseren, (1991).